

August 2020

Elucidation of UBQLN2 liquid-liquid phase separation mechanisms via point mutations and domain deletions

Holly Brianne Jones
Syracuse University

Follow this and additional works at: <https://surface.syr.edu/thesis>



Part of the [Life Sciences Commons](#)

Recommended Citation

Jones, Holly Brianne, "Elucidation of UBQLN2 liquid-liquid phase separation mechanisms via point mutations and domain deletions" (2020). *Theses - ALL*. 441.
<https://surface.syr.edu/thesis/441>

This Thesis is brought to you for free and open access by SURFACE. It has been accepted for inclusion in Theses - ALL by an authorized administrator of SURFACE. For more information, please contact surface@syr.edu.

Abstract

Organization, separation, and cellular regulation are all functions of membraneless organelles (MLOs), which arise by a biophysical phenomenon termed liquid-liquid phase separation (LLPS). By this process, macromolecules in a mixed liquid solution condense together to form liquid droplets within a liquid solution, comparable to oil droplets in water. Some known MLOs formed in cells via LLPS include nucleoli, stress granules, Cajal bodies, and processing-bodies, among other membrane-lacking liquid granules. Previous work has shown that many proteins which compose these liquid compartments also undergo LLPS isolated *in vitro*, and thus have become model systems to investigate the forces that drive these macromolecules to undergo phase transitions.

Currently, the LLPS field has identified key features of proteins which contribute to phase separation. Included in this are sequences of intrinsic disorder and structured sequences, prion-like regions, oligomerization, and multivalent interactions. In this thesis, the protein of interest, UBQLN2, contains all such features. Additionally, prior work in the Castañeda lab and others has shown that UBQLN2 is recruited to stress granules, and disease-related inclusion bodies. *In vitro*, UBQLN2 phase separates into spherical liquid droplets in a concentration and temperature-dependent manner. As UBQLN2 exhibits LLPS both *in vitro* and *in vivo*, it serves as a model system to uncover, on a molecular level, the driving forces of phase separation.

The studies provided herein, investigate the properties of UBQLN2 phase separation and how they are modified with the introduction of mutations and domain deletions. By identifying how molecular variations modify UBQLN2 LLPS properties, one

can identify a molecular code which UBQLN2 follows to drive and modulate its LLPS. Through experimental investigation via turbidity assays, phase diagram construction, microscopy, and self-association studies, we elucidate the molecular foundations of UBQLN2 LLPS.

Here, I propose that UBQLN2 LLPS is driven by “sticker” sequences which contribute to interchain interactions, and that hydrophobic and polar interactions are important sequence-intrinsic features which drive LLPS and control material properties of UBQLN2 droplets. Additionally, I look at UBQLN2 on a domain-by-domain level to uncover how sequence features like structure, disorder, and prion propensity may contribute differently to phase separation. Finally, I propose a method of UBQLN2 purification that potentially incorporates native post-translational modifications (PTMs) to create a more physiologically relevant system for study.

**Elucidation of UBQLN2 liquid-liquid phase separation mechanisms
via point mutations and domain deletions**

By

Holly Jones

B.S. Eastern Illinois University, 2018

Thesis

Submitted in partial fulfillment of the requirements for the
degree of Master of Science in Biology

Syracuse University

August 2020

Copyright Holly Jones 2020

All Rights Reserved

Acknowledgments

I would like to express my sincere gratitude for all of those who have made this dissertation possible, and to those who have assisted me as I have journeyed through graduate school. I wish to thank Dr. Carlos Castañeda first and foremost for giving me the opportunity to join his research team. I am truly grateful for all the ways he has shaped my time at graduate school—by allowing me to pursue my own research interests, for providing direction and support to my research projects, and for guiding me as I explore and define my own career interests and passions. I will always remember Dr. Castañeda’s encouragement and passion for our field. I would also like to thank my committee members, Dr. James Hougland, Dr. Eleanor Maine, and Dr. Heidi Hehnly.

I would also like to thank my current graduate lab members, Tongyin Zheng, Yiran Yang, and Peter Raymond-Smiedy for being of great assistance, and partners, in the lab. I am especially thankful to have had lab mates who have been incredibly helpful, and who have also become great friends. I am also grateful for the current and previous Castañeda lab undergraduates who, though younger in age, have left me with impressionable traits of great scientists. I consider it an honor to have worked alongside of, and learned from, great fellow researchers. I would like to give a special thanks to Thuy Dao, our lab manager, who has been of great assistance in teaching me lab procedures, and who has helped me appreciate the science behind them.

I also express my deepest gratitude for the Hougland lab, who welcomed me into their lab to learn and perform experiments, and who invited me on many needed coffee runs. I am genuinely thankful for Michelle Sieburg, the Hougland lab manager, who acted as a research mentor, and also a mentor in faith.

Finally, I would like to sincerely thank my family and friends who have supported, prayed for, and encouraged me along this journey. I undoubtedly have grown in skill, knowledge, and faith throughout my time at Syracuse University, by which much is owed to the guidance of my loved ones and mentors.

Contents

Abstract

Copyright Notice

Acknowledgments

List of Illustrative Material

Chapter 1: Introduction	1
<i>1.1 Membraneless organelles form via liquid-liquid phase separation</i>	2
<i>1.2 Multivalent interactions maintain phase-separated compartments</i>	4
<i>1.3 Dysfunction of LLPS leads to pathological states</i>	7
<i>1.4 In vitro analysis of phase-separating protein solutions</i>	8
<i>1.5 Ubiquilin-2 (UBQLN2) phase separates in vitro and is recruited to stress granules</i>	12
<i>1.6 Dissertation overview</i>	13
Chapter 2: Single Amino Acid Substitutions Substantially Alter UBQLN2 Droplet Morphology and Dense Phase Material Properties	19
<i>2.1 Introduction</i>	21
<i>2.2 Results</i>	23
<i>2.2.1 Turbidity assay analyses describe effect of amino acid substitutions</i>	23
<i>2.2.2 Dense phase properties and dynamics are altered by hydrophobic sticker but not spacer substitutions</i>	27
<i>2.2.3 Effects of amino acid substitutions on LLPS properties can be explained by changes in oligomerization propensity</i>	28
<i>2.2.4 SAXS analysis confirms presence of large oligomers in stickers</i>	29

2.3 Discussion and Conclusions.....	31
2.4 Materials and Methods.....	41
2.4.1 Subcloning, Protein Expression, and Purification.....	41
2.4.2 Spectrophotometric Absorbance/Turbidity Measurements.....	41
2.4.3 Phase diagram measurements.....	42
2.4.4 Bright-field Imaging of Phase Separation.....	43
2.4.5 Droplet Fusion Assays.....	43
2.4.6 Size Exclusion Chromatography.....	44
2.4.7 Small Angle X-Ray Scattering.....	45
Chapter 3: Domain Deletion Constructs Map Domain Contributions to UBQLN2	
Phase Separation.....	46
3.1 Introduction.....	48
3.2 Results.....	52
3.2.1 Generation of UBQLN2 Domain Deletion Constructs and Mutants.....	52
3.2.2 Turbidity Assays Screened for Differential Effects on UBQLN2 LLPS.....	53
3.2.3 Phase Diagrams Quantitatively Describe the Effects of Domains on LLPS.....	55
3.2.4 Phase Diagrams Quantitatively Describe the Effects of Mutations.....	57
3.2.5 Size Exclusion Chromatography Describes UBQLN2 Self- Association.....	58
3.3 Discussion and Conclusions.....	59
3.4 Materials and Methods.....	74
3.4.1 Subcloning, Protein Expression, and Purification.....	74
3.4.2 Spectrophotometric Absorbance/Turbidity Measurements.....	74

3.4.3 Phase diagram measurements.....	75
3.4.4 Size Exclusion Chromatography.....	76
Chapter 4: Eukaryotic Expression of UBQLN2 in Sf9 Insect Cells.....	77
4.1 Introduction.....	79
4.2 Results.....	83
4.2.1 Generation of UBQLN2 baculovirus.....	83
4.2.2 Sf9 cell preparation and infection.....	85
4.2.3 Purification of UBQLN2.....	85
4.3 Conclusions and Future Studies.....	85
Chapter 5: Conclusions and future work.....	96
5.1 Conclusions.....	97
5.2 Future Directions.....	99
List of Abbreviations.....	103
References.....	104
Publication “Single Amino Acid Substitutions in Stickers, but Not Spacers, Substantially Alter UBQLN2 Phase Transitions and Dense Phase Material Properties”	112
Curriculum Vitae.....	124

List of Illustrative Materials

1.1 Membraneless Organelles which arise via LLPS.....	15
1.2 Schematic diagram of multivalent interactions which drive LLPS.....	16
1.3 Microscopic imaging of UBQLN2 confirms LLPS and UBQLN2 domain map.....	17
1.4 Temperature—ramp spectroscopic data is used to construct phase diagrams.....	18
2.1 UBQLN2 450C composition and experimental sticker residues.....	33
2.2 Spectrophotometric turbidity assay results.....	34
2.3 Temperature–Concentration phase diagrams for representative sticker and spacer residues in UBQLN2.....	35
2.4 Light microscopy probes dense phase droplet properties.....	37
2.5 Oligomerization propensities of different UBQLN2 mutants.....	39
2.6 Small angle x-ray scattering (SAXS) experiments reveal scattering intensities of WT and mutant UBQLN2.....	40
3.1 Structure and function of UBQLN2.....	64
3.2 Phase separation properties of disease linked mutations in UBQLN2 FL and 450C.....	66
3.3 Domain deletion constructs of UBQLN2.....	67
3.4 Turbidity assays screen for LLPS in WT and P497L domain deletion constructs.	68
3.5 Phase diagrams map conditions of phase separation.....	69
3.6 Temperature-concentration phase diagrams for domain deletion constructs of wild-type and mutant UBQLN2.....	70
3.7 Oligomerization propensity of UBQLN2 domain deletion constructs.....	72

4.1 Phosphomimic mutant UBQLN2 perturbs LLPS properties.	89
4.2 Brightfield microscopy of WT and UBQLN2 mutants with phosphomimetic substitutions.....	90
4.3 Schematic of the generation of recombinant baculovirus and gene expression adapted from Bac-to-Bac Expression System.....	91
4.4 PCR product confirms successful production of recombinant donor plasmid pFastBacDual with UBQLN2 and RFP.....	92
4.5 SDS-Page gel electrophoresis confirms successful transposition of UBQLN2 into bacmid DNA.....	93
4.6 Western blot confirms expression of UBQLN2.....	94
4.7 Purification of UBQLN2 from Sf9 cells.....	95

Chapter 1: Introduction

Membraneless organelles form via liquid-liquid phase separation

Cellular organization is a key factor of normal cell function. Classically, the idea of membrane-bound organelles and compartments form the foundation of cellular organization. However, scientists have recently discovered the importance of membraneless organelles (MLOs), though the presence of MLOs has been recognized for nearly two centuries (Wilson, 1899). Membraneless organelles (MLOs) introduce a novel paradigm of cellular organization. MLOs add compartmentalization of cellular components through separation of cellular material, without a discrete external barrier like a lipid bilayer. Unlike their membrane-bound counterparts, these organelles are dynamic, allow constituents to easily enter and exit, and are thought to be regulated by various factors like cellular stressors, post-translational modifications (PTMs), or post-transcriptional RNA modifications (Drino and Schaefer, 2018; Saito et al., 2019; Shapouri et al., 2016). Different MLOs hold distinct physiological functions which impact stress response, development, and regulation of gene expression (Drino and Schaefer, 2018). Given different functions, MLOs must recruit different members, and thus can include proteins, mRNA, and DNA (Alberti and Carra, 2018). Largely, these MLOs function to allow sub-compartmentalization of biochemical reactions and biological processes (Nott et al., 2015).

MLOs exist as liquid droplets within the cell and arise from condensation of cellular material (Gomes and Shorter). Observations have described these organelles as having liquid-like material properties such as fusion, dripping, and wetting, with molecules continuously entering and exiting (Alberti and Carra, 2018; Brangwynne, 2011; Brangwynne et al., 2009). Membraneless organelles are advantageous to the

cellular environment due to their ability to sequester macromolecules and to spatiotemporally compartmentalize specific biochemical reactions, while also allowing diffusion of biomolecules into and out of the organelle. Nucleoli, Cajal bodies, P-bodies, and stress granules are all examples of MLOs in cells, and their function is largely contingent on the macromolecules they contain (Figure 1A). Functioning as more than just an organizational compartment, Cajal bodies, for example, can also tune biochemical reactions such as the assembly of U4/U6.U5 tri-snRNP, a spliceosomal complex (Novotná et al., 2011). Cajal bodies are able to accelerate this reaction and others, due to the high concentration of reactants sequestered inside the MLO. Processing bodies (P-bodies) play fundamental roles in mRNA degradation, storing, and repression, and thus contain many types of mRNAs and enzymes required for mRNA degradation (Kulkarni et al., 2010). Stress granules are MLOs which are thought to improve fitness during stressed conditions by stalling translation initiation, and by regulating signaling events (Alberti and Carra, 2018; Gomes and Shorter; Lin et al., 2015). Stress granules contain an array of translation initiation factors, RNA binding proteins (RBPs), protein quality control regulators, and many other non-RBP proteins (Protter and Parker, 2016). Thus, MLOs add an important aspect of cellular organization and function in many systems and processes.

Though common in the cellular environment, many questions remain as to how MLOs form, how they are regulated, and how their dysregulation may contribute to human disease. The formation and maintenance of membraneless organelles is thought to arise through a biological phenomenon called liquid-liquid phase separation (LLPS) (Hyman et al., 2014). LLPS is the thermodynamic process of converting a well-mixed

solution of interacting macromolecules into an energetically favored demixed state. This demixed state places liquid droplets, which contains a high concentration of macromolecules, in equilibrium with an aqueous solution, which is depleted of the macromolecules (Figure 1B) (Alberti and Carra, 2018). These droplets display liquid-like properties in that they are spherical in shape, are dynamic, have internal rearrangement, and fuse together with contact (Brangwynne et al., 2009). The field has recognized LLPS as a functional aspect of cell dynamics and molecular properties for many years. Indeed, protein crystallographers are well aware of LLPS, as the process is observed frequently at high protein concentrations required for crystallization. Nevertheless, the questions of what underpins LLPS, and how this is regulated in cells, still remain.

Multivalent interactions maintain phase-separated compartments

MLOs, with their many macromolecular components, require LLPS as the establishment of a network of interactions among macromolecules (Figure 2A) (Alberti and Carra, 2018). The network that drives the condensation of phase-separated macromolecules consists of multivalent binding domains, which transiently form intra- and intermolecular contacts. Here, multivalency refers to dynamically forming non-covalent interactions between and within phase-separated molecules. Multivalency can arise from interactions between both ordered and disordered domains of proteins. Intrinsically disordered regions (IDRs), or regions which lack three-dimensional structure, are a common attribute of proteins which phase separate at physiological

conditions (Uversky, 2017). Evidence also supports that structured domains can contribute to and modulate LLPS (Dao et al., 2018; Li et al., 2012; Wang et al., 2018).

FUS family proteins, which exhibit phase separation and have been studied extensively, are a good example of proteins with multivalent interactions between ordered and disordered regions (Wang et al., 2018). Included in this family are proteins FUS, hnRNPA1, and TDP-43, among others. These proteins are characterized together because they share similar domain structures. They have two key features: a low complexity, prion-like domain (PLD), and an RNA binding domain (RBD) which contain folded RNA recognition modules (Malinowska et al., 2013). Together, interactions among these domains are believed to work synergistically to drive LLPS. Additionally, with nuclear Overhauser effect (NOE) experiments, which are used to determine intra- and inter- molecular distances, the Fawzi group observed that all major residue types within the FUS PLD participate in interaction contacts, thus supporting the idea that FUS forms dynamic, multivalent interactions in its liquid phase (Murthy et al., 2019).

Underpinning multivalency are classical modes of molecular interactions including π — π stacking, cation— π interactions, and charge—charge interactions between the proteins' amino acid side chains (Figure 2B). π — π interactions can form between two amino acids which have aromatic side chains. Because aromatic molecules have planar geometry and contain delocalized π electrons, these molecules can form interactions in a stacked configuration. Several studies have uncovered the critical role of π — π stacking in the phase separation of proteins such as nephrin, FUS, and hnRNPA2 (Boeynaems et al., 2017; Pak et al., 2016; Xiang et al., 2015). Charge—charge interactions also contribute to phase separation through charge neutralization,

which occurs when a positively charged amino acid interacts with a negatively charged amino acid. These electrostatic interactions may arrange the proteins in a configuration that favors phase separation (Pak et al., 2016). Cation— π interactions provide points of contact between positively charged amino acids (lysine and arginine) and aromatic amino acids (tryptophan, tyrosine, and phenylalanine), which are rich in π electrons. FUS has emerged as a protein which is dependent on cation— π interactions to maintain its LLPS properties (Wang et al., 2018).

Beyond this, it is sensible that domains which contribute to oligomerization also increase the propensity for LLPS. It is thought that oligomerization nucleates a locally high concentration of a protein to promote phase separation (Shin et al., 2017). Nucleophosmin (NPM1), a protein involved in ribosome biogenesis, for example, mediates LLPS with partner proteins through its N-terminal oligomerization domain in a pentameric state (Mitrea et al., 2016). Additionally, recent studies suggest that NPM1 also can mediate LLPS itself via self-association under crowded conditions (Mitrea et al., 2018). Speckle-type POZ protein (SPOP) is a protein dependent on its ability to oligomerize in order to be recruited to MLOs (Marzahn et al., 2016). Interestingly, oligomerization has also been posed as a mechanism of solidification of liquid granules (Boke et al., 2016; Kato et al., 2012). Multivalency and oligomerization are currently suggested as main principles behind LLPS, however the exact biophysical mechanisms which drive molecules to phase separate, and what regulates this, is still under investigation.

Because of the prominent role multivalency plays in LLPS, researchers in the field have adopted the “sticker” and “spacer” framework from polymer physics to

describe these sites of dynamically forming contacts between phase-separated molecules. Stickers are the associative motifs which drive LLPS, or sequences that contribute to multivalency, and spacers connect the sticker regions (Harmon et al., 2017; Rubinstein and Dobrynin, 1997; Semenov and Rubinstein, 1998). Importantly, spacers can tune LLPS by either enabling or suppressing contact between stickers (Martin et al., 2020).

Dysfunction of LLPS leads to pathological states

Interestingly, LLPS, and the mechanism of how this transition occurs, may predispose MLOs to dysfunction. As a consequence of LLPS, and the network of interactions which it requires, MLOs tend to have very crowded and highly concentrated environments in comparison to the surrounding cytoplasm. Though these properties are necessary for proper, and beneficial, condensation, they can also increase the propensity for protein misfolding and aggregation. Additionally, IDRs and multi-domain proteins, both of which are common in key phase-separating proteins, increase the propensity for dysfunction (Alberti & Carra, 2018). As mentioned before, oligomerization may also predispose granules towards maturation to a solidified, dysregulated state (Boke et al., 2016; Kato et al., 2012).

Indeed, various pathological states have been associated with MLO dysfunction. For instance, dysregulation within phase-separated MLOs has been closely tied to neurological disorders such as amyotrophic lateral sclerosis (ALS) and frontotemporal dementia (FTD). ALS is a neurodegenerative disease which leads to muscle weakness and paralysis, where FTD leads to progressive cognitive impairment. A pathological

hallmark of ALS is the presence and formation of aggregates which resemble cytoplasmic inclusions (Lin et al., 2015). Interestingly, disease-linked mutations in proteins such as FUS, hnRNPA1/2, TIA-1, which are recruited to stress granules, facilitate a liquid-to -solid transition (Lin et al., 2015; Mackenzie et al., 2017; Patel et al., 2015). Importantly, each of these proteins undergo LLPS *in vitro* and in cells. Thus, it is suggested that disease-linked mutations alter the LLPS properties of these proteins, and may disrupt stress granule dynamics leading to ALS-associated pathological inclusions. The investigation of phase-separating proteins which harbor ALS-linked mutations has recently been prioritized, as their properties may reveal a central pathomechanism.

In vitro analysis of phase-separating protein solutions

The exact molecular mechanisms which link LLPS, MLOs, and cellular protein aggregates has yet to be discovered, and they are likely to be system- and context-specific. In order to systematically address these questions, our lab and others, have directed studies towards identifying the specific interactions underlying LLPS. Using an array of biochemical and biophysical techniques, researchers have found that regional hydrophobicity, the lack of or presence of ringed amino acids and other amino acid-based observations, and self-association have been identified as factors that may influence LLPS (Dao et al., 2018; Riback et al., 2017; Wang et al., 2018). In order to investigate how such variables may alter LLPS properties, a series of experiments can screen for, quantify, and describe phase-separating properties.

First, to screen for phase separation, many labs turn to brightfield microscopy. Phase-separated protein solutions contain micrometer sized droplets, which can be viewed under a microscope. Here, one can view liquid-like properties and characteristics of protein droplets in solution such as fusion events, sphericity, and mobility. By quantifying the size of the droplets after a specified amount of time, or the time it takes for two droplets to fuse, one can begin to describe the mobility of droplets. Fluorescent recovery after photobleaching (FRAP) is another technique often used in the field to describe the dynamic nature of phase-separated protein droplets. FRAP experiments can be performed on a microscope equipped with the necessary laser, where a region of interest is bleached with a laser, and the recovery of fluorescence is monitored. In a phase-separated system, this looks like photobleaching a small area of a fluorescently tagged protein droplet. The rate at which fluorescence recovers will be dependent on the dynamics of the protein exchange between the inside and outside of the droplet. For example, if fluorescence recovers quickly, the droplet is liquid-like, where if the fluorescence recovers slowly, the droplet is likely more gel-like, or aggregate-like.

Additionally, UV-visible (UV-Vis) spectrophotometry can be used to screen for LLPS by measurement of the absorbance of a phase-separated solution. Upon the induction of LLPS, often with the addition of salt or a change in temperature, a solution will become turbid due to the presence of liquid droplets. Therefore, as droplets appear in solution, they scatter light which causes an increase in absorbance. Previous work from our lab and others showed that high A_{600} values are associated with droplet formation, while lower absorbance values are associated with droplet clearance (Dao et

al., 2018). Typically, turbidity assays measure absorbance as a function of temperature (e.g. from 4°C to 60°C), which begins to map the conditions where the solution phase separates into a demixed state. Turbidity assays are also useful as a means to construct temperature—concentration phase diagrams.

The phase-separation field has adopted a method of quantifying LLPS at certain conditions through the construction of temperature—concentration phase diagrams (Figure 3). Temperature—concentration phase diagrams are valuable in that they map the conditions in which a protein solution is fully mixed and when a protein solution is demixed, or phase-separated. A technique commonly used to construct phase diagrams are temperature ramp turbidity assays, which are used herein and measure the absorbance of protein solutions of various concentrations across a specified temperature range (e.g. from 4°C to 60°C). At a protein concentration for which no LLPS is observed at the start of the experiment, temperature ramping turbidity assays are performed to determine T_{cp} , the temperature at the inflection point of the transition (Figure 3A). As this process is repeated over various concentrations, we are able to plot each T_{cp} as a function of protein concentration to construct the low-concentration arm of the phase diagram (Figure 3B). The low-concentration arm maps the phase boundary between the phase-separated and mixed states. For LCST (lower critical solution temperature) phase transitions, the solution changes from clear to turbid as temperature increases. Some phase-separating systems also exhibit an upper critical solution temperature (UCST), where the solution starts in a demixed state and returns to a fully mixed state as temperature increases. By constructing phase diagrams depicting the LCST and UCST arms, we can map phase transition behavior which describes the

conditions where the solution phase separates. Additionally, in these experiments we are able to test variables (such as pH, salt, protein concentration, or protein mutation) to quantify how they shift phase-separating conditions.

As self-association is a prominent mechanism underpinning LLPS, it is also important to detect oligomerization states of the protein of interest. Biophysical techniques commonly utilized to probe and describe self-association and oligomerization of phase-separating proteins are size exclusion chromatography (SEC) and small angle x-ray scattering (SAXS). SEC uses a column of tightly packed beads to separate solutions based on protein size and shape. Larger molecules, and thus larger oligomeric species in the solution will elute more quickly than smaller molecules. SAXS measures small angle scattering to determine the size and shape of nanoscale particles and macromolecules in solution. If larger oligomeric species are present in the protein solution, we would expect to see an increase in scattering intensity (cm^{-1}). Importantly, these experiments are performed with protein solutions in a non-phase-separating state.

An additional technique used to probe phase-separating proteins *in vitro* is nuclear magnetic resonance (NMR) spectroscopy, a technique which uses a magnetic field to measure the interaction of nuclear spins to identify molecular content and structure. An NMR analysis, chemical shift perturbation (CSP), has classically been used to map changes in chemical shifts of resonances in a series of protein concentration-dependent NMR spectra, and is used to identify residues that are affected by self-association and oligomerization. This technique is especially valuable as it has been used to predict “sticker” regions, a framework used to describe associative motifs which promote interchain interactions via non-covalent links and phase separation.

Conversely, “spacers” are the regions which link stickers, and can either support or suppress the formation of these interactions to modulate LLPS (Martin et al., 2020). The identification of sticker and spacer regions in a phase-separating protein is vital to understanding the molecular drivers of LLPS for that system. Ultimately, the techniques discussed above allow scientist to probe phase-separating behavior *in vitro* and analyze the contributing factors to LLPS.

Ubiquilin-2 (UBQLN2) phase separates in vitro and is recruited to stress granules

Our lab has shown that the human protein Ubiquilin-2 (UBQLN2) phase separates *in vitro* under physiological conditions, and is recruited to stress granules (Dao et al., 2018) (Figure 4 A&B). UBQLN2, a member of the ubiquilin family, is 66kDa and is composed of 624 amino acids. It is one of five known paralogs of UBQLN (-1, -2, -3, -4, and -L). UBQLN2 is a protein quality control factor found abundantly in the nervous system, and functions to transport ubiquitinated substrates to the proteasome for degradation, as well as stress response (Kleijnen, 2000; Walters, 2002; N’Diaye, 2009). UBQLN2 has an N-terminal ubiquitin-like domain (UBL) which associates with the proteasome, and a C-terminal ubiquitin-associating domain (UBA) which associates with ubiquitin (Ub) and polyubiquitin (Figure 4C). UBQLN2 also contains two heat shock chaperone-binding domains, STI1-I and STI1-II, which associate with chaperone proteins like HSP70 to further function in recycling proteins at the proteasome (Hjerpre, 2016; Kaye, 2000). Our lab recently showed that UBQLN2 features structured domains (UBL and UBA) and low-complexity intrinsically disordered regions (IDRs), both of which contribute to its phase separation (Dao et al., 2018). NMR studies confirmed that

the UBA, PXX, and STI1-II domains all contribute to multivalent interactions which drive its LLPS (Dao et al., 2018).

Importantly, UBQLN2 also is implicated in Amyotrophic Lateral Sclerosis (ALS). ALS is a proteinopathic disease where cytoplasmic inclusions, or protein aggregates, accumulate inside motor neurons. Liquid-liquid phase-separated MLOs like stress granules and P-bodies are thought to be precursors to cytoplasmic inclusions (Molliex et al., 2015). Notably, UBQLN2 is present in both stress granules and cytoplasmic inclusions (Alexander et al., 2018; Deng et al., 2011; Le et al., 2016). Additionally, mutations in UBQLN2 have recently been associated with familial ALS (Deng et al., 2011). Our lab previously characterized 11 disease-linked point mutations of UBQLN2, and found that ALS-linked mutations disrupt UBQLN2 phase-separating properties to different extents (Dao et al., 2019). Therefore, UBQLN2 is a model system of LLPS because of its phase-separating behavior, its link to stress granules, and its involvement in disease-linked proteinopathy.

Thesis overview

The studies provided here aim to further elucidate the molecular drivers of UBQLN2 LLPS. By using an array of techniques including microscopy, temperature—ramp turbidity assays, construction of temperature—concentration phase diagrams, SEC, and SAXS, I look at how mutations to UBQLN2 alter its phase separation, and how UBQLN2 domains contribute differently to its phase separation. First, I investigate how UBQLN2 stickers and spacers contribute to UBQLN2 LLPS via analysis of a library of UBQLN2 mutants. Chapter 3 focuses on domain-dependent interactions involved in

UBQLN2 LLPS via generation and analysis of six domain-deleted constructs. In Chapter 4 I provide proof of principle that UBQLN2 can be expressed and purified from Sf9 insect cells, which, importantly, yield post-translationally modified protein. Finally, I provide future directions for this work, and propose methods to further investigate UBQLN2 LLPS.

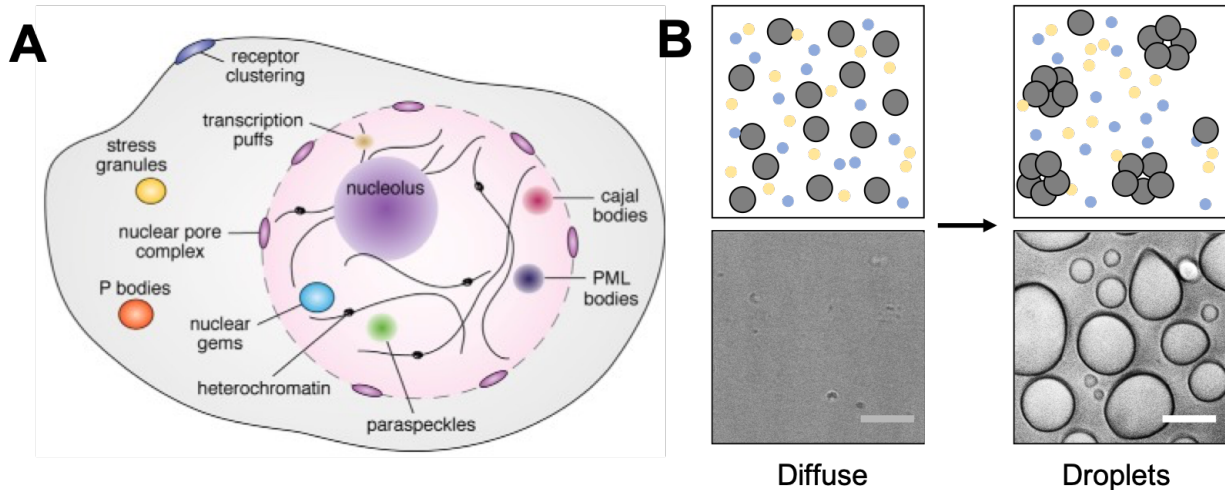


Figure 1. Membraneless organelles in cells and LLPS *in vitro*. (A) Membraneless organelles (MLOs) within the cell which arise via LLPS. Depicted here is a non-exhaustive list of organelles which arise via LLPS. Reproduced from (Gomes and Shorter, 2019). (B) A fully mixed solution of protein (grey) and buffer solution (blue and yellow) undergoes LLPS to a demixed state resulting in protein droplets. Below are brightfield microscopy images of UBQLN2 diffuse at time=0 in buffer solution and in a phase-separated state where time=30 min. Scale bar = 5 μm

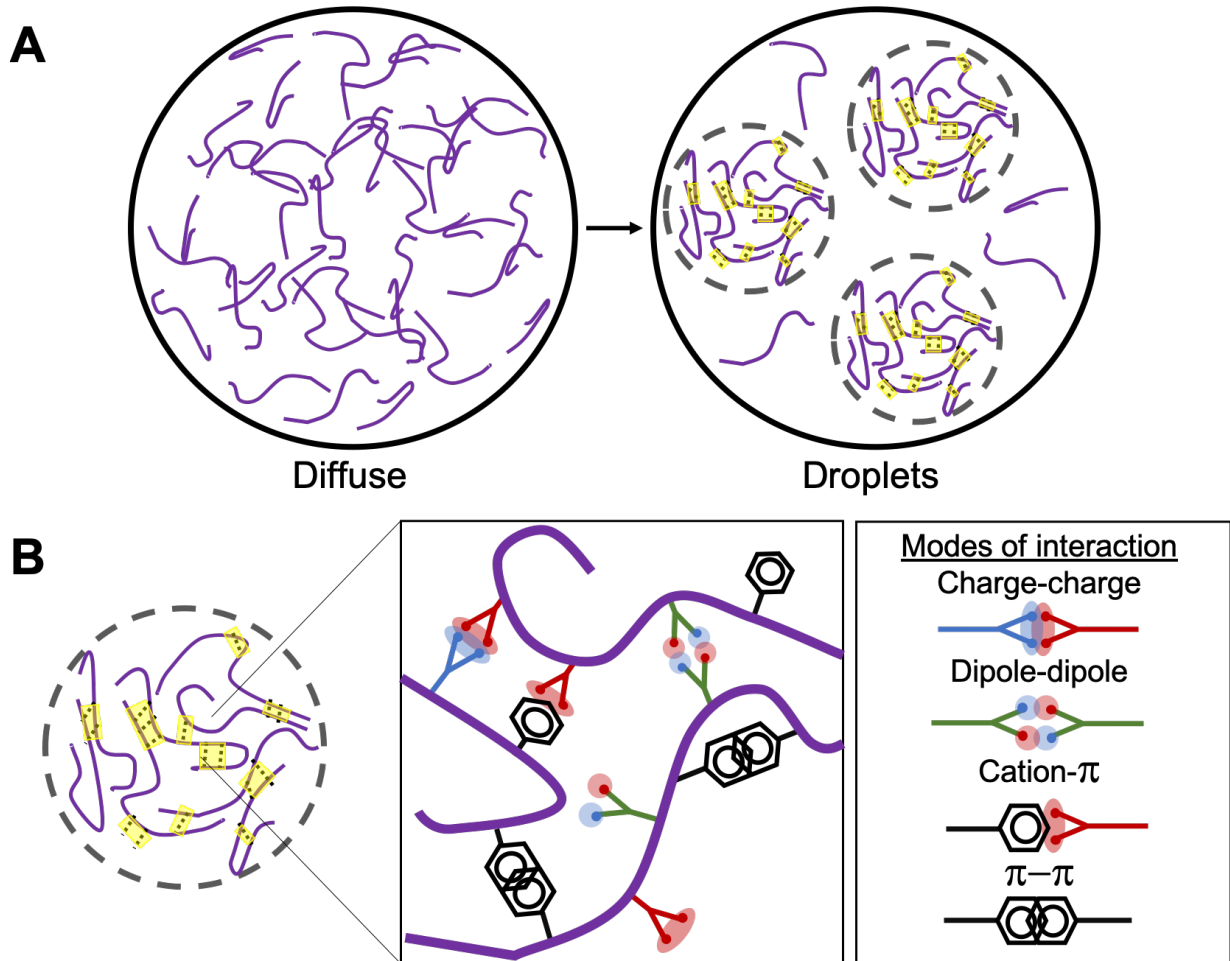


Figure 2. Determinants of LLPS. (A) Sites of multivalent intra- and intermolecular interactions (highlighted in yellow) are critical in driving and maintaining a phase-separated state between protein molecules (purple). (B) Depicted here is a protein phase-separated droplet (left) where purple represents protein molecules, and intra- and intermolecular interactions (stickers) are highlighted in yellow. View of droplet is zoomed in (right) to observe the interactions which contribute to multivalency. This non-exhaustive list of interactions important in multivalency includes charge-charge, cation- π , dipole-dipole, and π - π stacking. (adapted from *Shorter et al, 2016*).

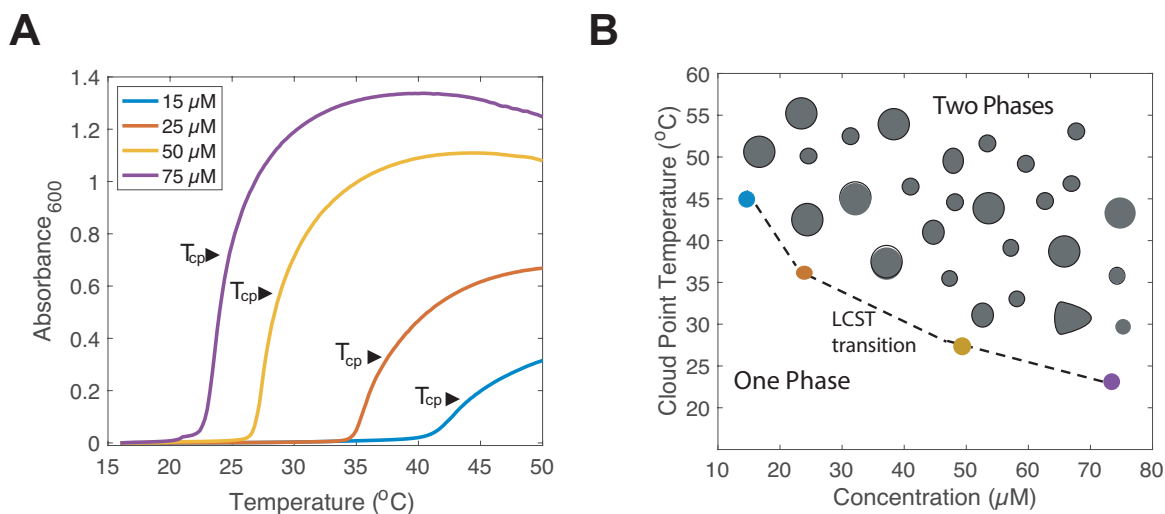


Figure 3. Temperature-concentration phase diagrams used to quantify LLPS. (A) Temperature—ramp spectroscopic data (colored lines) are fit with Four Parameter Logistic Regression analyses to determine the cloud point temperature (T_{cp}) at the inflection point of the transition at each concentration (in μM). (B) The LCST phase transition curve is mapped by plotting each T_{cp} , where the colored dots represent the experimental data points obtained.

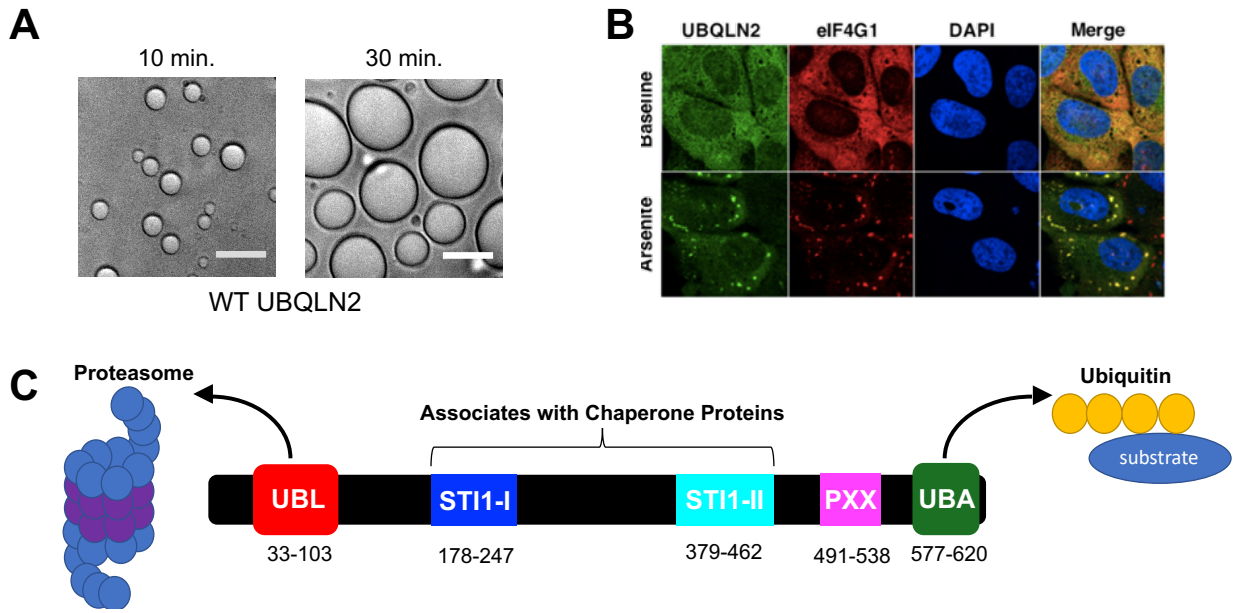


Figure 4. UBQLN2 phase separates *in vitro* and is recruited to stress granules in cells. (A) Brightfield microscopy of WT UBQLN2 in buffer containing 20 mM NaPhosphate and 200 mM NaCl (pH 6.8) at 37 C using 100 μM protein. (B) Immunostaining for endogenous UBQLN2 in U2OS cells shows that UBQLN2 is diffuse in cytoplasm, but form puncta under stress condition tested. UBQLN2 colocalizes with eIF4G1, a stress granule (SG) marker. DAPI is used to stain nuclei. (adapted from *Dao et al., 2018*) (C) Domain architecture and associations of UBQLN2.

Chapter 2

Single Amino Acid Substitutions Substantially Alter UBQLN2 Droplet Morphology and Dense Phase Material Properties

Yiran Yang,[†] Holly B. Jones,[‡] Thuy P. Dao,^{||} and Carlos A. Castañeda,^{§,||}

[†]Department of Chemistry, [‡]Department of Biology, [§]Interdisciplinary Neuroscience Program, and ^{||}Departments of Biology and Chemistry, Syracuse University, Syracuse, New York, United States

Note: This chapter was adapted from Single Amino Acid Substitutions in Stickers, but not Spacers, Substantially Alter UBQLN2 Phase Transitions and Dense Phase Material Properties published in The Journal of Physical Chemistry B and featured as an ACS Editors' Choice article. The work included in this chapter was divided between Yiran Yang and the author, Holly Jones.
<https://doi.org/10.1021/acs.jpcc.9b01024>

In this chapter, I present my contributions to the manuscript. These include all microscopy and droplet fusion experiments, size exclusion chromatography, protein purification, and writing and editing of the final manuscript. Additionally, I completed small angle x-ray scattering (SAXS) experiments, including protein sample preparation and data analysis, while experiments were collected at NIST (Gaithersburg, MD) by Dr. Alex Grishaev. SAXS data were not included in the published article, but are presented here and noted accordingly.

Abstract

UBQLN2 450–624 oligomerizes and undergoes temperature-responsive liquid–liquid phase transitions following a closed-loop temperature–concentration phase diagram. We recently showed that disease-linked mutations to UBQLN2 450–624 impart highly varying effects to its phase behavior, ranging from little change to significant decrease of saturation concentration and formation of gels and aggregates. However, how single mutations lead to these properties is unknown. Here, we use UBQLN2 450–624 as a model system to study the sequence determinants of phase separation. We hypothesized that UBQLN2 450–624 regions previously identified to promote its oligomerization are the “stickers” that drive interchain interactions and phase separation. We systematically investigated how phase behavior is affected by all 19 possible single amino acid substitutions at three sticker and two “spacer” (sequences separating stickers) positions. Overall, substitutions to stickers, but not spacers, substantially altered the shape of the phase diagram and dense phase material properties. Within the sticker regions, increasing hydrophobicity decreased saturation concentrations at low temperatures and enhanced oligomerization propensity and viscoelasticity of the dense phase. Conversely, substitutions to acidic residues at all positions greatly increased saturation concentrations. Our data demonstrate that single amino acid substitutions follow a molecular code to tune phase transition behavior of biopolymers.

Introduction

Liquid-liquid phase separation (LLPS) is a physical process whereby a fully mixed solution demixes into two different liquid states (Hyman et al., 2014). However, the exact mechanism which underpins this process is largely unknown. Emerging evidence points to a multitude of variables which work together to drive phase separation and tune its behavior. In a majority of phase-separating proteins, multivalency among intrinsically disordered regions and/or folded domains form the framework of protein phase separation (Banani et al., 2016; Li et al., 2012; Wang et al., 2018). Here, multivalency refers to multiple, non-covalent, reversible crosslinks that form among “sticker” regions in macromolecules. These multivalent interchain interactions (often present intrachain as well) are driven by properties of amino acids. For instance, amino acids possessing a positive charge can interact with aromatic amino acids to form cation- π interactions. Likewise, different types of amino acids contribute to π - π stacking interactions, hydrophobic, and electrostatic interactions. Examples of these can be found in phase-separating proteins FUS, Pab1, and TDP-43, and Ddx4. Phase-separating proteins in the FUS family, for example, are highly dependent on cation- π interactions, while proteins like Pab1 display hydrophobic interactions which drive their LLPS (Riback et al., 2017b; Wang et al., 2018b). DNA-binding protein, TDP-43, is highly dependent on aromatic residues for its ability to phase separate (Li et al., 2018). Charged residues in Ddx4 contribute to electrostatic interactions which contribute to its phase separation (Nott et al., 2015). These findings can be used to hypothesize how amino acid sequence can predict LLPS. Consequently,

it is hypothesized that phase-separating behavior is encoded in the amino acid sequence.

In this study, we created a system to which we could experimentally map the effects of single amino acid mutations in sticker and spacer regions on LLPS behavior. Using a C-terminal construct of UBQLN2 450C, we recently determined residues that were involved in self-association, or oligomerization (Dao et al., 2018). These residues were identified using concentration-dependent chemical shifts from NMR spectroscopy. The shortened C-terminal construct of UBQLN2 was chosen for analysis because its small size (~175 amino acids) enabled the use of nuclear magnetic resonance (NMR) spectroscopy to monitor backbone amide chemical shifts as a function of protein concentration on a residue-by-residue basis. Significant concentration-dependent chemical shifts were observed for residues 450-509, 555-570, 592-596, and 615-620, meaning that these sites contribute to self-association (Figure 1A) (Dao et al., 2018). With these data we hypothesized that these regions act as sites of multivalent interactions, and therefore drive UBQLN2 phase separation. Using the “sticker” and “spacer” framework we have predicted these sites to be stickers, which are the motifs that drive LLPS (Harmon et al., 2017; Rubinstein & Dobrynin, 1997). The amino acids which comprise the sticker regions are largely hydrophobic and polar (Figure 1B). The regions in between stickers are characterized as spacers. Spacers impart flexibility and can tune LLPS behavior.

We hypothesized that introducing mutations to sticker regions would significantly affect phase-separating properties, while mutations to spacers would affect phase-separating properties to a lesser extent. We expected to see significant differences in

saturation concentration (c_{sat}), and droplet morphology and droplet fusion kinetics in UBQLN2 constructs with mutated sticker positions. To test this hypothesis, we generated all 19 possible amino acid substitutions at three sticker residues and two spacer residues in the UBQLN2 450C background. We considered positions P497, P506, and V564 as “stickers”, and positions P525 and V538 as “spacers”. The resultant 95 constructs were subjected to temperature ramp turbidity assays to determine their saturation concentration, droplet morphology and kinetic studies via microscopy and droplet fusion assays, and self-association was observed via size exclusion chromatography (SEC) and small angle x-ray scattering (SAXS). Our data corroborate the hypothesis that sticker regions drive UBQLN2 phase separation given that sticker substitutions substantially altered temperature—concentration phase diagrams, droplet morphology and self-association propensity, whereas spacer substitutions altered these only marginally. Additionally, we show that individual amino acid substitutions modify phase transitions, and therefore show that phase-separating behavior is encoded in the amino acid sequence. With these data we hope to develop computational models and/or simulation to determine the molecular driving forces of phase separation.

Results

Turbidity assay analyses describe effect of amino acid substitutions

Temperature ramp turbidity assays were used to screen the experimental conditions, specifically protein concentration, for each mutant construct to undergo LLPS (Figure 2). We monitored the change of absorbance between 16 and 60°C of protein samples at different protein concentrations. Previous work from our lab showed

that high A_{600} values are associated with droplet formation, while lower absorbance values are associated with droplet clearance (Dao et al., 2018). These experiments were also used to construct temperature—concentration phase diagrams (Figure 3). WT UBQLN2 exhibited a LCST and a UCST, indicating two temperature-responsive phase transitions between 16 and 60°C (Figure 3A). As temperature increases from 16 to 45°C UBQLN2 demixes into phase-separated droplets, and as temperature further increases from 45°C to 60°C UBQLN2 returns to its fully mixed state. The first transition is a LCST transition, which means that there is a lower critical solution temperature (LCST) below which the solution is always mixed, and the second transition is a UCST transition, which means that there is an upper critical solution temperature (UCST) above which the solution is always mixed. Construction of turbidity profiles and phase diagrams allow for characterization of the conditions where phase transitions occur to compare across different protein samples.

We introduced amino acid substitutions at three sticker positions (497, 506, and 564) and two spacer positions (525 and 538) in UBQLN2 450C. First, using a fixed protein concentration of 50 μ M, we screened their phase-separating conditions using turbidity assays (Figure 2). Phase diagrams were constructed at two representative positions, a sticker (506) and a spacer (538), for each amino acid mutation. Across all positions, we initially noticed several major trends. When compared to the wild type amino acid at each position (proline at positions 497, 506, and 525, and valine at positions 525 and 538), substitutions impacted phase separation to different degrees (Figure 2, Figure 3B). In both turbidity assays and phase diagrams, substitutions to hydrophobic amino acids at sticker positions generally lowered the temperature at which

LLPS was first observed, or the LCST phase transition. As hydrophobicity increased with amino acid substitution, the protein concentration (c_{sat}) required for LLPS decreased and coexistence curves shifted to the left. Sticker position substitutions also widened the temperature range at which LLPS is observed. In contrast, spacer position substitutions generally reveal similar turbidity trends as wild type, except for some amino acid substitutions such as acidic amino acids D and E. Strikingly, temperature—concentration phase diagrams recapitulate general observations seen in our initial turbidity profiles. Here, we note that introducing mutations to UBQLN2 sticker position 506 shifted the position of the phase diagram and also changed the overall shape. In contrast, mutations at spacer position 538 generally left the phase diagram unchanged, with only mild perturbations from WT UBQLN2. These observations are consistent with our hypothesis that residues 497, 506, and 564 reside in sticker regions, where 525 and 538 are in spacer regions.

Beyond these general observations, there is considerable variation in droplet formation among the different types of amino acid substitutions. Our turbidity and phase diagram data are presented as amino acid type in decreasing hydrophobicity (Figure 2, Figure 3C). First, we have grouped amino acids by type: aromatic (F, W, Y), hydrophobic (A, G, I, L, M, P, V), polar (C, N, Q, S, T), basic (H, K, R), and acidic (D, E). We then organized these groups according to an experimentally determined hydrophobicity scale (Urry et al., 1992). We note the complication in assigning residues to these classes, particularly glycine and proline, due to their roles in modulating protein structure via flexibility and solubility (Holehouse and Pappu, 2018). Interestingly, among sticker positions increasing hydrophobicity promoted LLPS by lowering the

temperature and protein concentration needed for LLPS. This is especially seen with aromatic substitutions, where the threshold for UBQLN2 LLPS is below 16°C. Notably, slight differences between sticker positions and amino acid type were observed. For instance, UBQLN2 mutants with Ile or Phe substitutions at position 506 remained turbid for the entire temperature range (16–60°C) at 50 µM, whereas phase-separating solutions of P497F and P497I began clarifying at 40°C. These observations illustrated that Ile and Phe substitutions to both P497 and P506 impact LCST and UCST phase transitions but via different mechanisms. Spacer position mutations did affect UBQLN2 LLPS, however to a much lesser extent. Spacer mutations generally showed the same trend regarding the temperature onset of phase separation, however the absolute intensity of the absorbance signal increased after introducing a mutation, especially to aromatic and hydrophobic residues. It is possible that aromatic and hydrophobic residues increase sticker-like interactions, hence increasing the degree of phase separation of the solution. Interestingly, acidic mutations at both stickers and spacers greatly reduced the ability of UBQLN2 to phase separate. Together, these data show that LLPS properties are highly dependent on amino acid sequence, both in type of amino acid and position. Specifically, these data suggest the importance of hydrophobic amino acids in promoting UBQLN2 intermolecular interactions and driving its phase separation. Consistent with this idea, many amino acids found in sticker regions of UBQLN2 are hydrophobic.

Dense phase properties and dynamics are altered by hydrophobic sticker but not spacer substitutions

Mapping phase diagrams allowed us to elucidate the effects of the substitutions on phase transitions and determine driving forces for UBQLN2 phase separation. In order to evaluate the consequences of substitutions on the dense phase we first used brightfield microscopy to investigate the morphology of UBQLN2 droplets. To do this, we chose representative substitutions of each amino acid type including W (aromatic), G and L (hydrophobic), R (basic), Q (polar), and E (acidic) across all five positions studied (Figure 4). In general, droplet morphologies correlated well with turbidity assay results. Mutants with turbidity profiles similar to WT UBQLN2 also displayed spherical droplets of similar size as WT UBQLN2. Those mutations which resulted in significantly increased turbidity or shifted phase diagrams, such as aromatics and hydrophobics in sticker positions, also generally formed amorphous droplets. This was exhibited with mutants P497W, P497L, P506W, and P506L. Mutant P497Q, which appeared to form visible aggregates during turbidity assays, also exhibited aggregate-like morphology when viewed under the microscope. Acidic mutation E, which displayed little turbidity across all positions, formed small and dispersed aggregate-like species. Interestingly, after 30 minutes at these conditions, V538E showed the presence of spherical droplets after first appearing only as small aggregates. Consistent with our hypothesis, spacers (with the exclusion of P525R, P525E, and V538E) had minimal effects on droplet morphology, while sticker position substitutions showed a greater susceptibility to alter droplet dynamics and morphology. Future experiments will investigate the role of E and R mutations on droplet assembly kinetics and morphology.

To quantitatively describe the effects of sticker and spacer mutations on the dense phase, we analyzed droplet fusion kinetics. To determine the rate of fusion, we

measured the time it took for two fusing droplets to return to a spherical shape. We analyzed the rates of droplet fusions since the sphericity of droplets reports on surface tension and viscosity (Feric et al., 2016). For WT UBQLN2, two fusing droplets relax into one spherical droplet within seconds (Figure 4B). However, we observed that other mutations relaxed at a slower rate, while some did not achieve a spherical shape within a 3 minute experimental window (Figure 4B and 4C). Relaxation times were extracted for each amino acid type, at a representative sticker position, 506, and at a representative spacer position, 538. Consistent with our sticker-spacer hypothesis, V538 mutants all fused with similar relaxation times as WT UBQLN2, despite the type of amino acid substitution. In contrast, position 506 mutants varied in relaxation times based on the amino acid substitution. Polar and ionizable substitutions fused quickly, like WT. However aromatic and hydrophobic substitutions substantially slowed droplet relaxation. Again, these data suggest that hydrophobic and aromatic amino acids significantly impact UBQLN2 phase separation.

Effects of amino acid substitutions on LLPS properties can be explained by changes in oligomerization propensity

Previous work from our lab highlighted the importance of oligomerization in phase separation. Because of this, we probed UBQLN2 self-association via size exclusion chromatography (SEC) under non-phase-separating conditions. We previously demonstrated that UBQLN2 at low concentrations (up to ~100 μM) is monomeric, but at higher concentrations (~500 μM) UBQLN2 forms large oligomers (Dao et al., 2018). Indeed, as WT UBQLN2 concentration increased from 10 μM to 500

μM , SEC elution volumes decreased, as expected for UBQLN2 oligomerization (Figure 5). Therefore, we subjected representative mutants at each position to SEC using concentrations of 10, 100 and 500 μM (Figure 5).

All representative substitutions, across all positions, exhibited concentration-dependent oligomerization; increasing protein concentrations led to a decrease in elution volume (Figure 5). Again, consistent with our hypothesis, the SEC experiments for the spacer mutations were similar to those for WT UBQLN2. P525E was the only exception, as a small population of a large species eluted early in the SEC experiment. This is consistent with microscopy data, as P525E showed the most aggregates out of all other E mutants. At sticker positions 497 and 506 both W and L substitutions oligomerized substantially more than WT. At sticker position V564, W and L appeared to oligomerize more than WT but not as substantially as at other sticker positions. We suspect this difference is due to the fact that the WT amino acid at this position, valine, is already hydrophobic. These data further suggest that aromatic and hydrophobic residues promote UBQLN2 LLPS, as these substitutions also promote oligomerization and thus intermolecular interactions.

SAXS analysis confirms presence of large oligomers in stickers

To corroborate SEC conclusions, we also subjected representative UBQLN2 mutants to analysis via small angle x-ray scattering (SAXS). SAXS is a technique classically used to determine size and shape of nanoscale particles and macromolecules in solution through a measure of light scattering angles. Here, SAXS is used to monitor oligomeric species under non-phase-separating conditions in solution. If

larger oligomeric species are present in the protein solution, we would expect to see an increase in scattering intensity (cm^{-1}). Our studies herein pose that we will observe larger oligomeric species with increases in concentration and temperature, as well as with hydrophobic “sticker” UBQLN2 substitutions. In these experiments, we looked at WT UBQLN2 450C and mutations to sticker positions 497 and 506. We chose 497L because of its tendency to phase separate at lower temperatures and protein concentration as compared to WT, and we chose glutamic acid mutations because of their tendency to experience very little phase separation. We also did these experiments at two temperatures to show the relationship between oligomerization and temperature. Completely in line with our predictions, WT UBQLN2 had increased scattering intensity with increasing concentration (100 μM to $\sim 250\mu\text{M}$) and increasing temperature (4°C and 25°C) (Figure 6A). Additionally, leucine substitutions in sticker positions P497 and P506 drastically enhanced scattering when compared to WT at the same concentration (Figure 6B). The acidic substitution glutamic acid, at sticker positions 497 and 506, had a similar scattering profile as WT, which supports data from SEC (Figure 6C). All protein solutions displayed increased scattering with increased temperatures, consistent with previous data which describes oligomerization as a prerequisite for LLPS (Dao et al., 2019). These results together confirm the role of self-association in UBQLN2 LLPS—where we see greater oligomerization, phase separation is easier to promote at lower protein concentrations.

Discussion and Conclusions

Here, we have demonstrated that UBQLN2 phase separation can be modulated, to different extents, by single amino acid substitutions. The observations herein provide evidence that both substitution position and amino acid type are important in tuning the behavior of UBQLN2 LLPS. These data demonstrate that the sticker-spacer framework is useful in predicting the driving motifs of phase separation. Substitutions at sticker but not spacer positions elicited major changes to the overall shape and characteristics of the phase diagram, droplet morphologies and viscoelascity, and self-association. Therefore, we can conclude that stickers drive phase-separating properties, where spacers modulate LLPS to a lesser degree. Beyond this, we also confirmed trends across types of amino acids. It was observed that bulky aromatic, hydrophobic and some polar amino acids tend to alter LLPS properties more substantially than others. This was especially true from analyzing the strikingly different droplet morphologies and viscoelastic properties in the sticker position P506. Additionally, acidic mutations elicited major changes in phase separation by greatly increasing saturation concentration, which notably, occurred in both sticker and spacer substitutions. Because acidic mutations impart a negative charge similarly to a phosphate group, this specific finding highlights the potential impact of post-translational modifications such as phosphorylation on modulating phase separation behavior.

With these combined data, we have determined that UBQLN2 LLPS is driven by the hydrophobic effect and polar interactions. The interactions posed by these substitutions add to UBQLN2's overall multivalency. It is thought that the introduction of more hydrophobic residues increased the "stickiness" of both stickers and spacers. This

idea can be justified through self-association studies provided herein—those mutations which showed major deviation from WT in droplet morphology also showed the presence of higher-order oligomeric species. The particular trends witnessed in these experiments address a rich molecular code which governs UBQLN2 LLPS. Our work here provides a rich data set to be used as a benchmark for analytical and computational models of phase separation.

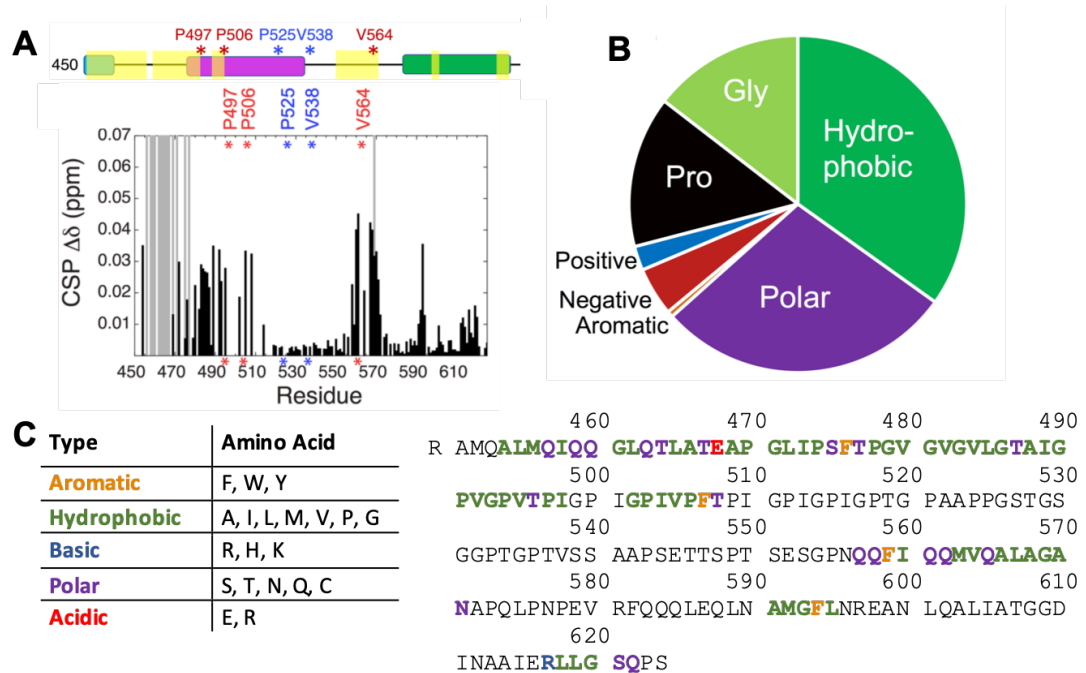


Figure 1. UBQLN2 450C experimental sticker residues and composition. (A) CSPs represent residue-specific chemical shift differences between low (45 μ M) and high (600 μ M) protein concentrations. Grey bars mark resonances only visible at 45 μ M. Domain map marks residues that exhibit concentration-dependent peak broadening or significant CSPs. All spectra were collected at 25 $^{\circ}$ C in pH 6.8 buffer under non-LLPS conditions. Experimental sticker residues are highlighted and marked with asterisks in red, and experimental spacer residues are highlighted and marked with asterisks in blue. (B) Fraction of different types of amino acids in UBQLN2 450C, which is high in polar, hydrophobic, glycine and proline residues, and depleted in charged and aromatic residues. (C) UBQLN2 450C sequence where residues highlighted in color are found in sticker regions with colors corresponding to its type of amino acid. Sticker regions are high in hydrophobic and polar residues, and low in aromatic and charged residues.

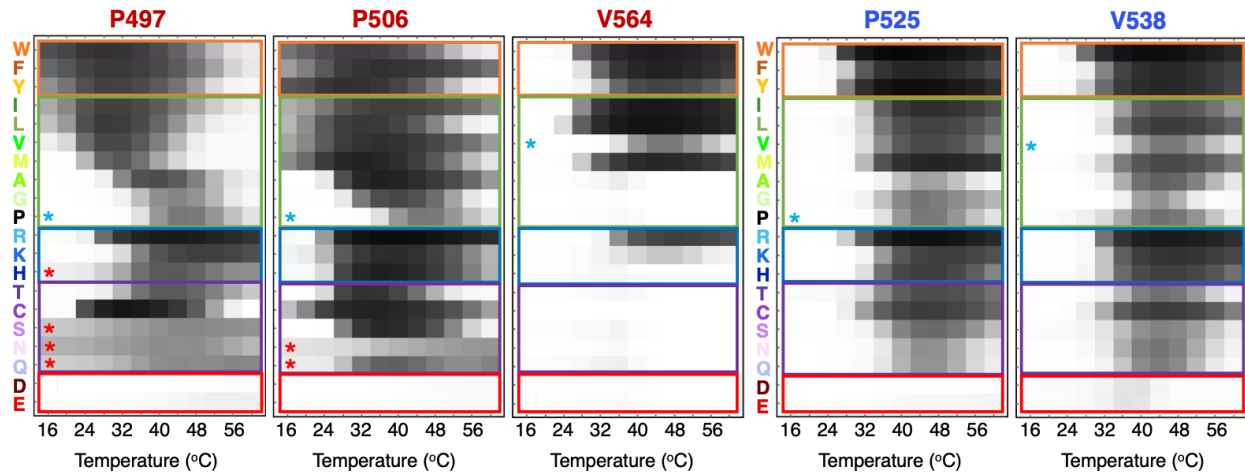


Figure 2. Turbidity profiles at sticker and spacer positions. Results from spectrophotometric turbidity assay as a function of temperature comparing LLPS of different UBQLN2 mutants using 50 μ M protein in 20 mM NaPhosphate and 200 mM NaCl (pH 6.8). The blue asterisks represent WT UBQLN2 turbidity profile for each position. The red asterisks represent mutants that form unevenly distributed aggregates at one point during the assay. P497H, S, N, and Q formed aggregates early in the experiment, whereas P506N and Q aggregated at temperatures above 44 $^{\circ}$ C. Turbidity profiles of amino acid substitutions at each position are separated by amino acid type: aromatic, hydrophobic, basic, polar, and acidic. Hypothesized stickers and spacers are color-coded red and blue, respectively, at the top.

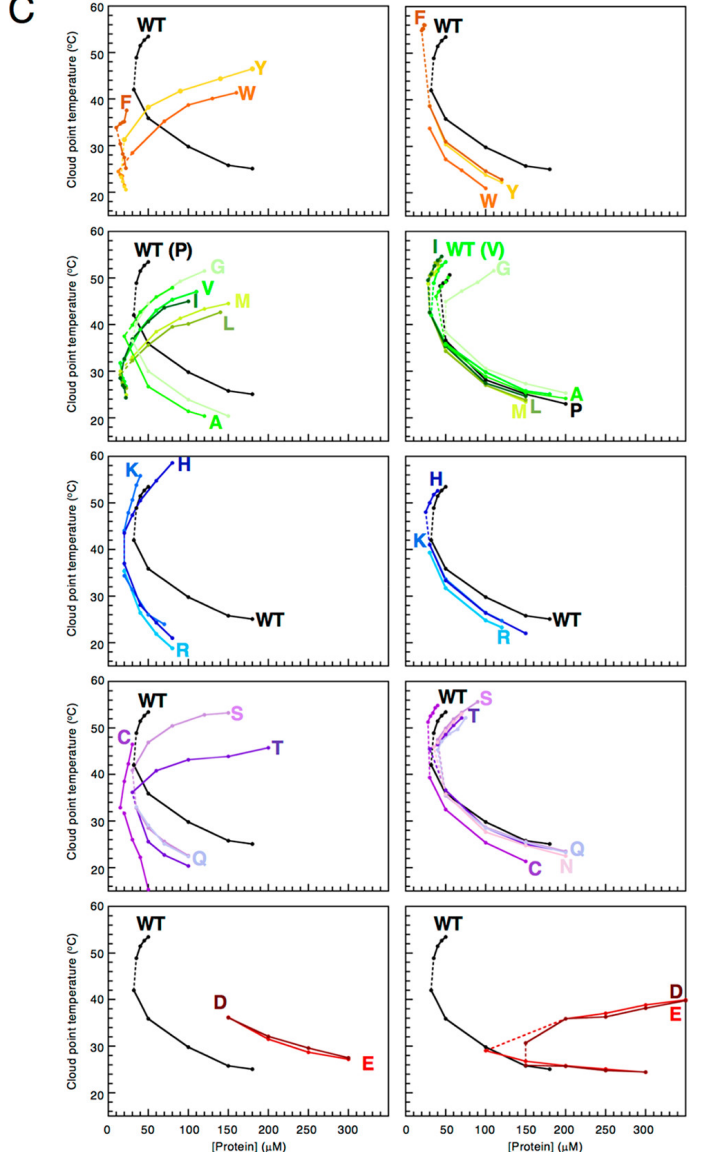
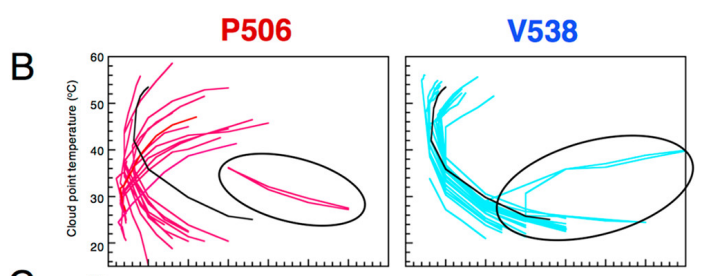
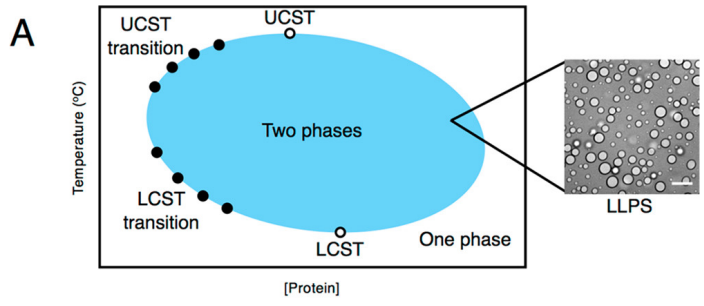


Figure 3. Temperature–Concentration phase diagrams for representative sticker and spacer residues in UBQLN2. (A) Schematic of a closed-loop phase diagram showing both UCST and LCST behaviors. The black dots represent the experimental data points for the low concentration arm obtained in this study to partially map the phase diagram. (B) Effects of amino acid substitutions in the sticker (pink, P506) region and in the spacer (cyan, V538) region compared to WT UBQLN2 (black). Circled in black are D and E mutants for each position. (C) Effects of amino acid substitutions separated by amino acid type: aromatic (F, W, Y), hydrophobic (A, G, I, L, M, P, V), basic (H, K, R), polar (C, N, Q, S, T), and acidic (D, E). The dashed lines are guides that connect the UCST phase transition cloud-point temperatures to the LCST ones. Both arms of P506N and the UCST arm of P506Q are missing due to formation of aggregates during the assays. The UCST arms for V538W, V538Y, V538R, V538K, P506D, and P506E are missing, since we observed either no turbidity or nonzero turbidity values at 60 °C at all concentrations tested.

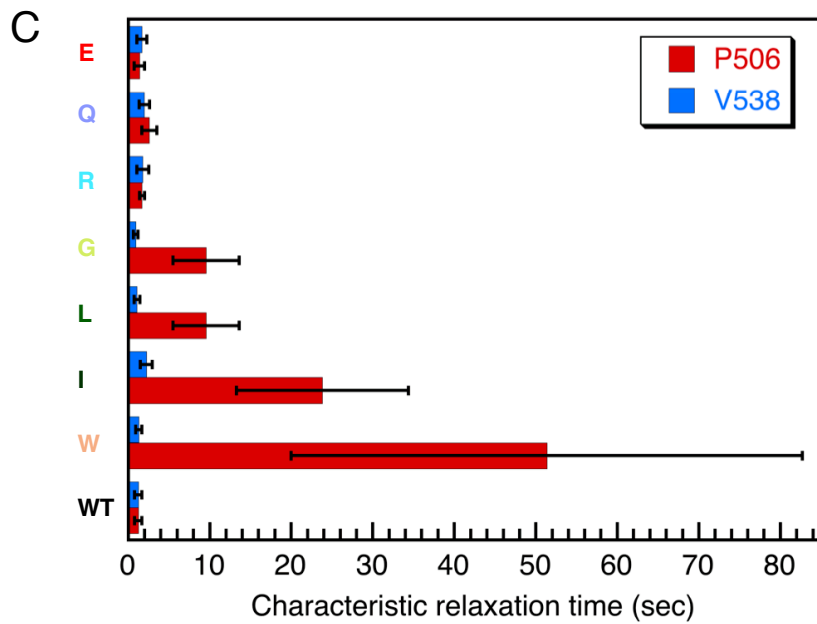
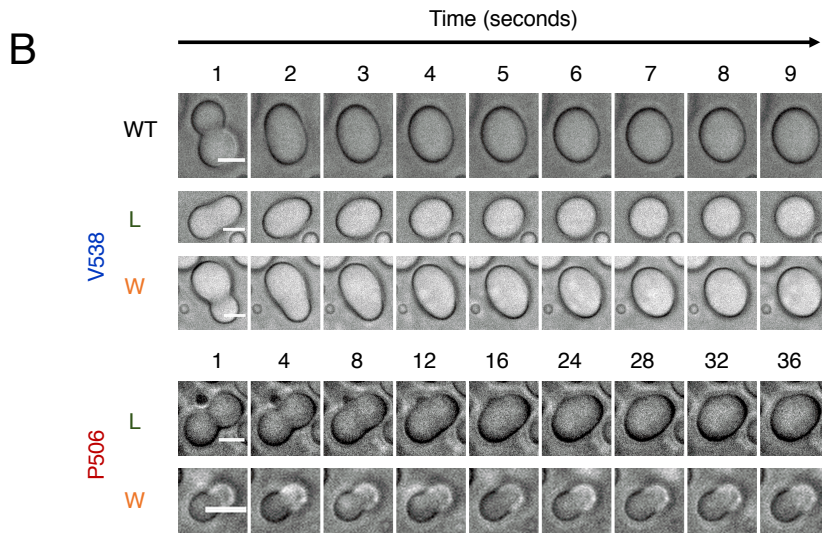
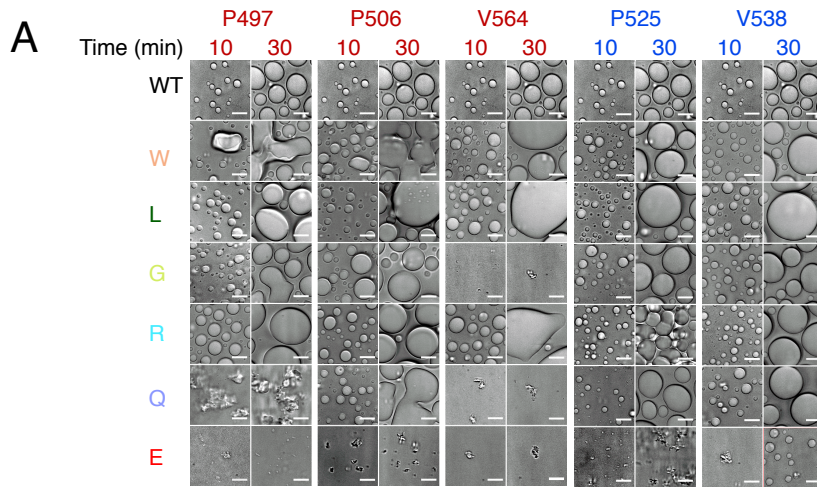


Figure 4. Amino acid substitutions in the sticker, but not spacer, regions affect droplet properties. (A) Light microscopy of different UBQLN2 mutants over 10 and 30 min at 37 °C using 100 μ M protein at sticker (P497, P506, V564) and spacer (P525, V538) positions. Scale bar = 5 μ m. (B) Snapshots of droplet fusion over a nine second window (for WT and V538L and V538W) and a 36 s window (for P506L and P506W), indicating differences in droplet fusion kinetics between substitutions at a sticker position (P506) and a spacer position (V538). Droplets were imaged 10 min after incubating 100 μ M protein (except for P506W (25 μ M), P506E and V538E (300 μ M)) at 37 °C in buffer containing 20 mM NaPhosphate and 200 mM NaCl (pH 6.8). Scale bar = 2 μ m. (C) Average characteristic relaxation times for WT and mutant droplet fusion. Error bars represent the standard deviation over eight droplets.

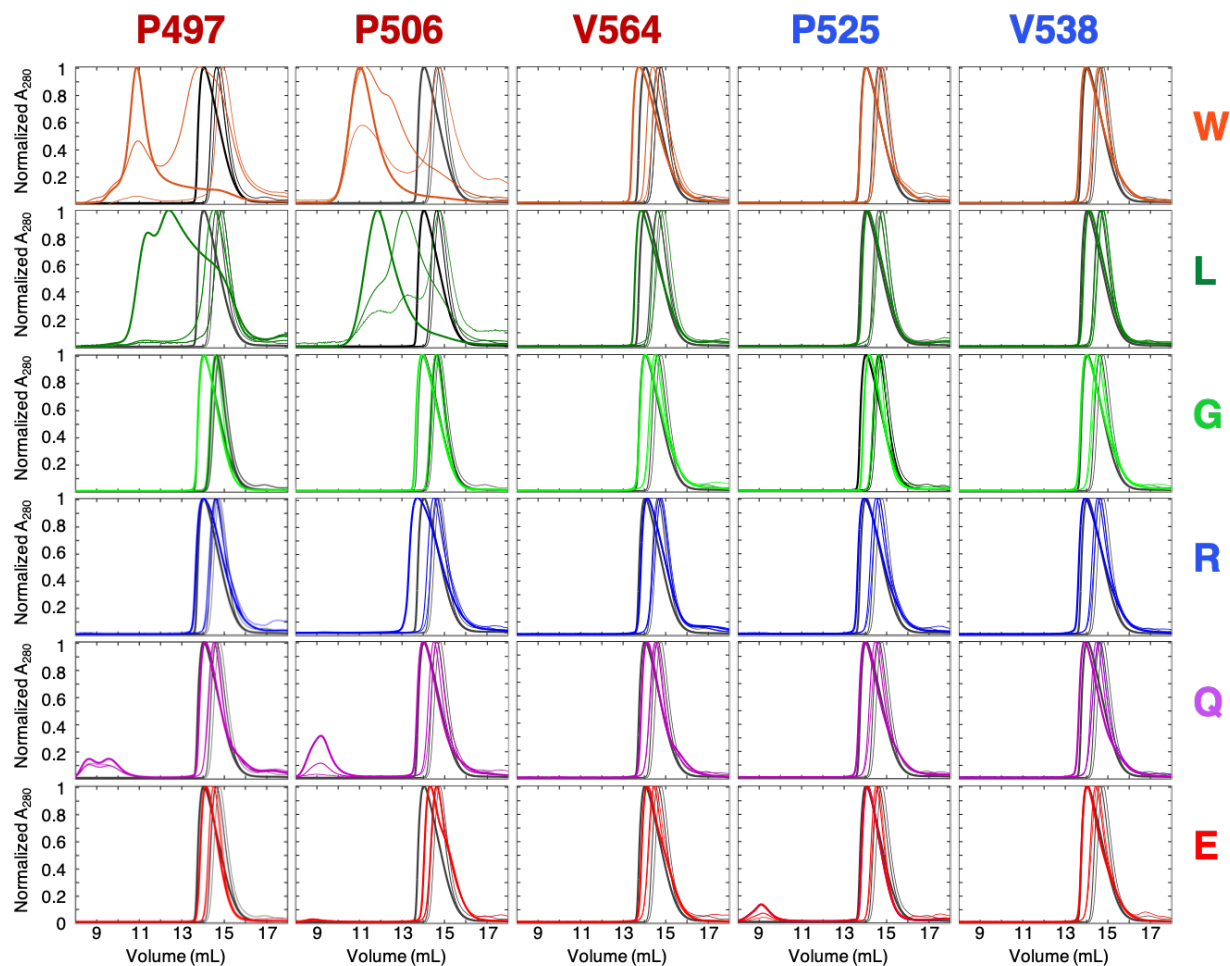


Figure 5. Oligomerization propensities of different UBQLN2 mutants.

Representative SEC profiles of UBQLN2 mutants at 10 μM (thinnest line), 100 μM (medium-thick), and 500 μM (thickest) protein concentrations. For each mutant, WT SEC curves were plotted in gray for visual comparison.

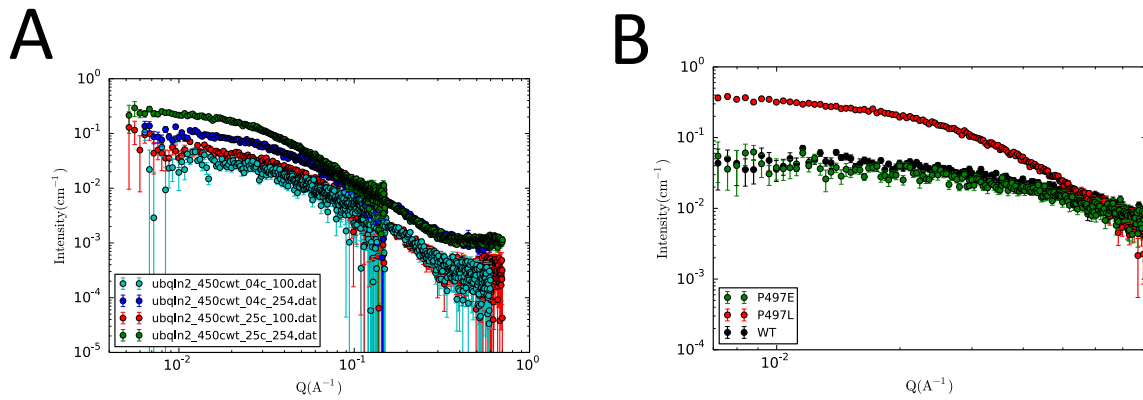


Figure 6. Small angle x-ray scattering (SAXS) experiments reveal scattering intensities of WT and mutant UBQLN2. (A) WT 4°C 100 μM (aqua), WT 25°C 100 μM (red), WT 4°C 254 μM (blue), WT 25°C 254 μM (green). (B) P497L (red), P497E (green), WT (black).

Materials and Methods

Subcloning, Protein Expression, and Purification

UBQLN2 mutants were generated from UBQLN2 450-624 using Phusion Site-Directed Mutagenesis Kit (Thermo Scientific). A tryptophan codon was added to the C-terminal end of all constructs to facilitate determination of protein concentration. UBQLN2 450-624 and all the mutants were expressed and purified as described in (Dao et al., 2018). Briefly, the constructs were expressed in *E. coli* Rosetta 2 (DE3) pLysS cells in Luria-Bertani (LB) broth at 37°C overnight. Bacteria were pelleted, frozen, lysed, then purified via a “salting out” process. NaCl was added to the cleared lysate to the final concentration of 0.5 M - 1 M. UBQLN2 droplets were pelleted and then resuspended in 6 M urea, 20 mM NaPhosphate, 0.5 mM EDTA, 0.1 mM TCEP, 0.02% NaN₃ (pH 6.8). Leftover NaCl and urea were removed through HiTrap desalting column (GE Healthcare). All the cysteine mutants were subjected to size exclusion chromatography over a Superdex 75 HiLoad 16/600 column (GE Healthcare) or an ENrich™ SEC 650 10 x 300 column (Biorad) to remove dimer contaminations. SDS-PAGE gels were performed to confirm the purity of the proteins. The identity and molecular weight of each mutant was verified using electrospray mass spectrometry in positive mode on a Shimadzu 8040 MS. Purified proteins were frozen at -80°C.

Spectrophotometric Absorbance/Turbidity Measurements

Protein samples were prepared by adding protein (from stock to a final concentration of 50 µM unless otherwise noted) to cold sodium phosphate buffer (pH 6.8, 20 mM

NaPhosphate, 0.5 mM EDTA, 0.1 mM TCEP, 0.02% NaN₃) containing 200 mM NaCl and were kept on ice for at least 5 minutes before the assay. Absorbance at 600 nm was recorded as a function of temperature by a Beckman DU-640 UV/Vis spectrophotometer using a temperature ramp rate of 2°C/min increasing from 16°C to 60°C and then ramped down to 16°C. Net absorbance values were recorded after subtracting the absorbance value of a buffer control. Results were averaged from data collected using proteins from at least two separate preps and four trials for each (total n ≥ 8). Data were plotted using Mathematica (Wolfram Research).

Phase diagram measurements

For the LCST (lower critical solution temperature) phase transition, i.e. mapping the phase boundary as temperature is increased, protein samples were prepared as described for the turbidity measurements. For the UCST (upper critical solution temperature) arm, protein samples were prepared by mixing protein and buffer/salt solutions that were incubated at 63°C for at least 10 minutes. Absorbance at 600 nm was recorded as a function of temperature by a Beckman DU-640 UV/Vis spectrophotometer using a temperature ramp rate of 2°C/min decreasing from 60°C to 16°C. Two trials (n = 2) were conducted using four to five different concentrations of wild-type and mutant UBQLN2 450-624 proteins for each arm. The protein concentrations were chosen to cover as wide a range as possible to allow observation of phase separation during the temperature ramps but not at the starting temperatures (16°C and 60°C for LCST and UCST arms, respectively). Cloud point temperatures were determined by fitting a Four Parameter Logistic Regression model to the data.

$$y = d + \frac{a-d}{1+\left(\frac{x}{c}\right)^b} \text{ (Equation 1)}$$

Cloud point temperatures used were the point of inflection (c). Cloud point temperatures were then used to define the coexistence curve as a function of protein concentration. The temperature ramp rate was either 1°C or 2°C/min, whichever yielded the most reproducible, consistent turbidity profiles and phase diagrams. Fitting and plotting of data were done with Kaleidagraph (Synergy Software).

Bright-field Imaging of Phase Separation

UBQLN2 450-624 constructs were prepared to contain 100 µM protein in 20 mM NaPhosphate, 200 mM NaCl, 0.1 mM TCEP, and 0.5 mM EDTA (pH 6.8). Samples were added to MatTek glass bottom dishes that had been coated with 5% bovine serum albumin (BSA) to minimize changes as a result of surface interactions, and incubated at 37 °C. Phase separation was imaged on an ONI Nanoimager (Oxford Nanoimaging Ltd, Oxford, UK) equipped with a Hamamatsu sCMOS ORCA flash 4.0 V3 camera using an Olympus 100×/1.4 N.A. objective. Images were prepared using Fiji (Schindelin et al., 2012) and FigureJ plugin (Mutterer and Zinck, 2013).

Droplet Fusion Assays

UBQLN2 450-624 constructs were prepared to contain 100 µM protein in 20 mM NaPhosphate, and 0.5 mM EDTA (pH 6.8), with the exception of P506W at 25 µM protein and P506E and V538E at 300 µM protein. Samples were added to MatTek glass bottom dishes that had been incubated with 5% BSA (to minimize changes as a result of surface interactions), and incubated at 37 °C. Phase separation was initiated with the

addition of NaCl to a final concentration of 200 mM. After 10 minutes of incubation, droplet formation was imaged as time-lapsed sequences for three minutes on an ONI Nanoimager (Oxford Nanoimaging Ltd, Oxford, UK) equipped with a Hamamatsu sCMOS ORCA flash 4.0 V3 camera using an Olympus 100×/1.4 N.A. objective. Five trials were performed for each mutant. Droplets chosen for analysis were of similar size and ranged between 2 and 4 microns, except for V538E (8 microns) and P506E (5 microns). For each mutant, eight fusion events were chosen for analysis and saved as separate .tif images including frames from the initial fusion event.

Relaxation times (time it takes for two fusing droplets to return to a round shape) were determined by manually measuring the major axis (a) and the minor axis (b) in pixels using Fiji software (Schindelin et al., 2012) and calculating the aspect ratio as $(\alpha)=a/b$. (Schindelin et al., 2012) We monitored the fusion events in this way until the droplets reached their most relaxed state, or until the aspect ratio was approximately equal to 1. The aspect ratio for each fusion event was fit to an exponential decay curve in Matlab (Mathworks).

$$y = (\alpha_0)^{-\tau*x} + c \quad (\text{Equation 2})$$

where α_0 is the initial aspect ratio, x is time, and $1/\tau$ gives the characteristic relaxation time.

Size Exclusion Chromatography (SEC)

Purified UBQLN2 constructs at different concentrations (10 μ M, 100 μ M, 500 μ M) were subjected to chromatography over a ENrich™ SEC 650 10 x 300 column (Biorad) on a Biorad NGC system. Experiments were conducted using 250 μ L of protein at ambient

temperature using 1 mL/min flow rate in pH 6.8 buffer containing 20 mM NaPhosphate, 0.5 mM EDTA, 0.1 mM TCEP with no added NaCl.

Small Angle X-ray Scattering (SAXS)

Purified UBQLN2 constructs were prepared in pH 6.8 buffer containing 20 mM NaPhosphate, 0.5 mM EDTA, 0.1 mM TCEP with no added NaCl. SAXS experiments were performed at NIST (Gaithersburg, MD) by Dr. Alex Grishaev. SAXS data analysis was performed on SASview.

Chapter 3

N-terminal Domain-Deleted Constructs Predict Role of Domains in UBQLN2 Phase Separation

Holly B. Jones,[‡] Thuy P. Dao,^{||} and Carlos A. Castañeda,^{§,||}

[‡]Department of Biology, [§]Interdisciplinary Neuroscience Program, and ^{||}Departments of Biology and Chemistry, Syracuse University, Syracuse, New York, United States

Abstract

The human protein UBQLN2 undergoes temperature-responsive liquid-liquid phase separation driven by sticker amino acid sequences which contribute to intra- and intermolecular multivalent interactions. Previously, hydrophobicity and enhanced oligomerization have been identified as drivers of UBQLN2 phase separation. Additionally, it was demonstrated by single amino acid substitutions, that UBQLN2 follows a molecular code to tune phase behavior. However, how UBQLN2 domains contribute to this behavior is unknown. UBQLN2 features a mix of structured, disordered low-complexity regions, and prion-like regions. All of these regions are believed to modulate phase behavior via different mechanisms. In this study, we created six N-terminally domain deleted constructs in order to investigate the role of UBQLN2 domains and linkers in its phase separation. By obtaining temperature-concentration phase diagrams, we determined that some domain deletion constructs promoted phase separation while others inhibited phase separation. Additionally, two representative disease-linked mutations were introduced to these constructs, and we found that mutations further modulate the phase boundaries for UBQLN2 phase separation. We propose that domain deletion constructs may differentially expose or conceal sticker sequences, which then modulates its phase separation behavior. The investigation of these constructs creates the opportunity to mimic various bound states of UBQLN2 in the cell. We speculate that UBQLN2 phase separation will be modulated as UBQLN2 associates with different partners at various domains.

Introduction

In the cell UBQLN2 acts as a proteasomal shuttle factor through the ubiquitin-proteasome system and autophagy (Ko et al., 2004). Misfolded proteins and/or proteins destined for degradation are covalently modified with ubiquitin (ubiquitination) and later bound to UBQLN2. UBQLN2 then shuttles these proteins to the proteasome to be recycled by the cell. This one function of UBQLN2 portrays its different “binding states” in the cell. First, unbound, full length UBQLN2 likely exists in the cytosol. Next, UBQLN2’s ubiquitin-associated (UBA) domain binds the ubiquitin tag of the protein marked for degradation (Ko et al., 2004). Then, the ubiquitin-like (UBL) domain binds the regulatory cap of the 26S proteasome (Ko et al., 2004). In this scenario, UBQLN2 is observed in three different bound states: 1) unbound 2) ubiquitin-bound and 3) ubiquitin and proteasome bound (Figure 1A). As presented in previous chapters, UBQLN2 alone phase separates under physiological conditions (Dao et al., 2018). As UBQLN2 phase-separating properties are highly dependent on multivalent interactions among amino acids in its sequence, it is expected that domain interactions with other binding partners would modulate UBQLN2 phase separation properties. Upon binding, domains of UBQLN2 are no longer available to partake in interactions driving and modulating LLPS. Therefore, it is important to identify how different domains may contribute to or modulate UBQLN2 LLPS behavior.

In addition to shuttling proteins to the proteasome for degradation, UBQLN2 functions in other protein quality control (PQC) mechanisms. Via UBQLN2’s central ST11 domains, UBQLN2 binds chaperone proteins, autophagy components, and ubiquitinated substrates (Hjerpe et al., 2016; Kaye et al., 2000; Kurlawala et al., 2017;

Yun Lee et al., 2013). Evidence suggests that UBQLN2 associates with HSP70, a stress-induced protein involved in disaggregase machinery, via the middle STI1 domains in order to chaperone misfolded proteins to the proteasome (Hjerpe et al., 2016). Corroborating this, mutations to UBQLN2 hindered association with HSP70 chaperone proteins (Hjerpe et al., 2016). Additionally, UBQLN2 is believed to bind Stch, a heat-shock protein similar in structure and sequence to HSP70 (Kaye et al., 2000). As a part of the ubiquilin family, UBQLN2 shares high sequential similarity with its homologs UBQLN1 and UBQLN4. UBQLN1 also associates with proteins BCLb and LC3, an anti-apoptotic protein and an autophagy component, respectively via UBQLN1's middle STI1 domains, therefore UBQLN2 may interact with these same proteins as well (Beverly et al., 2012; Kurlawala et al., 2017). Figure 1A highlights the domain architecture of UBQLN2, and its associations with potential binding partners.

UBQLN2 contains both structured domains and intrinsically disordered low-complexity domains (LCDs). Intrinsically disordered LCDs are domains which do not hold a fixed three-dimensional structure. Its 71-residue UBL and 44-residue UBA domains are structured and function in the ubiquitin-proteasome system, and both have been biophysically characterized (Figure 1) (Walters et al., 2004; Zhang et al., 2008). The majority of the rest of the sequence (residues 1-58, 105-267, 283-363, 373-466, and 486-586) is predicted to be disordered based on the average of three disorder prediction algorithms (Figure 1B) (Li et al., 1999; Obradovic et al., 2003; Romero et al., 1997; Xue et al., 2010). Often, disordered LCDs are important drivers for the phase separation of macromolecules, but both folded and disordered domains contribute to LLPS. However, in some systems, disease-linked mutations in LCDs promote

maturation of phase-separated droplets into pathological fibrils (Molliex et al., 2015). Depending on the phase-separating system, domains with three-dimensional structure can contribute to or drive phase separation, though their exact role is currently unclear (Milkovic et al., 2020). Interestingly, NMR studies identified structured and unstructured domains (UBA, PXX, and ST11-II) that contribute to UBQLN2 self-association, and mutational studies confirmed these as driving regions of phase separation (Dao et al., 2018; Yang et al., 2019). Beyond these C-terminal regions, UBQLN2 offers other distinct sequence regions which likely contribute to its phase-separating profile. PLAAC prion predictions suggest prion-like domains between linker residues 105-143, linker and ST11-II residues 337-461, and residues 555-574. Prion-like sequences are classically thought to be especially prone to aggregation (Figure 1B) (Lancaster et al., 2014; Sabate et al., 2015). Notably, recent findings suggest that prion-like sequences have chaperone-like functions and are a key regulator of LLPS by enhancing self-association (Franzmann and Alberti, 2019). A phase separation predictor algorithm, from the Forman-Kay group, is based on amino acid propensity for π - π contacts and predicts UBQLN2 to phase separate (Fig 1B) (Vernon et al., 2018). Here, positive P-score values represent a higher probability of phase separation. Interestingly, the higher P-score values are seen in all linker regions of UBQLN2. As we investigate UBQLN2 LLPS, it is vital to understand how such features contribute to its phase-separating ability.

Furthermore, elucidating how disease-linked mutations modulate domain-domain interactions could further inform on the mechanism of UBQLN2 LLPS and how mutations disrupt LLPS. Our lab has previously characterized effects of disease-linked

mutations at positions 487, 497, and 506 using the C-terminal construct UBQLN2 450-624 (Dao et al., 2019). These mutations altered UBQLN2 450C phase separation in that they 1) lowered phase transition temperatures and decreased saturation concentrations (c_{sat}) necessary for LLPS, 2) disrupted droplet morphology wherein some cases gel-like and amorphous aggregates were observed, and 3) increased oligomerization propensity of UBQLN2. Interestingly, in a preliminary study, we found that the same mutations in full length UBQLN2 altered LLPS to a much less severe extent (data not shown). Thus, we hypothesize that mutations modulate phase separation differently in various bound-states of UBQLN2.

For this study, we purified and expressed six N-terminal domain deletions (full-length (FL), 109C, 178C, 248C, 379C, and 450C) to identify how different domains, and domain features, may contribute to, or modulate UBQLN2 LLPS behavior (Figure 3). Additionally, we introduced two representative ALS-linked mutations, T487I and P497L, one at a time, into full-length UBQLN2 and each domain deletion construct. We hypothesize that that disease-linked mutations differentially tune LLPS across these six domain deletion constructs. By analyzing the phase-separating behavior of domain deletion constructs via temperature-ramp turbidity assays and size exclusion chromatography, we have begun to understand how each domain differentially tunes phase separation.

Results

Generation of UBQLN2 Domain Deletion Constructs and Mutants

UBQLN2 constructs were designed to successively remove each N-terminal domain and linker region (Figure 3A). First the full-length protein was expressed and purified using established protocols (Dao et al., 2018, 2019). Removal of the UBL domain generated the 109C construct. The UBL domain and the first linker region was removed with the 178C construct. Deletion of successive N-terminal domains and linker regions was continued up to the ST11-II region (constructs 248C and 379C) (Figure 3B). Construct 450C was also included in our domain-deletion library as it is the smallest construct of UBQLN2 that undergoes LLPS similarly to FL, (Dao et al., 2018). All domain deletion constructs were subjected to brightfield microscopy under phase-separating conditions to verify that all constructs do indeed phase separate (Figure 3C). All protein constructs were expressed in *E. coli*. We took advantage of the ability of each construct to phase separate with increasing salt to purify UBQLN2 from the rest of *E. coli* cell lysate (see methods) (Dao et al., 2018, 2019). No construct contains any affinity tag for purification. After generation of the domain deletion constructs for wild-type UBQLN2, we introduced ALS-linked mutations, T487I and P497L, one at a time into each domain deletion construct via site-directed mutagenesis. The resulting proteins were expressed in *E. coli* and purified via a similar salting-out method as wild-type since all mutated constructs phase-separated with increasing salt concentration.

Turbidity Assays Screened for Differential Effects on UBQLN2 LLPS

To systematically investigate the differences in phase separation properties of UBQLN2 domain deletion constructs, we subjected each protein to temperature-ramp turbidity assays at conditions which induced phase separation. We previously adopted this technique to monitor LLPS of UBQLN2 450C constructs as a function of temperature (Chapter 2) (Yang et al., 2019). We monitored the change of absorbance (A_{600}) values between 16 and 60°C of protein samples at a fixed protein concentration. These assays were repeated for a minimum of four times to ensure reproducibility. Initially, we observed two major trends—a class of constructs which significantly promoted phase separation in that they lowered the protein saturation concentration needed for LLPS, and a class of constructs which decreased phase separation in that they increased the saturation concentration. Because of this, we screened those which promoted LLPS (109C, 178C, and 379C) using a low protein concentration of 10 μ M, and we screened those with decreased LLPS (FL, 248C, and 450C) using 50 μ M protein (Figure 4A). However, 450C phase-separated much less in comparison to FL and 248C. Using 10 μ M protein, 109C, 178C, and 379C were clustered together, though with decreasing cloud point temperatures, respectively. All constructs exhibited an increase in turbidity (phase separation) as temperature was raised from 16 to 45°C. This transition is called a LCST (lower critical solution temperature) phase transition, as there is a temperature below which the solution is well mixed, and above this temperature the protein solution is demixed, or phase-separated. Consistent with previous findings, as temperature is further increased from 45 to 60°C, the 450C construct exhibits a second phase transition. This transition is called UCST (upper

critical solution temperature), as there is a critical temperature below which the solution is phase-separated and above which the solution is mixed and single-phase (Yang et al., 2019). Interestingly, 248C presents relatively diminished absorbance from 45 to 60°C, though we do not see a return to a completely mixed solution. This indicates 248C may also have a UCST phase transition, though it would be outside of these experimental conditions. This initial screen informs us that UBQLN2 domains modulate phase separation properties to different extents. Moreover, we can postulate that N-terminal domains and linkers contribute to UBQLN2 multivalency to different capacities.

Given the differences observed across N-terminal domain deletion constructs, we hypothesized that mutations to these constructs would also modulate the phase-separating properties incongruously. Disease-linked mutation P497L was introduced into each domain deletion construct, and subsequently purified and screened for LLPS in the same manner as WT constructs presented above (Figure 4B). It should be noted that turbidity assays for P497L mutant constructs were performed over a temperature range of 4-60°C since they phase-separated at lower temperatures than WT. Interestingly, the same group of constructs that exhibited phase separation at lower concentrations in WT (109C, 178C, and 379C) also exhibited phase separation at lower concentrations in the P497L mutant domain deletion constructs (Figure 4B). Likewise, the group of WT constructs that required higher concentrations for phase separation (FL, 248C, and 450C) also required higher concentrations with the introduction of the mutation. Interestingly, WT FL behaves similarly to P497L FL (Figure 4B). However, the introduction of P497L mutation to construct 450C resulted in phase separation at significantly lower temperatures. Similarly, the P497L 248C begins to phase separate at

lower temperatures than WT 248C. Interestingly, mutation P497L to constructs 109C, 178C and 379C results in a downward shift in the temperature which initiates phase separation, though the overall absorbance was diminished in each mutant construct. In general, the mutation P497L appears to shift phase separation initiation to a lower temperature in all constructs. However, this is not the case in FL. This further suggests that mutations have differential effects on UBQLN2 phase separation, dependent on which domain-deleted construct to which it is introduced.

Phase Diagrams Quantitatively Describe the Effects of Domains on LLPS

To quantitatively describe how domains and linkers alter the conditions which induce phase separation, and how mutations may also alter this, we experimentally obtained the low protein concentration arm of temperature—concentration phase diagrams. (The high protein concentration arm would reveal the protein concentration inside the protein droplets.) At a protein concentration which did not induce phase separation at the beginning of the experiment (4°C), I performed temperature-ramp turbidity assays and obtained the cloud-point temperature (T_{cp}) at the inflection point of the phase transition (Figure 5A). This was repeated using a series of four protein concentrations to map the phase boundary (Figure 5B). This process was repeated with all six WT domain deletion constructs, and was repeated a minimum of four times at each protein concentration to ensure reproducibility (Figure 6). With WT full-length UBQLN2 as a point of reference, we observed that domain deletion constructs impacted LLPS both positively and negatively, in terms of promoting (lowering saturation concentration) and inhibiting (raising saturation concentration) phase separation. The

248C and 450C constructs do not phase separate as readily as they significantly increased saturation concentration necessary for LLPS. Conversely, constructs 109C, 178C, and 379C all tend to promote UBQLN2 LLPS. From these three constructs, 109C and 178C behave strikingly similar within error. Construct 379C, though only 71 amino acids longer than 450C, shows a greatly increased propensity to phase separate, as this construct is observed to have the lowest saturation concentrations at all temperatures tested.

Overall, domain deletion constructs do not follow a specific pattern, but rather suggest distinct tendencies for each construct (Figure 6). For instance, starting with the smallest construct, 450C, we observe the least amount of phase separation. This is plausible since 450C, being the shortest, has the least amount of residues available to partake in multivalent interactions. Moving forward, 379C shows much more phase separation at the temperatures and concentrations tested. Reasonably, this makes sense given it incorporates the second prion-rich region, and has more residues potentially involved in multivalency. However, 248C has far less phase separation tendency even though it is longer than 379C. With the addition of the first ST11-I region (178C), we again observe increased phase separation. Construct 109C is longer still, and contains the first proline rich region, though no appreciable change is observed. Finally, with the incorporation of the UBL domain in the FL construct, we again observe decreased phase separation at the conditions tested. This back-and-forth nature suggest that UBQLN2 domains and linkers differentially tune LLPS in a non-straightforward manner.

Phase Diagrams Quantitatively Describe the Effects of Mutations

To investigate how mutations alter phase separation in a domain-dependent manner, ALS-linked mutations P497L and T487I were introduced to UBQLN2, and temperature—concentration phase diagrams were obtained (Figure 6). When P497L was introduced into full-length UBQLN2, there was no appreciable change to the overall phase diagram as compared to wild-type FL UBQLN2. However, this trend did not hold for any of the domain deletion constructs tested here. In general, the introduction of the P497L mutation appears to shift the phase transition to lower protein concentrations and temperatures for all domain deletion constructs (Figure 6). For P497L constructs 109C, 178C, 379C, and 450C, phase separation was drastically promoted, in that phase separation was observed at low temperatures even at a low concentration of 5 μ M. P497L 248C was particularly interesting in that the shape of the phase boundary remained generally the same between mutant and WT, but the phase transition was observed at lower temperatures for P497L, shifting its phase diagram in a downward manner.

Previous data produced by the lab indicated that disease-linked mutation T487I drastically altered phase-separating properties for the 450C domain deletion construct (Dao et al., 2019). We introduced this mutation into domain deletion constructs 109C, 178C, 248C, 379C, and 450C. In accordance with data presented above, constructs 109C, 178C, and 379C exhibited a significantly large downward shift in saturation concentrations (data not shown). Because of this, it was not experimentally feasible to acquire reproducible temperature—concentration turbidity data at such low concentrations (<5 μ M). However, in constructs 248C and 450C, this mutation lowered

saturation concentrations to different degrees (Figure 6). In 248C we observed a mild downward shift of the phase boundary. Interestingly, the phase boundaries for both the T487I and P497L mutations overlap at some protein concentrations (Figure 6). Based on these conditions, we can broadly say that mutations T487I and P497L affect 248C phase separation in a similar manner. However, mutation T487I drastically shifts 450C phase diagram when compared to both WT and P497L (Figure 6). The T487I mutation in the 450C background shifts the saturation concentrations to 5-15 μM , with cloud point temperatures between 15 and 20°C, a significant shift from WT and P497L 450C.

Size Exclusion Chromatography Describes UBQLN2 Self-Association

Under non-phase-separating conditions, we probed UBQLN2 domain deletion constructs for self-association since oligomerization is a prerequisite for UBQLN2 LLPS (Dao et al., 2018). All purified WT constructs were subjected to size exclusion chromatography (SEC) in increasing protein concentrations (10 and 100 μM) over an Enrich SEC 650 10 X 200 column (Biorad). The lab previously confirmed that WT 450C UBQLN2 is monomeric at low concentrations (10 μM and 100 μM) but forms large oligomers at higher concentrations (500 μM), consistent with concentration-dependent oligomerization. As expected, FL and all five domain deletion constructs exhibited a decrease in elution volume with increasing protein concentration from 10 to 100 μM (Figure 7). Interestingly, most constructs (109C, 379C and 450C) appear to elute in a similar trend as WT FL UBQLN2, based on their relative differences in size. However, constructs 178C and 248C have a population of large species which elutes around 9 mL. Interestingly, the 178C construct has a much larger population of this species,

whereas 248C also shows the presence of mixed oligomeric species at the 9 mL elution volume peak. Notably, the 248C construct exhibits a broad peak at 12 mL, indicative of numerous oligomeric species.

Discussion

Elucidating the role that each domain plays in UBQLN2 phase separation is critical to understanding how UBQLN2 behaves in cells and how phase separation contributes to UBQLN2 function *in vivo*. In these studies, we have demonstrated how domains contribute differently to UBQLN2 phase separation. We postulate that various domain deletion constructs mimic different bound states of UBQLN2. For instance, the 109C construct, which does not contain the UBL domain, may mimic the state which UBQLN2 is engaged with the proteasomal receptors Rpn10 or Rpn13 (Chen et al., 2016). The 248C, 379C, and 450C constructs could all possibly mimic the association of UBQLN2 with a client protein via the STI1-I or STI1-II domains. While the *in vitro* data herein cannot predict the precise behavior of UBQLN2 when introduced to the cellular milieu, we suggest that bound states of UBQLN2 may alter the available multivalent interactions for phase separation, which therefore likely tunes UBQLN2 behavior in cells.

Recent literature describes phase-separating proteins as containing stickers, regions which drive LLPS via interchain interactions, and spacers, those sequences which connect stickers and can modulate LLPS in a manner that exposes stickers, or conceals stickers (Martin et al., 2020). Similarly, the field has adopted terms like primary driving regions (PDRs) and modulating regions (MRs), which describe sequences as

those which largely contribute to LLPS, and those which modulate LLPS properties, respectively (Bratek-Skicki et al., 2020). The data herein begin to uncover which domains of UBQN2 may act more as stickers, and those which may be spacers. We have observed trends which lead us to several general conclusions.

Based on these data, we hypothesize that the structured UBL domain may modulate UBQLN2 LLPS in a way that hinders the formation of multivalent contacts. The 109C construct, which deletes only the UBL domain, exhibits enhanced phase separation in comparison to FL at the same concentration and temperature, regardless of whether the protein is WT or mutated (Figure 6). Therefore, it is sensible to suggest that the structured UBL domain may sterically hinder the formation of intra- and intermolecular contacts which drive LLPS. Supporting this, the 178C construct also presents a similar phase-separating profile as 109C, which is sensible considering 109C and 178C only differ by the linker region between the UBL and ST11-I regions (Figure 6). With this theory in mind, it is plausible that UBQLN2 has a greater phase-separating propensity as it contacts the proteasome via its UBL domain in the cell.

The 109C and 178C constructs both present increased phase separation when compared to FL UBQLN2. This informs us that the UBL domain may modulate LLPS such that it diminishes multivalent contacts resulting in a reduced propensity to phase separate. This may stem from UBL interactions with other parts of the UBQLN2 sequence. However, the linker between UBL and ST11-I domains (residues 109-177) does not significantly change LLPS behavior, indicating that this region may minimally tune phase separation. In contrast to this idea, SEC results reveal that the 178C construct has greater propensity for self-association, which would predict a greater

degree of phase separation (Yang et al., 2019). Additionally, the predicted prion-like sequence between residues 100-150 would suggest this linker as a site of self-association (Figure 1B). However, this prediction was not supported by SEC data, nor did the region appear to significantly alter phase behavior between constructs 109C and 178C (Figure 6 and 7). Alternatively, SEC data could be corroborated in that UBQLN2 oligomerization is mainly dependent upon the STI1-II region, which is present in all constructs except 450C (Dao et al., 2018; Ford and Monteiro, 2006; Kurlawala et al., 2017)

Similarly, the linker region between the two STI1 domains appears to hinder LLPS to a degree. This is shown by the vast difference in phase-separating profiles of the 248C and 379C constructs. We hypothesize that the enhanced phase-separating behavior of construct 379C could be linked to the full exposure of the predicted prion-like sequence between residues 350 and 450 in the STI1-II domain (Figure 1). Supporting this, NMR studies have previously identified the STI1-II as a domain contributing to UBQLN2 self-association (Dao et al., 2018). Thus, it is reasonable to suggest that the 248-378 linker region blocks interaction contacts at the prion-like STI1-II domain.

In these experiments, we have also introduced mutations T487I and P497L. Generally, mutation T487I induced higher phase separation tendencies to all constructs—so much so that phase diagrams could not experimentally be constructed for T487I 109C, 178C, and 379C. Interestingly, in constructs 248C and 450C, mutation T487I tuned LLPS to very different degrees. In 450C we observe an enormous increase in phase separation, indicated by decreased cloud point temperature at decreased concentrations. In 248C an increase in phase separation is observed,

however to a much lesser degree than what is observed in 450C. The difference in effect of this mutation suggests that mutations alter phase behavior via a different mechanism in different constructs. Similarly, mutation P497L also induced higher phase separation tendency, though this was also seen to different extents in different constructs. Therefore, we can insinuate that in cells, disease-linked mutations may alter phase behavior differently, dependent on the binding state of UBQLN2.

We also must consider that domain deletion constructs vary in size and shape, and consequently may not be directly comparable. By successively deleting N-terminal domains, UBQLN2 obviously becomes smaller in size, and also likely changes the three-dimensional shape for the remaining part of the construct. A conformational change of shape to UBQLN2 may expose or conceal sites of multivalent interactions, or stickers. For instance, if the UBL domain interacts with the UBA domain on the C-terminal end of UBQLN2, the protein could fold over the inner domains, sterically hindering the inner domains from making multivalent contacts. In this case, the construct deleting the UBL would expose this section, resulting in more multivalent contacts, and thus a higher propensity for phase separation. Additionally, successive deletion of domains and linkers removes residues involved in multivalency. With this rationale, longer constructs have more residues partaking in multivalent contacts, where shorter constructs have fewer residues involved in contact.

These data suggest that UBQLN2 domains modulate LLPS differentially, though additional investigation is warranted to fully elucidate how these domains, and their respective characteristics contribute to LLPS as a whole. Importantly, these data can be interpreted to suggest that the structured UBL domain and the disordered linker region

between ST11- domains may hinder UBQLN2 LLPS. Additionally, we can predict that the prion-like region in the ST11-II domain is a main site of multivalent interactions, and thus drives UBQLN2 LLPS. Importantly, these data further confirm that liquid-liquid phase separation is not straight forward, and is highly dependent on a variety of factors.

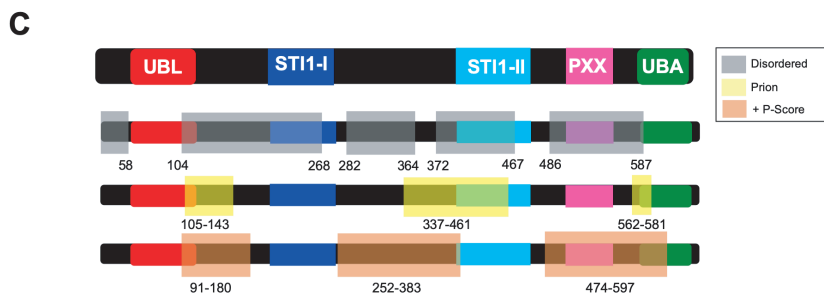
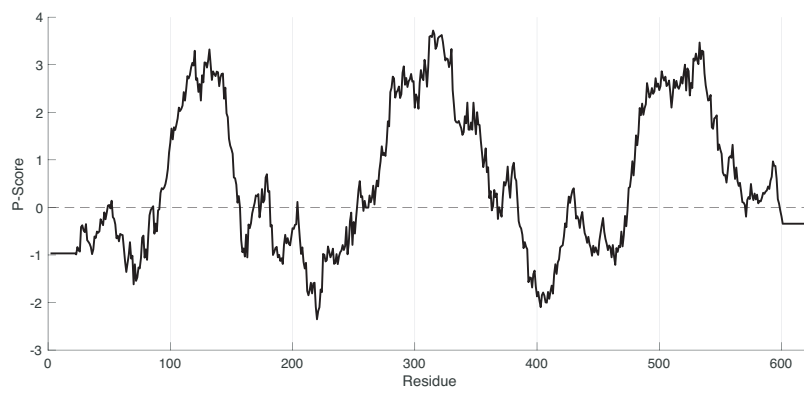
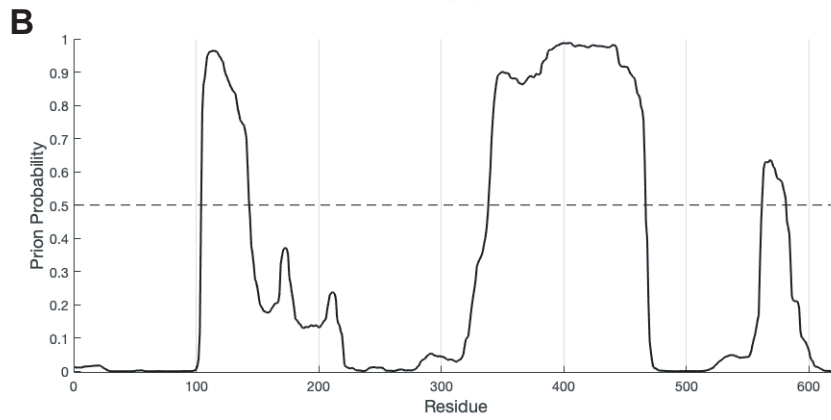
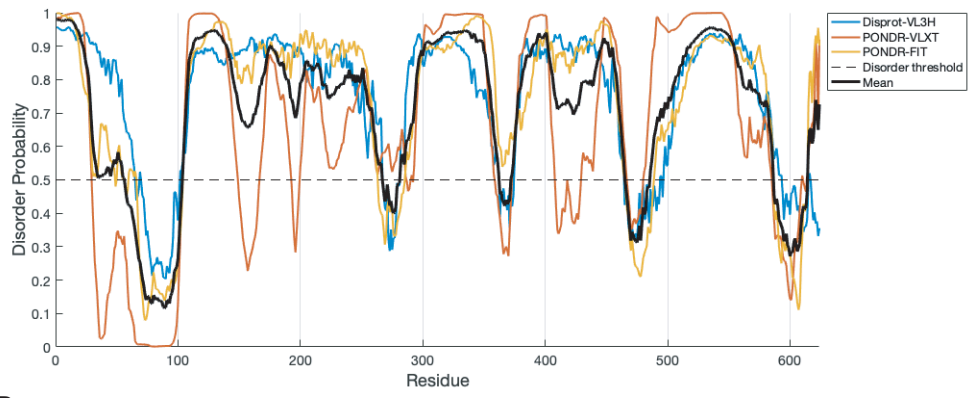
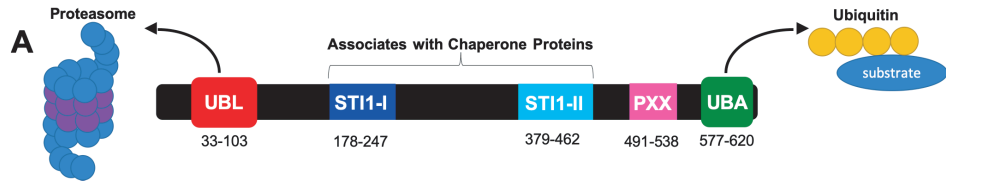


Figure 1. Structure and Function of UBQLN2. (A) Domain architecture and associations of UBQLN2. (B) Sequence-based disorder, prion-like predictions, and P-score predictions of UBQLN2. Disorder probability was calculated using PONDR-FIT, Ponder-VLXT, and Disprot-VL3H, where the average of the three is shown in black (Li et al., 1999; Obradovic et al., 2003; Romero et al., 1997; Xue et al., 2010). Prion-like probability was calculated using PLAAC, and identified prion-like regions are highlighted in yellow on the domain map (Lancaster et al., 2014). P-score values predict phase separation propensity, and were calculated using Phase Separation Predictor (Vernon et al., 2018). (C) Disordered (gray), prion (yellow), and positive P-score (orange) residues are highlighted along UBQLN2 domain map, and residues are labeled below.

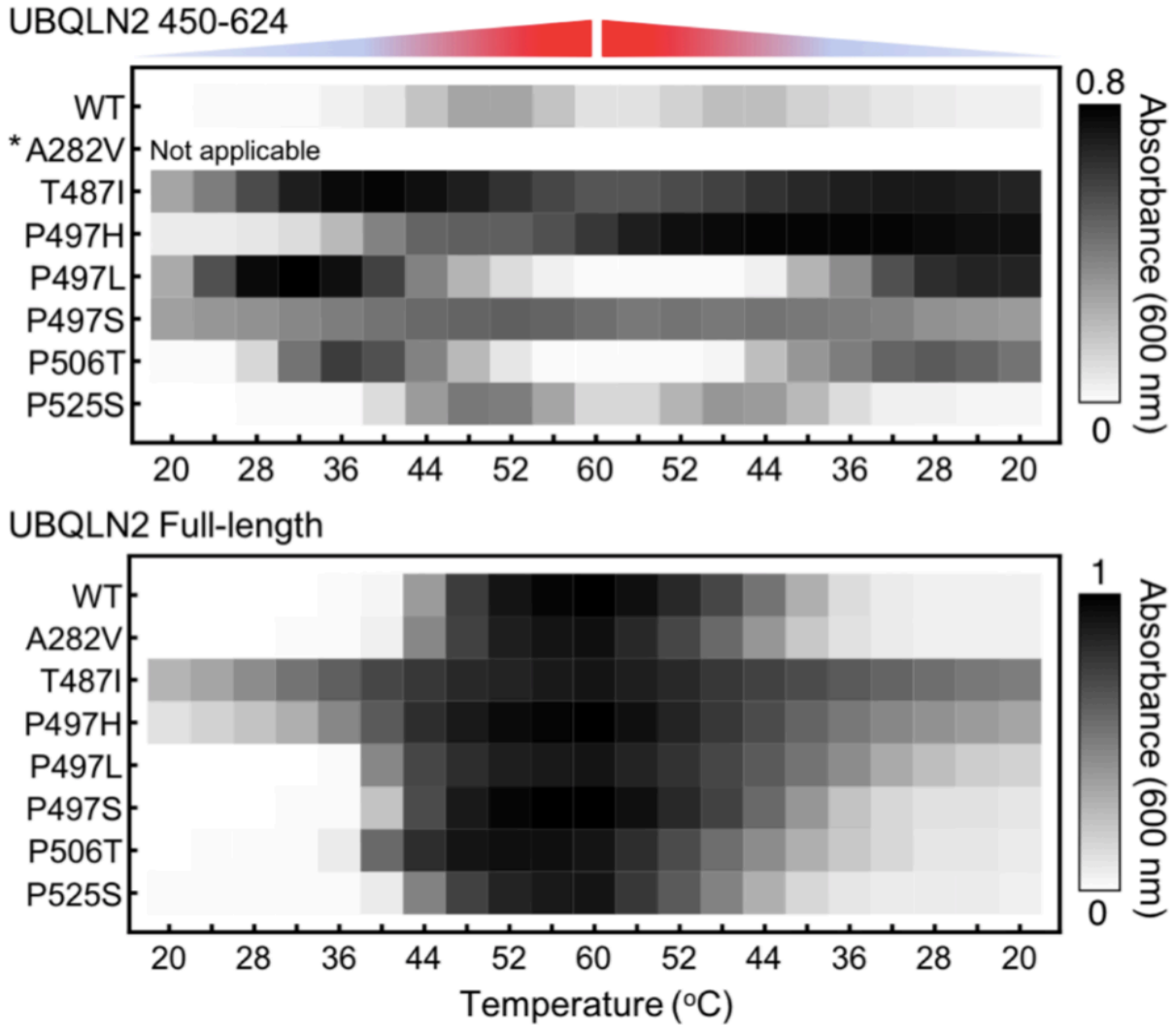


Figure 2. Disease-linked mutant phase separation properties are different in UBQLN2 450C and FL. Protein concentration for 450C is 50 μ M and FL is 20 μ M. Protein is in 200 mM NaCl, 20 mM HEPES pH7 buffer. Data collected by Thuy Dao.

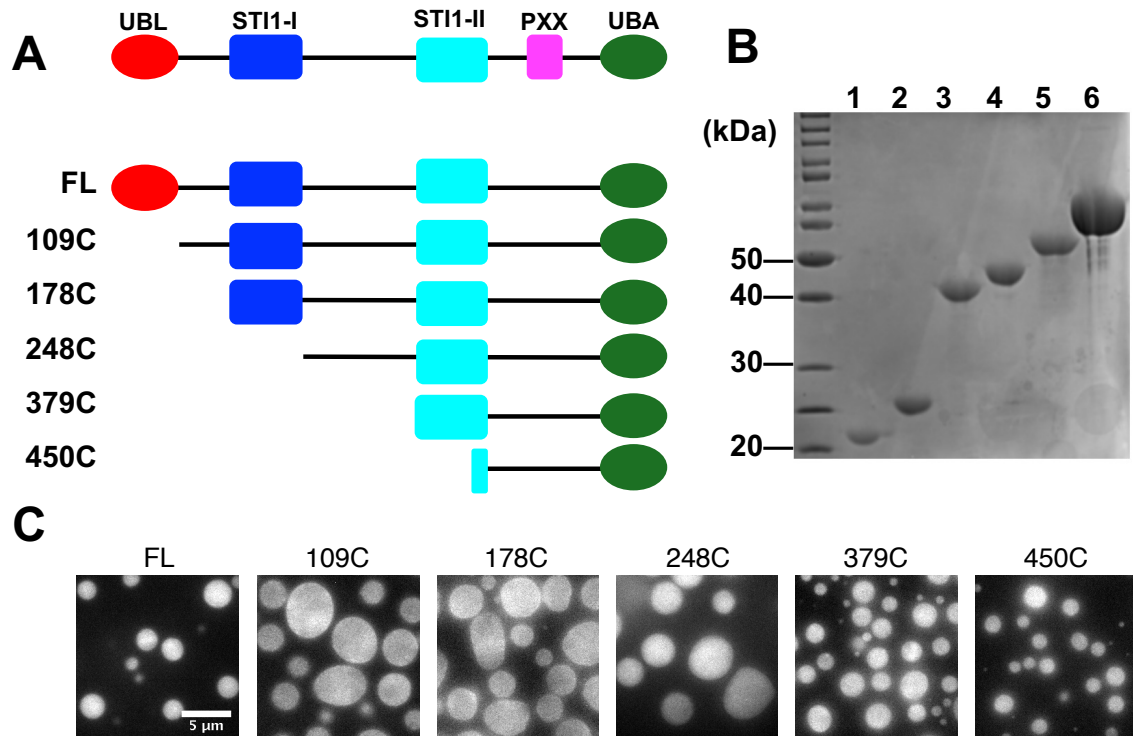


Figure 3. Domain Deletion constructs of UBQLN2. (A) N-terminally domain deleted constructs. (B) Purified UBQLN2 protein samples on SDS-PAGE gel are loaded as: 1: 450C, 2: 379C, 3: 248C, 4: 178C, 5: 109C, 6: FL. Molecular weight markers are labeled on the left side in kDa. (C) Brightfield microscopy imaging of UBQLN2 domain deletion constructs. Protein concentration is 50 μ M for FL, 109C, 178C, and 379C, and 200 μ M for 248C and 175 μ M for 450C. Protein is in 200 mM NaCl, 20 mM Hepes pH7 buffer, at 30°C after 10 minutes. Microscopy images are from Thuy Dao.

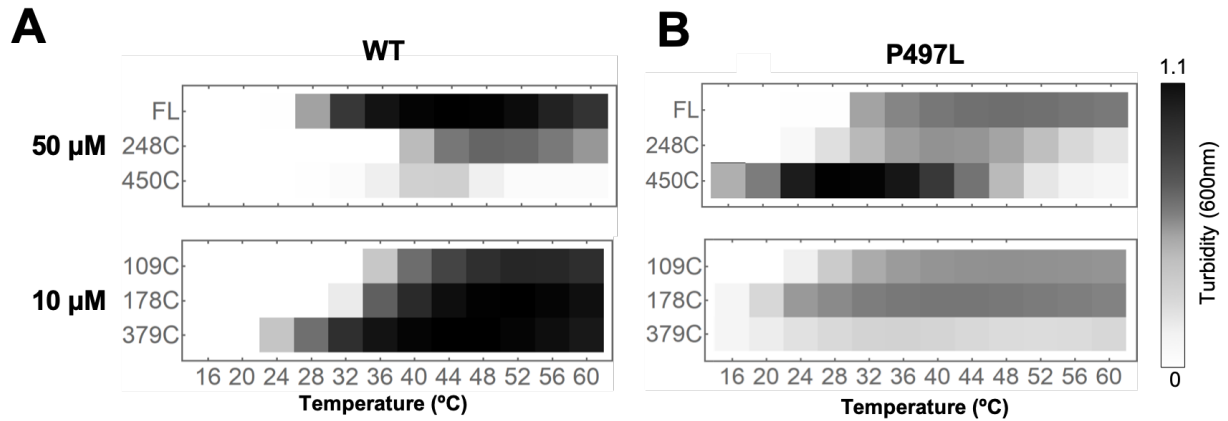


Figure 4. Turbidity assays screen for LLPS in WT and P497L domain deletion

constructs. (A) Spectrophotometric turbidity assay results for WT UBQLN2 domain deletion constructs at 50 μM (FL, 248C, 450C) and 10 μM (109C, 178C, 379C) in 20 mM NaPhosphate and 200 mM NaCl (pH 6.8). (B) Spectrophotometric turbidity assay results from mutant P497L UBQLN2 domain deletion constructs at 50 μM (FL, 248C, and 450C) and 10 μM (109C, 178C, 379C) in 20 mM NaPhosphate and 200 mM NaCl (pH 6.8). Darkness of the square correlates with cloudiness of the solution, such that black squares are phase-separated samples.

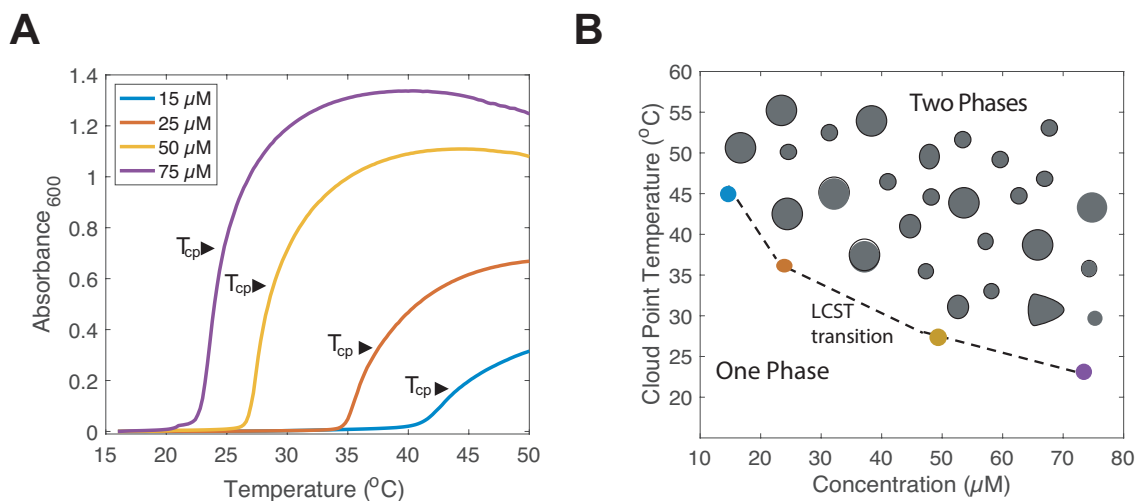


Figure 5. Phase diagrams map conditions of phase separation. (A) Temperature—ramp spectroscopic data is fit to a Four Parameter Logistic Regression model to determine the cloud point temperature (T_{cp}) at the inflection point of the transition at each concentration (in μM). (B) The phase boundary (dotted) is mapped, where the colored dots represent the experimental cloud point temperatures obtained. UBQLN2 samples above the phase boundary are in the phase-separated state, whereas samples below the phase boundary are completely miscible and clear (one phase).

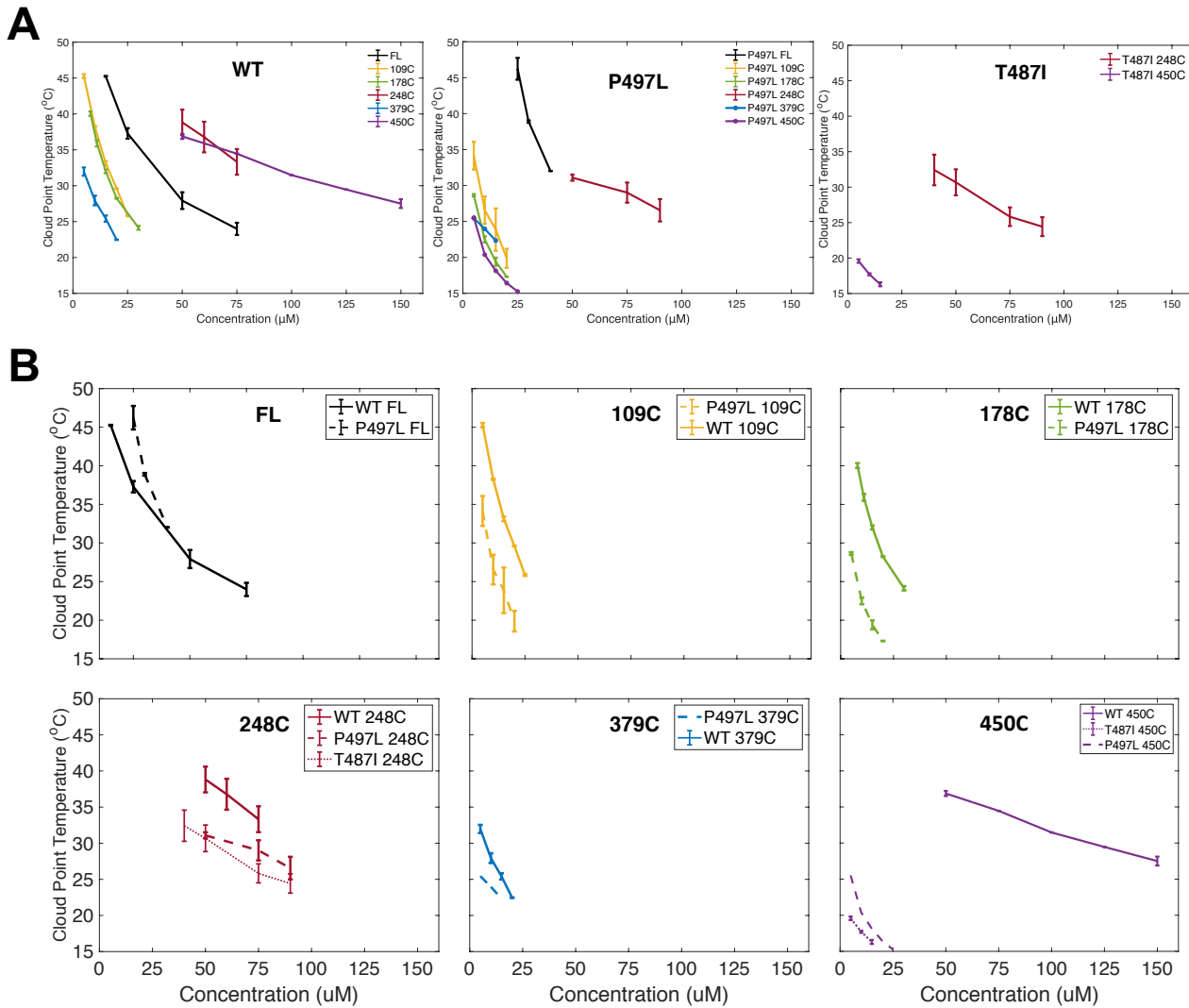


Figure 6. Temperature-concentration phase diagrams for domain deletion

constructs of wild-type and mutant UBQLN2. (A) Phase diagrams for full-length and domain deletion constructs of wild-type UBQLN2 and disease-linked P497L and T487I mutants. (B) Phase diagrams as in panel A, except they are organized according to domain deletion construct. Experimental cloud point temperatures are plotted which map the LLPS phase boundary, and the lines connecting points are guides to visualize the low-concentration arm of the phase boundary. Domain deletion constructs are color-coded (black: full-length (FL), etc.) Error bars represent standard deviation of cloud point temperatures using $n=4$ trials from two separate protein purifications, with the

exception of P497L 379C and P497L 450C, which both had n=2 trials from one protein purification. All protein was in buffer containing 20 mM NaPhosphate and 200 mM NaCl (pH 6.8).

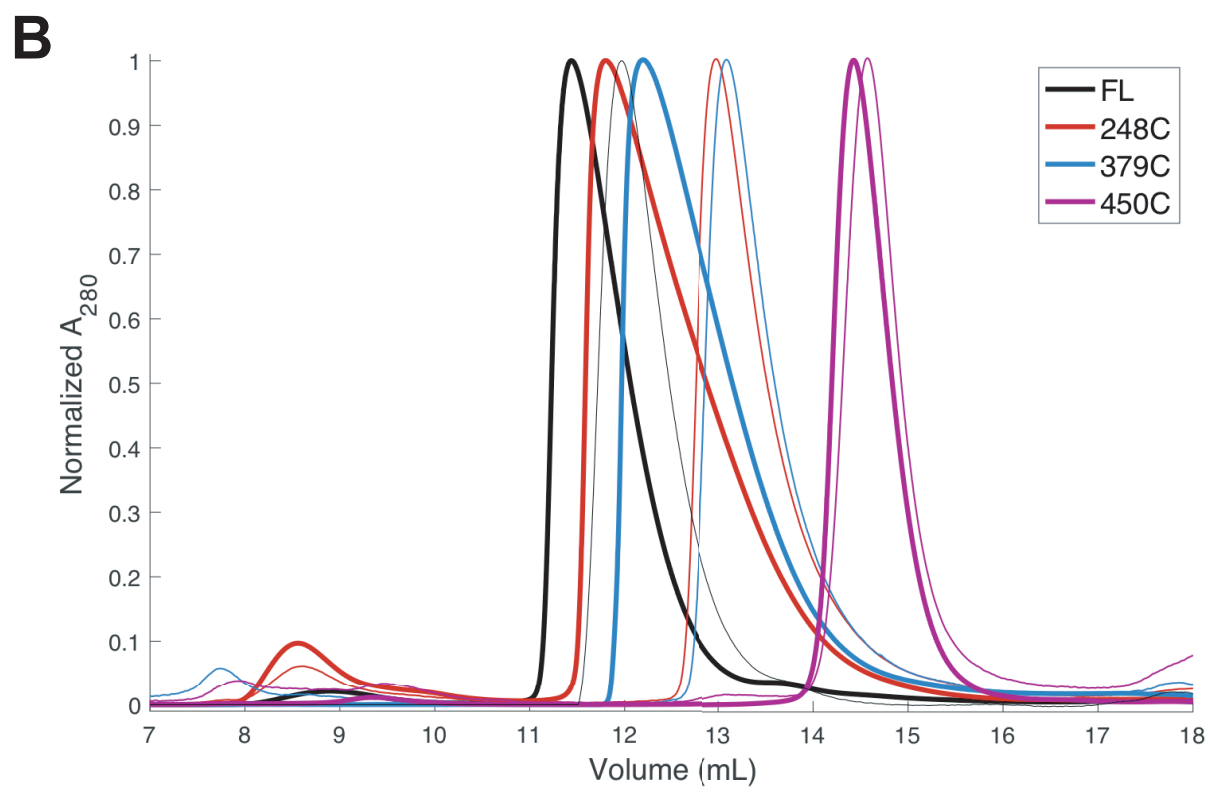
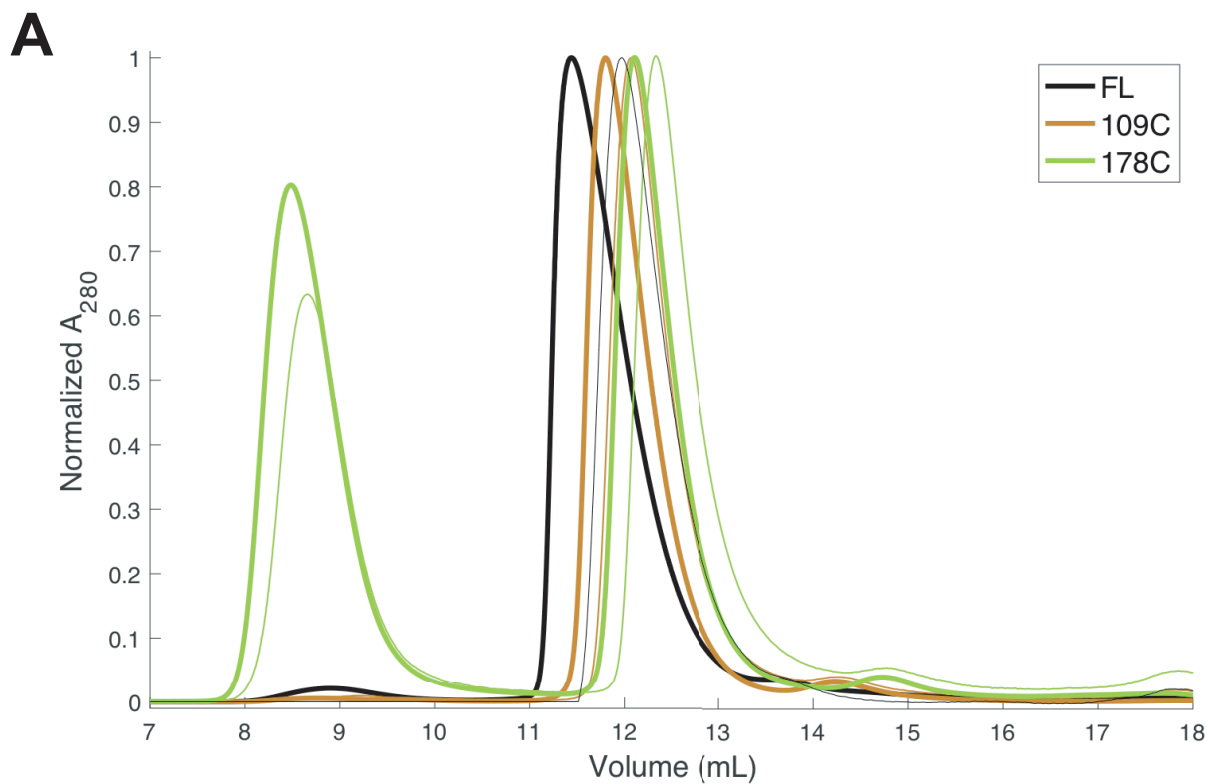


Figure 7. Oligomerization propensity of UBQLN2 domain deletion constructs. Size exclusion chromatography (SEC) profiles of (A) FL, 109C, and 178C and (B) FL, 248C, 379C, and 450C domain deletion constructs. The thinnest lines represent protein concentration of 10 μ M, and the thickest lines represents 100 μ M. Plots were divided by those constructs with higher molecular weights and lower molecular weights, where FL was plotted in black on both plots for visual comparison. Proteins were in pH 6.8 buffer containing 20 mM NaPhosphate.

Methods

Subcloning, Protein Expression, and Purification

UBQLN2 mutants were generated from UBQLN2 using Phusion Site-Directed Mutagenesis Kit (Thermo Scientific). A tryptophan codon was added to the C-terminal end of all constructs to facilitate determination of protein concentration. UBQLN2 constructs and all mutants were expressed and purified as described in (Dao et al., 2018). Briefly, the constructs were expressed in *E. coli* Rosetta 2 (DE3) pLysS cells in Luria-Bertani (LB) broth at 37°C overnight. Bacteria were pelleted, frozen, lysed, then purified via a “salting out” process. NaCl was added to the cleared lysate to the final concentration of 0.1 M - 1 M. UBQLN2 droplets were pelleted and then resuspended in 20 mM NaPhosphate, 0.5 mM EDTA, 0.1 mM TCEP, 0.02% NaN₃ (pH 6.8). Leftover NaCl was removed through HiTrap desalting column (GE Healthcare). SDS-PAGE gels were performed to confirm the purity of the proteins. Purified proteins were frozen at -80°C.

Spectrophotometric Absorbance/Turbidity Measurements

Protein samples were prepared by adding protein (from stock to a final concentration noted for each experiment) to cold sodium phosphate buffer (pH 6.8, 20 mM NaPhosphate, 0.5 mM EDTA, 0.1 mM TCEP, 0.02% NaN₃) containing 200 mM NaCl and were kept on ice before the assay. Absorbance at 600 nm was recorded as a function of temperature by an Agilent Cary 3500 UV-visible (UV-Vis) spectrophotometer using a temperature ramp rate of 1°C/min increasing from 16°C or 4°C to 60°C. Net absorbance values were recorded after subtracting the absorbance value of a buffer

control. Results were averaged from data collected using proteins from at least two separate preps and two trials for each (total $n \geq 4$) for most constructs. Data were plotted using Mathematica (Wolfram Research).

Phase diagram measurements

For the LCST (lower critical solution temperature) phase transition, i.e. mapping the phase boundary as temperature is increased, protein samples were prepared as described for the turbidity measurements. Absorbance at 600 nm was recorded as a function of temperature by a Beckman DU-640 UV/Vis spectrophotometer using a temperature ramp rate of 1°C/min increasing from 4°C to 60°C. Four trials ($n = 4$) were conducted using three to five different concentrations of wild-type and mutant UBQLN2 protein constructs for each arm. The protein concentrations were chosen to cover as wide a range as possible to allow observation of phase separation during the temperature ramps but not at the starting temperature of 4°C. Cloud point temperatures were determined by fitting a Four Parameter Logistic Regression model to the data.

$$y = d + \frac{a-d}{1+\left(\frac{x}{c}\right)^b} \text{ (Equation 1)}$$

Cloud point temperatures used were the point of inflection (c). Cloud point temperatures were then used to define the coexistence curve as a function of protein concentration. Fitting and plotting of data were done in Matlab.

Size Exclusion Chromatography

Purified UBQLN2 constructs at different concentrations (10 μ M and 100 μ M) were subjected to chromatography over a ENrich™ SEC 650 10 x 300 column (Biorad) on a Biorad NGC system. Experiments were conducted using 300 μ L of protein at ambient temperature using 1 mL/min flow rate in pH 6.8 buffer containing 20 mM NaPhosphate, 0.5 mM EDTA, 0.1 mM TCEP with no added NaCl.

Chapter 4

Eukaryotic Expression of UBQLN2 in Sf9 Insect Cells to examine post-translational modifications

Holly B. Jones,[‡] Michelle Sieburg,^{||} and Carlos A. Castañeda,^{§,||}

[‡]Department of Biology, [§]Interdisciplinary Neuroscience Program, and ^{||}Departments of Biology and Chemistry, Syracuse University, Syracuse, New York, United States

Abstract

A principle advantage of membraneless organelles (MLOs), which form via liquid-liquid phase separation (LLPS), is that they rapidly and dynamically respond to cellular and environmental cues. In response to biological signals, MLOs can assemble, disassemble, and change their own material properties, for example. The dynamic nature of MLOs requires that they have regulatory mechanisms to condense and dissipate upon response. Post-translational modifications (PTMs) have emerged as one of these regulators. PTMs are common in physiological environments, and previous work has shown that PTMs play a large role in LLPS regulation *in vivo*. Recent studies using glutamic acid mutations to UBQLN2 as a phosphomimetic illustrate that PTMs have the ability to alter UBQLN2 LLPS properties. A disadvantage of bacterial expression of UBQLN2 is that bacteria do not possess machinery to install PTMs. Here, I propose experimental methods to examine PTMs in UBQLN2 by recombinantly expressing and purifying UBQLN2 from eukaryotic Sf9 insect cells. Insect cells contain machinery to add 'mammalian-like' PTMs. Through *in vitro* studies of post-translationally modified UBQLN2, we can determine if UBQLN2 is modified by PTMs, how PTMs may alter its LLPS properties, and begin to understand how PTMs regulate UBQLN2 phase separation.

Introduction

Membraneless organelles are distinct from their membrane-bound counterparts in that they can readily form and dissolve within the cytoplasm in response to environmental signals (Bah and Forman-Kay, 2016). MLO components regulate their inter- and intramolecular contacts such that these recruited molecules either condense, or dissipate into the cytoplasm. Certain physiological mechanisms must be responsible for varying the concentration at which the proteins or other macromolecules phase separate in order to regulate controlled dissolution and condensation of MLO components. Though the regulation of MLO formation and dissolution is widely unknown, groups have begun to discover what types of cellular mechanisms may be responsible for the reversible nature of MLOs.

Early on, Brangwynne and colleagues described P granules in germline cells of *Caenorhabditis elegans* as controlled liquid droplets. They found that these P granules localize via a physicochemical mechanism controlled by the dispersion of polarity proteins (Brangwynne et al., 2009). Another MLO commonly studied, the stress granule, rapidly assembles upon the presentation of cellular stress (Dao et al., 2018). Many of the proteins found inside stress granules also undergo LLPS. Significant knowledge of ribonucleoprotein granule regulation has been discovered through the study of the protein FUS, a phase-separating protein driven by its intrinsically disordered low-complexity (LC) domain. Cell studies have shown that FUS granule condensation can be regulated by manipulating the number of arginine and tyrosine residues within the protein (Wang et al., 2018). Furthermore, post-translational arginine methylation modulates these interactions, and thus its phase separation, wherein removal of methyl

groups on arginine promotes condensation (Qamar et al., 2018). Dissolution of FUS granules was found to be modulated by transportin, a molecular chaperone (Qamar et al., 2018).

As mentioned above with arginine methylation, PTMs have emerged as a major regulator of condensates. Since PTMs of specific amino acids modify physicochemical properties of proteins by altering charge, bulkiness, and sterics, it is not surprising that they are an important regulator of LLPS (Bah and Forman-Kay, 2016). Therefore, modifications to key phase-separating proteins have the ability to modulate the condensation and dissolution of cellular MLOs. Several groups have studied how phase-separating proteins are modified, and have analyzed how these modifications alter their phase-separating properties and their recruitment into MLOs. Phosphorylation of serine-rich IDPs has been shown to regulate RNA granules (Wang et al., 2014). Additionally, the Bonini lab has shown that the addition of ADP-ribose to the protein TDP-43 instigates recruitment of the protein into stress granules, while phosphorylation of TDP-43 is required for TDP-43 recruitment into cytoplasmic inclusions and leads to neurodegeneration (McGurk et al., 2018). Even studies which investigate phase separation *in vitro* have exposed PTMs as modulators of LLPS properties (Ferreon et al., 2018; Li et al., 2012).

Interestingly, UBQLN2 possesses nine disease-linked mutations which reside within its unique proline-rich (PXX) region (Dao et al., 2019; Deng et al., 2011). These mutations have been shown to cause dominant X-linked inheritance of amyotrophic lateral sclerosis (ALS) and ALS/dementia, and facilitate the formation of cytoplasmic inclusions (Deng et al., 2011; Lin et al., 2015; Mackenzie et al., 2017; Molliex et al.,

2015). Of these nine PXX mutations, six are mutated to either a serine, or threonine, both of which are residues which can be phosphorylated. These features make the UBQLN2 PXX region and phosphorylation interesting avenues for investigation of UBQLN2 regulation via PTMs. Notably, mass spectrometry (MS) experiments do not find that the PXX region is PTM-modified. However, this is largely due to the fact that UBQLN2 cannot be digested in typical ways for PTM analysis, as trypsin is typically used as a protease which cleaves at lysine and arginine residues, and the PXX region does not contain lysine or arginine residues.

In an effort to recapitulate the effect of phosphorylation on UBQLN2 properties, we have used glutamic acid substitutions as phosphomimetic substitutions for preliminary studies on the effect of PTMs on UBQLN2 phase separation. Because glutamic acid mutations introduce a negative charge much like a phosphate group, researchers have used Glu residues to introduce phosphomimetic modifications to phase-separating proteins (Wang et al., 2018). In a recent study, glutamic acid mutations at positions P497, P506, P525, V538, and V564, incorporating both “sticker” and “spacer” positions and three positions within the PXX region, were expressed and purified via site directed mutagenesis in the UBQLN2 C-terminal construct, 450C (Chapter 2). The resulting protein was screened for LLPS with temperature ramp turbidity assays. Strikingly, all glutamic acid mutations show extremely diminished phase separation in comparison with WT 450C UBQLN2 (Figure 1A). It is interesting to note that the phosphomimetic mutation resulted in diminished phase separation at both sticker (P497, P506, and V564) and spacer (P525 and V538) positions. Self-association of phosphomimetic UBQLN2 was also investigated, as self-association is known to be a pre-requisite of

UBQLN2 LLPS (Dao et al., 2018). However, SEC revealed little difference between WT UBQLN2 and glutamic acid mutants, with the exception of P525E, where a small population eluted near void volume (Figure 1B). Additionally, phosphomimetic protein was subjected to analysis via microscopy, which largely showed disperse, micron-sized 'granules', rather than spherical fusing droplets which appears after 10 minutes in WT UBQLN2 (Figure 2). Mutant V538E formed phase-separated droplets after 30 minutes, and mutant P525E formed large aggregates after 30 minutes. Though these preliminary studies were not conducted in the full-length protein, it portrays the ability of a phosphomimetic substitution to significantly alter phase-separating behavior.

As PTMs have emerged as important modulators of LLPS, and as preliminary studies have shown that phosphorylation has the capacity to significantly alter LLPS, it is important that studies on UBQLN2 phase separation include native PTMs. Pioneers in the field, Alberti and Hyman, have suggested that phase separation assays be performed with protein expressed from insect cells, which ensures that they receive PTMs (Alberti et al., 2018). Studying the effect of native PTMs on UBQLN2 phase separation *in vitro* could give insight into how PTMs regulate condensation, dissolution, or material properties of UBQLN2-containing condensates *in vivo*. With this in mind, it is also important to note that UBQLN2 features intrinsically disordered regions (IDRs) which are regions often modified with PTMs (Hofweber and Dormann, 2019). Databases also suggest sites for modification via phosphorylation, ubiquitylation, and acetylation (Hornbeck et al., 2015).

Here, I describe the novel expression and purification of full length UBQLN2 in Sf9 insect cells, an isolate of *Spodoptera frugiperda*, via a baculoviral expression

system. Baculoviral expression in Sf9 cells was chosen because: 1) proteins receive the post-translational modifications that are required for normal protein activity and behavior, 2) recombinant proteins are processed, modified, and targeted to their appropriate cellular location in insect cells, which makes them functionally similar to their authentic counterparts, 3) genes are abundantly transcribed during late stages of infection, as opposed to other eukaryotic expression systems and 4) the insect cell expression system is safe in that baculoviruses have limited host range, specific to invertebrates (Invitrogen, 2015).

Results

The methods presented below provide a proof of principle that full length UBQLN2 can be expressed and purified from Sf9 insect cells. In overview, UBQLN2 is first cloned into pFastBacDual + RFP (red fluorescent protein), the donor plasmid. This plasmid is transformed and transposed into DH10Bac cells, and the resulting recombinant bacmid DNA is used to transfect Hi5 cells for the production of passage 1 (P1) baculovirus. P1 virus is used to infect Sf9 cells for passage 2 (P2) baculoviral production. Finally, P2 baculovirus infects Sf9 cells for expression, and later purification.

Generation of UBQLN2 baculovirus

UBQLN2 baculoviral stock was generated using the Bac-to-Bac Baculoviral Expression System and the pFastBac Dual plasmid containing UBQLN2 under the control of the polyhedron promoter and RFP under the p10 promoter. RFP is used here as a visual marker of baculovirus production and processing, not of UBQLN2 specific

expression. Baculovirus stocks were prepared according to the manufacturer's protocol, and slightly adapted to the Hougland lab protocol (Figure 3) (Invitrogen, 2015; Sieburg et al., 2019).

pFastBacDual plasmid was supplied by the manufacturer, and RFP was cloned under the p10 promoter by the Hougland lab. PCR-amplified UBQLN2 was cloned into this plasmid downstream of the polyhedron promoter and transformed into DH5alpha cells. These cells were grown overnight on selection plates; single colonies were miniprepmed from overnight liquid cultures, and the DNA was eluted in water (Figure 4). pFBD p10RFP UBQLN2 was then transformed into DH10Bac™ *E. coli* cells, and plated on Bac plates, which are prepared with kanamycin, gentamycin, tetracycline, Blue-gal, and IPTG. UBQLN2 transposition was confirmed with a x-gal blue-white screen, PCR amplification of the transposed region using pUCM13 rev/for primers, and gel electrophoresis (Figure 5). DH10Bac™ competent cells were used for bacmid extraction and amplification. Bacmid DNA was used for transfection of Hi5 cells (Passage 1; P1). Hi5 cells were used for P1 because they have a very good viral yield, and adhere better to a flask than our stock of Sf9 cells. When cells were ~80% lysed, and media was visibly pink, Passage 1 UBQLN2 baculoviral stock was collected. Passage 1 UBQLN2 baculoviral stock was used for the infection of Sf9 cells for the generation of Passage 2 UBQLN2 baculovirus, which is necessary for the virus to be in the same media as the final expression. When the Sf9 cells were ~80% lysed, and media was visibly pink, P2 UBQLN2 baculoviral stock was harvested and stored for the infection of Sf9 cells for recombinant gene expression.

Sf9 cell preparation and infection

Sf9 cells were propagated and grown in Sf900-III medium at 28°C with shaking at 140rpm. This expression culture was inoculated with P2 UBQLN2 baculovirus particles. UBQLN2 was expressed for 48 hours at 28°C with shaking (140 rpm). A western blot confirmed UBQLN2 expression, though the blot appeared to be overloaded (Figure 6A). For visual comparison, a western blot of various volumes of purified UBQLN2 is included (Figure 6B). The expression culture was harvested, and the cells were pelleted via centrifugation at 500 x g for 5 minutes at room temperature. The supernatant, which contained UBQLN2 as the cells were lysed, was aspirated from the pink-colored pellet, which was stored at -80°C until purification.

Purification of UBQLN2

Cells were lysed and purified via a “salting out” process. NaCl was added to the lysate to a final concentration of 1M, which produced UBQLN2 droplets in solution. UBQLN2 droplets were pelleted and then resuspended in 20 mM NaPhosphate, 0.5 mM EDTA (pH 6.8). Leftover salt was removed through a HiTrap desalting column (GE Healthcare). A SDS-PAGE gel was performed to confirm the identity and purity of UBQLN2 (Figure 7). These experiments indicate that full-length UBQLN2 was expressed and purified from insect cells.

Conclusions and Future Studies

Eukaryotic expression of UBQLN2 will begin the development of a more physiologically-based expression system for the study of post-translationally modified

UBQLN2. The work presented in this chapter is a proof of principle study to show that we can express and purify full-length UBQLN2 from insect cells. Further experiments are required to examine the PTM state of UBQLN2 (discussed below). The expression system discussed herein will permit us to determine the effect of PTMs on its phase-separating behavior. These studies have the potential to direct future *in vivo* investigation of PTMs on the ability of UBQLN2 to form stress-induced condensates in the cell as well as examine how UBQLN2 recruitment to stress granules affect stress granule condensation and dissipation.

Initially, as a screen for post-translational modification, the molecular weight of purified UBQLN2 would be analyzed via mass spectroscopy. In an effort to identify sites and types of modification, chymotrypsin and glutamyl peptidase can be used to cut UBQLN2 in optimal pieces for proteomics. These proteases were chosen because their specificity for the hydrolysis of peptide bonds at tryptophan, tyrosine, phenylalanine, or leucine. By cutting the sequence at these residues, the resulting fragments are small enough for a residue-by-residue analysis. High resolution mass spectroscopy can be used to localize sites and identify types of post-translational modification. It is important to note that eukaryotic-expressed UBQLN2 may result in populations of mixed modification, or populations of unmodified UBQLN2. Hypothesized from UBQLN2 phosphomimetic data, some modified protein may not phase separate, which would require a different method of purification, since our existing purification method is dependent on the ability of UBQLN2 to phase separate. In this case, an affinity tag (e.g. His-tag) could be added to UBQLN2 to ensure a viable method of purification.

Post-translationally modified UBQLN2 may then be investigated via *in vitro* biochemical and biophysical techniques utilized in the Castañeda lab including structural studies via NMR, temperature—concentration phase diagram analysis, self-association analysis via SEC, and droplet properties via microscopy. By comparing these results to those from unmodified UBQLN2, we can tease out what effect PTMs have on UBQLN2 LLPS *in vitro*. As we have shown that UBQLN2 LLPS is modulated in an amino acid-dependent manner, we hypothesize that the addition of a PTM would also vary LLPS phase behavior and droplet properties.

Importantly, the data from these experiments could inform how PTMs may regulate MLO condensation and dissolution. For instance, if insect cell expression resulted in a population of hyperphosphorylated UBQLN2, which showed severely diminished phase-separating properties, we could hypothesize that phosphorylation of UBQLN2 could be a mechanism for UBQLN2 to exit stress granules or regulate the dissolution of stress granules. We then could propose future *in vivo* studies to test this hypothesis. Based on the outcomes of experiments performed on modified UBQLN2, we can better direct our *in vitro* experiments to assess the role of PTMs. Future investigation of UBQLN2 post-translational modification would focus on its function in MLO condensation/dissolution regulation and its effects on the physical properties of stress granules. Investigation of PTM-modified UBQLN2 and its implications in disease-linked aberrant phase transition is of specific interest as many ALS-linked mutations result in residues which can be phosphorylated. Notably, these mutations have been shown to disrupt LLPS by facilitating a liquid-to-solid transition, and the formation of cytoplasmic inclusions (Dao et al., 2019; Lin et al., 2015; Mackenzie et al., 2017; Molliex

et al., 2015; Patel et al., 2015). These observations suggest that disease mutations alter LLPS properties of MLOs, and PTMs may be a worthwhile mechanism to investigate how this may occur.

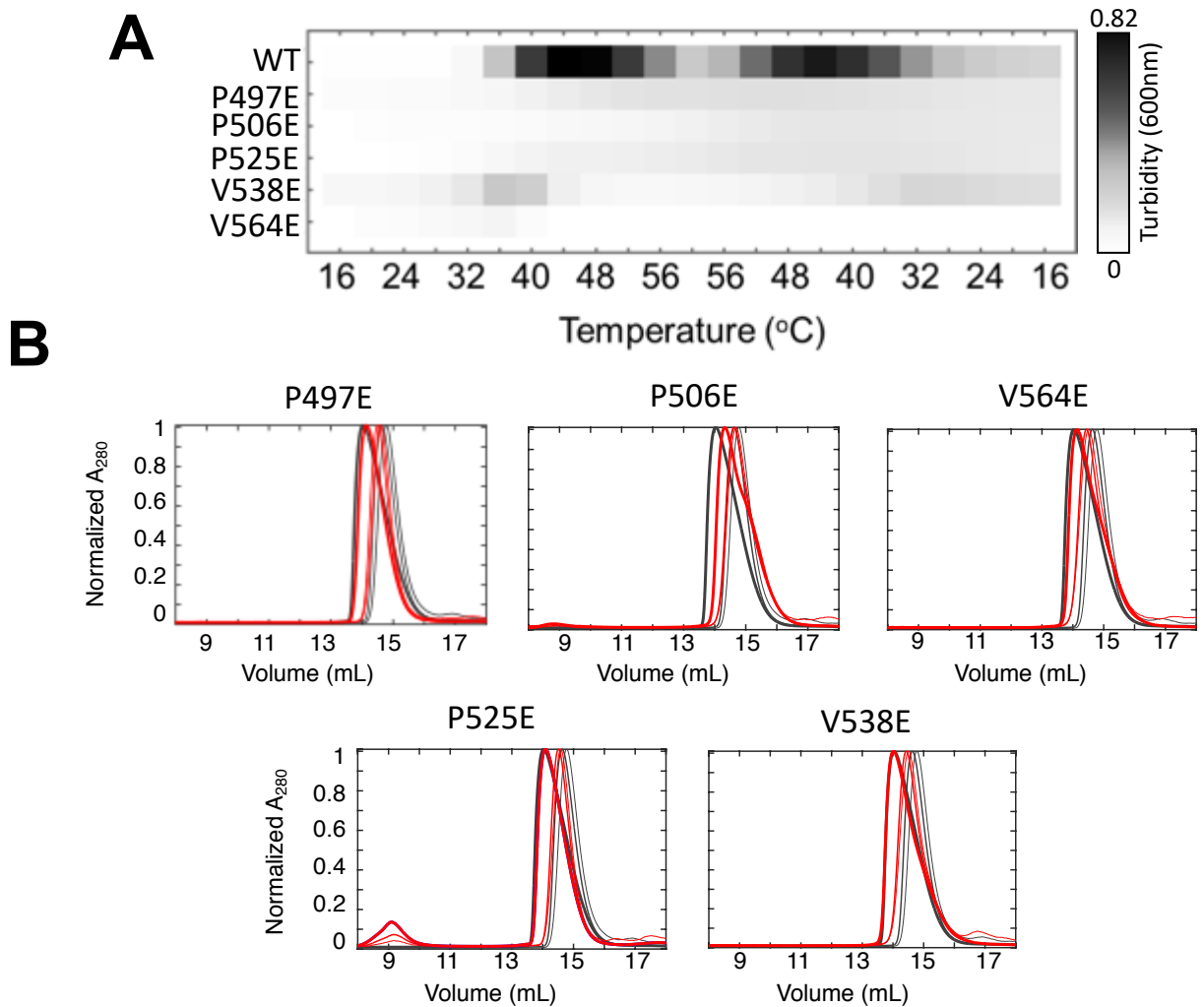


Figure 1. Effects of phosphomimetic substitutions on UBQLN2 LLPS and self-association. (A) Turbidity assays screen for phase separation in UBQLN2 mutants with phosphomimetic substitutions. Results from spectrophotometric turbidity assay as a function of temperature comparing LLPS of UBQLN2 mutants using 50 μ M protein in 20 mM NaPhosphate and 200 mM NaCl (pH 6.8). (B) Oligomerization propensities of phosphomimetic UBQLN2 mutants (red). Representative SEC profiles of UBQLN2 mutants at 10 μ M (thinnest line), 100 μ M (medium-thick), and 500 μ M (thickest) protein concentrations. For each mutant, WT SEC curves were plotted in gray for visual comparison.

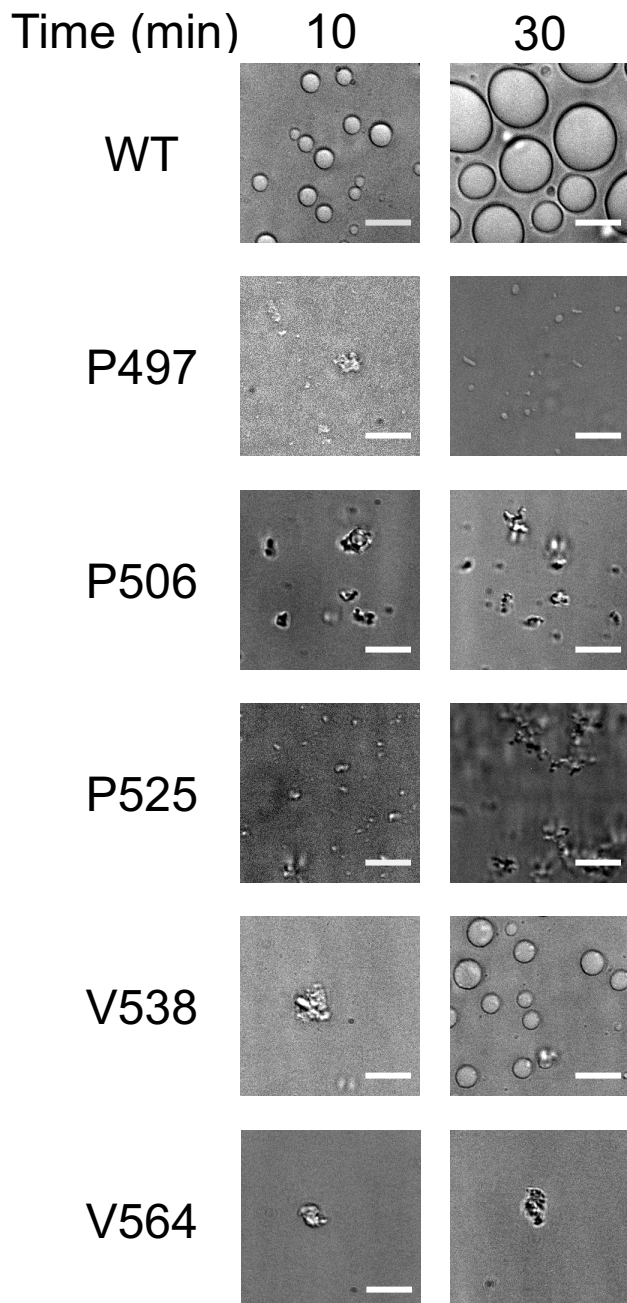


Figure 2. Brightfield microscopy of WT and UBQLN2 mutants with phosphomimetic substitutions. Samples were collected at 10 and 30 min at 37 °C using 100 μ M protein in 20 mM NaPhosphate and 200 mM NaCl (pH 6.8). Scale bar = 5 μ m.

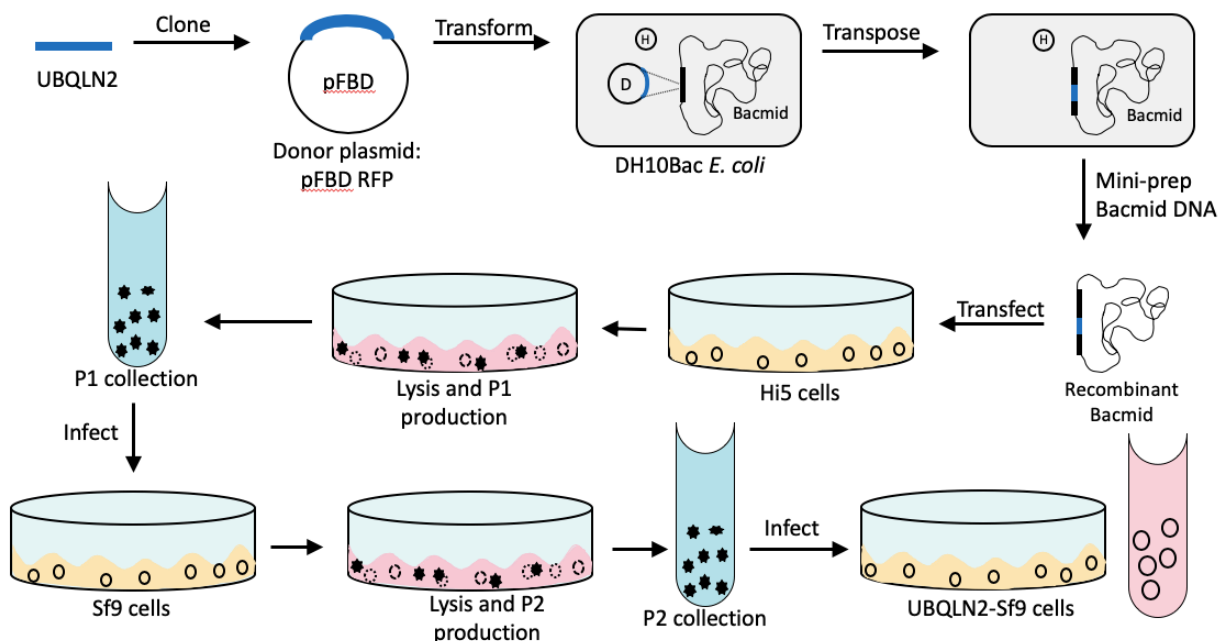


Figure 3. Schematic of the generation of recombinant baculovirus and gene expression adapted from Bac-to-Bac Expression System (Invitrogen, 2015).

UBQLN2 is cloned into pFastBacDual (pFBD) + RFP (red fluorescent protein) donor plasmid, and the recombinant plasmid is transformed into DH10Bac *E. coli* competent cells which contain the bacmid with a mini-attTn7 target site and the helper plasmid. The mini-Tn7 element on the pFastBac™ donor plasmid can transpose to the mini-attTn7 target site on the bacmid in the presence of transposition proteins provided by the helper plasmid. Colonies containing recombinant bacmids are identified by disruption of the *lacZα* gene. High molecular weight mini-prep DNA is prepared from selected *E. coli* clones containing the recombinant bacmid, and this DNA is then used to transfect hi5 cells. Once these cells lyse (represented by circles with dashed-line) the passage 1 virus is collected (star shaped particles). Passage 1 virus is used to infect Sf9 cells. Once the Sf9 cells lyse, passage 2 virus is collected and used to infect Sf9 cells for the expression of UBQLN2.

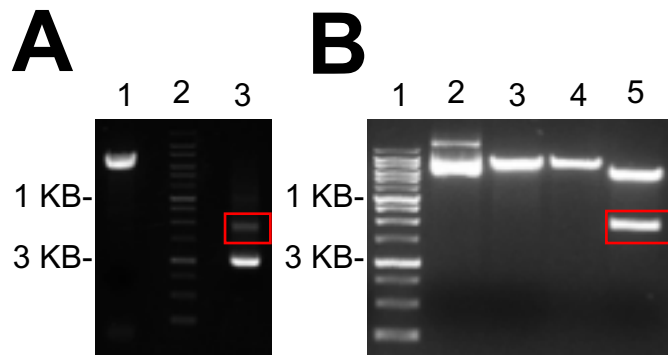


Figure 4. Preparation of pFastBacDual plasmid with UBQLN2 and RFP. (A) PCR product confirms successful production of recombinant donor plasmid pFastBacDual with UBQLN2 and RFP at 2 KB (product labeled in red). Lanes: 1) digested pFBD p10RFP; 2) ladder; 3) PCR product. (B) DNA miniprep confirms successful molecular cloning of UBQLN2 into pFBD + RFP. Lanes: 1) ladder; 2) undigested DNA; 3) DNA digested with BamH1; 4) DNA digested with HindIII; 5) DNA digested with BamH1 and HindIII.

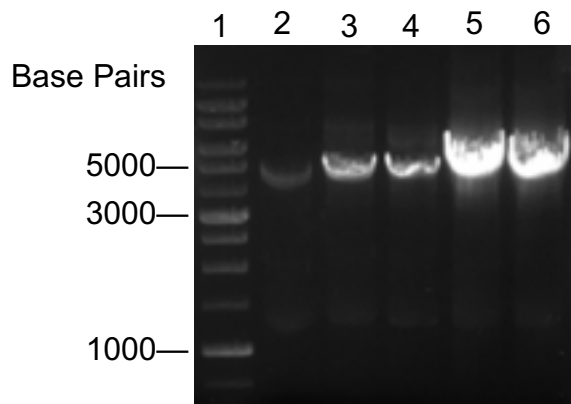


Figure 5. SDS-PAGE confirms successful transposition of UBQLN2 into bacmid DNA using pUCM13 for/rev primers. Lanes 2-6 show PCR product of bacmid transposed with pFastBacDual with UBQLN2 + RFP (~ 4560 base pairs). Lanes: 1) ladder; 2-6) individual DH10Bac™ *E. coli* cell colonies with UBQLN2 bacmid DNA.

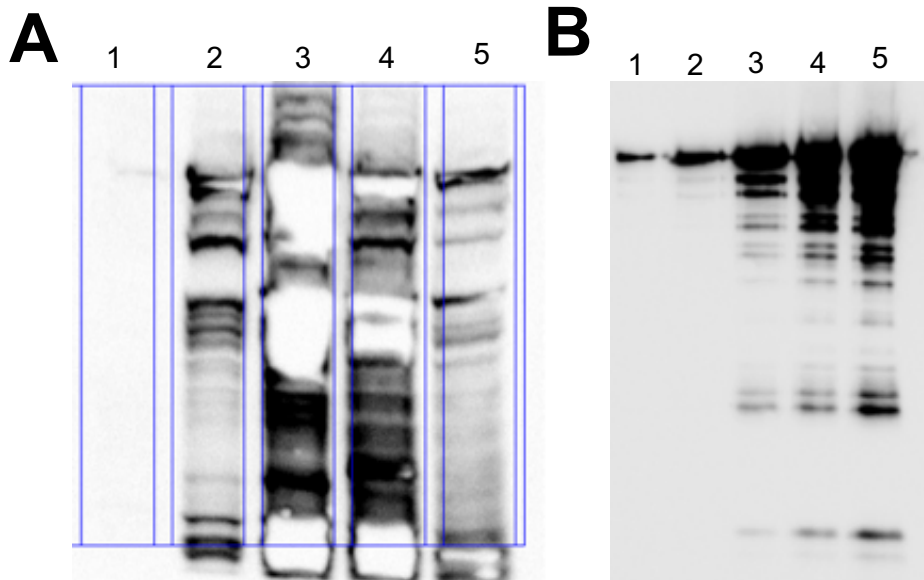


Figure 6. Western blot confirms expression of UBQLN2. (A) Mouse-Anti Ubiquilin2 western blot of UBQLN2 expression time points. Lanes are outlined in blue and are loaded as: 1) 0 hrs; 2) 24 hrs; 3) 48 hrs; 4) 72 hrs; 5) 96 hrs post baculoviral infection. (B) Western blot of full-length UBQLN2 at various loading volumes for visual comparison of overloaded UBQLN2. Lanes were loaded with 1) 10 ng; 2) 20 ng; 3) 50 ng; 4) 100 ng; and 5) 200 ng purified UBQLN2.

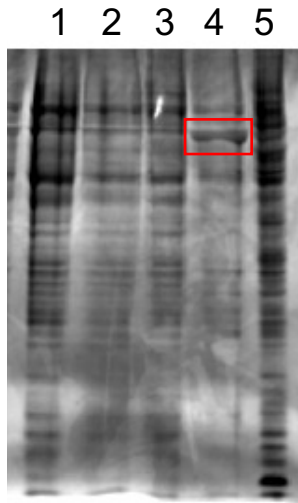


Figure 7. Purification of UBQLN2 from Sf9 cells. SDS-PAGE gel lanes were loaded as: 1) total protein; 2) post-salt supernatant 1; 3) post-salt supernatant 2; 4) elution 1; and 5) elution 2. UBQLN2 was identified in elution 1, lane 4.

Chapter 5: Conclusions and Future Directions

Conclusions

Regarding the molecular underpinnings of UBQLN2 LLPS, the research provided herein identifies several driving mechanisms which largely contribute to the ability of UBQLN2 to phase separate. Our research on C-terminal construct, 450C, corroborates the “sticker” and “spacer” framework, which predicts that “stickers” are sequences which drive interchain interactions and phase separation, where “spacers” are sequences separating stickers which modulate phase separation properties by either enabling or suppressing contact between stickers (Chapter 2) (Yang et al., 2019). Within these stickers, we have shown that LLPS can be modulated by single amino acid substitutions, and that UBQLN2 LLPS follows a molecular code. For instance, mutations to hydrophobic amino acids and polar amino acids decreased cloud point temperatures, seemingly promoting LLPS at lower temperatures and lower concentrations. Therefore, the hydrophobic effect and polar interactions likely are the driving forces underlying UBQLN2 phase separation. This idea is also supported in that more than 25% of the UBQLN2 450C sequence consists of polar residues, and almost 50% of the construct consists of hydrophobic residues. In contrast, mutations to acidic mutations resulted in diminished phase separation. As acidic mutations introduce negative charges much like phosphorylation, and glutamic acid mutations have classically been used as phosphomimetic substitutions, this highlights the potential for regulation of LLPS via post-translational modifications, and highlighting the importance of electrostatics in phase-separating systems.

We have also initiated investigation of the specific role of UBQLN2 domains in its phase separation (Chapter 3). By obtaining temperature-concentration phase diagrams

of six successive N-terminal domain deletion UBQLN2 constructs, we have discovered that each domain, does indeed tune phase separation differently. Interestingly, our data corroborate evidence that prion-like regions contributes to phase separation. However, in the case of UBQLN2, deletion of prion-like domains did not significantly alter self-association behavior as expected, since prion regions have been shown to act as sites of oligomerization. This project helped identify how sequence features such as disorder, structure, and prion-like propensity may govern UBQLN2 LLPS.

Additionally, in chapter 4, I have proposed a method of UBQLN2 purification via insect cell expression, which would include the incorporation of native post-translational modifications (PTMs). Insect cells were chosen for expression because they possess the eukaryotic machinery necessary to modify recombinant proteins in a functionally similar way as their authentic counterparts. A baculoviral expression system was chosen because it ensures a high level of transcription and is safe in that baculoviruses have a host range limited to invertebrates (Invitrogen, 2015). PTMs are an important factor to consider when studying LLPS because several studies have demonstrated that PTMs regulate phase separation, and that many phase-separating proteins are modified. Here, I have described successful expression of full length UBQLN2 in Sf9 insect cells, which provides various avenues for future research.

Furthermore, investigation of UBQLN2 in a domain-by-domain manner indicates the importance of studying full-length protein in phase separation studies. Currently in the field, it is common to perform experiments on smaller protein constructs due to ease of protein purification, and the ability to do certain *in vitro* analyses on smaller proteins, like nuclear magnetic resonance (NMR). As the domain-deletion studies herein have

suggested that each segment of UBQLN2 plays a direct role in driving or modulating LLPS, it would be most physiologically significant to study phase-separating behavior of full-length protein.

Future Directions

In the previous chapters, I have discussed the role of mutations and domain-deletions on UBQLN2 LLPS, with the overarching goal to elucidate the molecular mechanisms which drive UBQLN2 phase separation *in vitro*. Here, I propose methods and potential directions to further investigate UBQLN2 LLPS in terms of analytical modeling, its behavior in cells, and its role in neurodegenerative pathology.

The experimental data contributed here provides a benchmark for future analytical modeling and/or molecular simulation. By obtaining experimental phase diagrams, we determined that UBQLN2 exhibits LCST (lower critical solution temperature) phase transitions. With our experimental data, we can provide a basis for which simulations can reproduce sequence-specific LCST behavior. Ultimately, these data would provide key input for machine-learning algorithms to model phase behavior (Ruff et al., 2018). In addition to predicting phase behavior, an interesting application of these data is to the design of thermoresponsive biopolymers. Thermoresponsive polymer design is of recent interest due to their application in cell sheet fabrication, drug delivery, and 3D-printing (Suntornnond et al., 2017; Ward and Georgiou, 2011).

Indeed, much is left to discover concerning the molecular foundation of UBQLN2 LLPS. Questions remain as to how UBQLN2 facilitates interactions to drive its phase separation *in vitro*, and great questions remain as to how this is translated into cellular

behavior. Specifically, how mutated UBQLN2 behaves *in vivo* is of specific interest due to its link to human disease. Current and future studies in our lab aim to introduce disease-linked mutations into cells to understand how this may alter its phase-separating properties. Disease-linked mutations studied here (Chapter 2), P497H and P497S are of particular interest as they visibly aggregated in turbidity assays using the 450C C-terminal construct (Chapter 2, Figure 2). Similarly, disease-linked mutation P497L showed significantly slower droplet fusion rates compared to WT, characterizing it as an additional mutation of interest. These *in vitro* experiments suggest that disease-linked mutations could perturb phase behavior *in vivo*. Experiments to study these mutations would include live cell imaging and analysis of the dynamics of fluorescently tagged proteins. Understanding how these mutations may alter UBQLN2 recruitment into stress granules, change MLO dynamics and material properties, impair protein quality control (PQC) mechanisms, or promote liquid-to-solid transitions would be beneficial to elucidate disease mechanisms and to the phase-separating community as a whole.

As UBQLN2 shares sequential similarity with its homologs UBQLN1, and -4, analysis of these proteins would also be an interesting avenue to further elucidate the mechanisms behind UBQLN phase separation. UBQLN2 is 74% identical to UBQLN2, and UBQLN1 is 60% identical with UBQLN4. Ubiquilin proteins share a high degree of homology due to their common major domains (UBL, UBA, STI1-I, STI1-II), with the exception of the PXX domain, which is unique to UBQLN2. The Ubiquilin family of proteins functionally links the ubiquitination machinery with the proteasome and other protein quality control pathways. By performing similar biophysical analyses on these

UBQLN homologs, we can better understand the role of LLPS for the ubiquitin family as a whole. Additionally, by comparing and contrasting LLPS behavior between ubiquitin homologs, we may begin to elucidate how molecular variances across homologs alter their phase behavior.

With the role of UBQLN2 in protein quality control (PQC), it is equally important to direct future studies to understanding how LLPS partakes in this function. For instance, investigation of how disease-linked mutations may alter UBQLN2 engagement with PQC machinery could inform the field on potential pathomechanisms. UBQLN2 proteasomal shuttle functionality could be monitored by its association with proteasomal receptors Rpn10 and Rpn13, and ubiquitin (Ub) (Chen et al, 2016). Previous studies have suggested that UBQLN1 prefers association with K63-linked polyUb chains over K48 polyUb chains. Therefore, studies on full-length and mutated UBQLN2 are warranted to determine Ub binding preference and how this binding disrupts or modulates UBQLN2 LLPS. As mentioned in Chapter 3, UBQLN2 has a multitude of binding partners involved in PQC. Prospective studies characterizing UBQLN2 association with binding partners has the potential to further inform us on the role of UBQLN2 in PQC, and how disease may result in dysfunction of this system.

Generation of post-translationally modified UBQLN2 permits us to adopt many experimental directions—both *in vivo* and *in vitro*. As a starting point, analyses similar to those presented in this work would give insight to modified UBQLN2 phase-separating properties. Turbidity assays and phase diagram construction can inform about the protein's ability to phase separate under specific conditions. Importantly, size exclusion chromatography (SEC) could be utilized to see if modification alters the oligomeric

propensity of UBQLN2. Microscopy and NMR experiments would add additional information about the proteins' droplet dynamics, and structure, respectively.

Analysis of modified UBQLN2 via expression in eukaryotic Sf9 cells will direct future in-cell investigation on the role of post-translational modification (PTM) in UBQLN2 LLPS. Molecular weight analysis via mass spectrometry should reveal if, and what kind of modification was made to UBQLN2. With this information, we can then direct our in-cell experiments to study this specific modification. For example, if UBQLN2 is acetylated, we could fluorescently tag acetylated UBQLN2 with an antibody specific to acetylated UBQLN2. We could then utilize immunohistochemistry and immunoblots to identify where and when UBQLN2 is acetylated, and investigate the resulting phase-separating properties. As PTMs are recognized as a major regulatory mechanism of liquid-liquid phase-separated puncta in cells, elucidating where and when UBQLN2 is modified would provide insight on the regulatory role of PTMs on UBQLN2 LLPS. Similarly, such experiments could be done with hyperphosphorylation, and ubiquitination.

Certainly, there are a multitude of avenues to which this work can be applied and extrapolated. The work provided herein can be applied not just to fields investigating liquid-liquid phase separation, but also to fields studying thermodynamic polymers, disease mechanisms, and protein quality control. Overall, these data provide a solid groundwork which establishes the molecular foundation of UBQLN2.

Appendix

List of Abbreviations

LLPS	Liquid-liquid phase separation
PTM	Post-translational modification
MLO	Membraneless organelle
SG	Stress granule
RBP	RNA binding protein
IDR	Intrinsically disordered region
ALS	amyotrophic lateral sclerosis
FTD	Frontotemporal dementia
SAXS	Small angle X-ray Scattering
SEC	Size exclusion chromatography
FRAP	Fluorescent recovery after photobleaching
UBQLN2	Ubiquilin2
UBL	Ubiquitin-like
UBA	Ubiquitin associating
MS	Mass spectrometry
mRNA	Messenger ribonucleic acid
PLD	Prion-like domain
NOE	Nuclear Overhauser effect
NPM1	Nucleophosmin
TDP-43	TAR DNA binding protein
hnRNP	Heterogenous nuclear ribonucleoprotein
SPOP	Speckle-type POZ protein
UV-Vis	UV-visible spectrophotometry
T _{cp}	Cloud point temperature
LCST	Lower critical transition temperature
UCST	Upper critical transition temperature
NMR	Nuclear magnetic resonance
CSP	Chemical shift perturbation
Ub	Ubiquitin

References

- Alberti, S., and Carra, S. (2018). Quality Control of Membraneless Organelles. *J. Mol. Biol.* 430, 4711–4729.
- Alberti, S., Saha, S., Woodruff, J.B., Franzmann, T.M., Wang, J., Hyman, A.A., Pfotenhauerstrasse, :, and Kriwacki, R.W. (2018). A User's Guide for Phase Separation Assays with Purified Proteins. *J. Mol. Biol.* 430, 4806–4820.
- Alexander, E.J., Niaki, A.G., Zhang, T., Sarkar, J., Liu, Y., Nirujogi, R.S., Pandey, A., Myong, S., and Wang, J. (2018). Ubiquilin 2 modulates ALS/FTD-linked FUS–RNA complex dynamics and stress granule formation. *Proc. Natl. Acad. Sci. U. S. A.* 115, e11485-11494.
- Bah, A., and Forman-Kay, J.D. (2016). Modulation of intrinsically disordered protein function by post-translational modifications. *J. Biol. Chem.* 291, 6696–6705.
- Banani, S.F., Rice, A.M., Peeples, W.B., Lin, Y., Jain, S., Parker, R., and Rosen, M.K. (2016). Compositional Control of Phase-Separated Cellular Bodies. *Cell* 166, 651–663.
- Beverly, L.J., Lockwood, W.W., Shah, P.P., Erdjument-Bromage, H., and Varmus, H. (2012). Ubiquitination, localization, and stability of an anti-apoptotic BCL2-like protein, BCL2L10/BCLb, are regulated by Ubiquilin1. *Proc. Natl. Acad. Sci. U. S. A.* 109, 119–126.
- Boeynaems, S., De Decker, M., Tompa, P., and Van Den Bosch, L. (2017). Arginine-rich Peptides Can Actively Mediate Liquid-liquid Phase Separation. *BIO-PROTOCOL* 7, e2525.
- Boke, E., Ruer, M., Wühr, M., Coughlin, M., Lemaitre, R., Gygi, S.P., Alberti, S., Drechsel, D., Hyman, A.A., and Mitchison, T.J. (2016). Amyloid-like Self-Assembly of a Cellular Compartment. *Cell* 166, 637–650.
- Brangwynne, C.P. (2011). Soft active aggregates: Mechanics, dynamics and self-assembly of liquid-like intracellular protein bodies. *Soft Matter* 7, 3052–3059.
- Brangwynne, C.P., Eckmann, C.R., Courson, D.S., Rybarska, A., Hoege, C., Gharakhani, J., Jülicher, F., and Hyman, A.A. (2009). Germline P Granules Are Liquid Droplets That Localize by Controlled Dissolution/Condensation. *New Ser.* 324, 1729–1732.
- Bratek-Skicki, A., Pancsa, R., Meszaros, B., Van Lindt, J., and Tompa, P. (2020). A guide to regulation of the formation of biomolecular condensates. *FEBS J.* 287, 1924–1935.

Chen, X., Randles, L., Shi, K., Tarasov, S.G., Aihara, H., and Walters, K.J. (2016). Structures of Rpn1 T1:Rad23 and hRpn13:hPLIC2 reveal distinct binding mechanisms between substrate receptors and shuttle factors of the proteasome. *Structure* 24, 1257–1270.

Dao, T.P., Kolaitis, R.M., Kim, H.J., O'Donovan, K., Martyniak, B., Colicino, E., Hehnl, H., Taylor, J.P., and Castañeda, C.A. (2018a). Ubiquitin Modulates Liquid-Liquid Phase Separation of UBQLN2 via Disruption of Multivalent Interactions. *Mol. Cell* 69, 965–978.

Dao, T.P., Martyniak, B., Canning, A.J., Lei, Y., Colicino, E.G., Cosgrove, M.S., Hehnl, H., and Castañeda, C.A. (2019). ALS-Linked Mutations Affect UBQLN2 Oligomerization and Phase Separation in a Position- and Amino Acid-Dependent Manner. *Structure* 27, 937–951.

Deng, H.-X., Chen, W., Hong, S.-T., Boycott, K.M., Gorrie, G.H., Siddique, N., Yang, Y., Fecto, F., Shi, Y., Zhai, H., et al. (2011). Mutations in UBQLN2 cause dominant X-linked juvenile and adult onset ALS and ALS/dementia. *Nature* 477, 211–215.

Ford, D.L., Monteiro, M.J. (2006). Dimerization of ubiquitin is dependent upon the central region of the protein: evidence that the monomer, but not the dimer, is involved in binding presenilins. *Biochem. J.* 399, 397-404.

Drino, A., and Schaefer, M.R. (2018). RNAs, Phase Separation, and Membrane-Less Organelles: Are Post-Transcriptional Modifications Modulating Organelle Dynamics? *BioEssays* 40, e1800085.

Feric, M., Vaidya, N., Harmon, T.S., Mitrea, D.M., Zhu, L., Richardson, T.M., Kriwacki, R.W., Pappu, R. V., and Brangwynne, C.P. (2016). Coexisting Liquid Phases Underlie Nucleolar Subcompartments. *Cell* 165, 1686–1697.

Ferreon, J.C., Jain, A., Choi, K.J., Tsoi, P.S., Mackenzie, K.R., Jung, S.Y., and Ferreon, A.C. (2018). Acetylation disfavors tau phase separation. *Int. J. Mol. Sci.* 19, 1360.

Franzmann, T.M., and Alberti, S. (2019). Prion-like low-complexity sequences: Key regulators of protein solubility and phase behavior. *J. Biol. Chem.* 294, 7128–7136.

Gomes, E., and Shorter, J. (2019). The molecular language of membraneless organelles. *J. Biol. Chem.* 294, 7115–7127.

Harmon, T.S., Holehouse, A.S., Rosen, M.K., and Pappu, R. V. (2017). Intrinsically disordered linkers determine the interplay between phase separation and gelation in multivalent proteins. *Elife* 6, e30294.

Hjerpe, R., Bett, J.S., Keuss, M.J., Solovyova, A., McWilliams, T.G., Johnson, C., Sahu, I., Varghese, J., Wood, N., Wightman, M., et al. (2016). UBQLN2 Mediates Autophagy-Independent Protein Aggregate Clearance by the Proteasome. *Cell* 166, 935–949.

Hofweber, M., and Dormann, D. (2019). Friend or foe-Post-translational modifications as regulators of phase separation and RNP granule dynamics. *J. Biol. Chem.* 294, 7137–7150.

Holehouse, A.S., and Pappu, R. V. (2018). Collapse Transitions of Proteins and the Interplay Among Backbone, Sidechain, and Solvent Interactions. *Annu. Rev. Biophys.* 47, 19–39.

Hornbeck, P. V., Zhang, B., Murray, B., Kornhauser, J.M., Latham, V., and Skrzypek, E. (2015). PhosphoSitePlus, 2014: Mutations, PTMs and recalibrations. *Nucleic Acids Res.* 43, 512-520.

Hyman, A.A., Weber, C.A., and Ulicher, F.J." (2014). Liquid-Liquid Phase Separation in Biology. *Annu. Rev. Cell Dev. Biol* 30, 39–58.

Invitrogen (2015). Bac-to-Bac® Baculovirus Expression System. User Guid.

Kato, M., Han, T.W., Xie, S., Shi, K., Du, X., Wu, L.C., Mirzaei, H., Goldsmith, E.J., Longgood, J., Pei, J., et al. (2012). Cell-free formation of RNA granules: Low complexity sequence domains form dynamic fibers within hydrogels. *Cell* 149, 753–767.

Kaye, F.J., Modi, S., Ivanovska, I., Koonin, E. V., Thress, K., Kubo, A., Kornbluth, S., and Rose, M.D. (2000). A family of ubiquitin-like proteins binds the ATPase domain of Hsp70-like Stch. *FEBS Lett.* 467, 348–355.

Ko, H.S., Uehara, T., Tsuruma, K., and Nomura, Y. (2004). Ubiquilin interacts with ubiquitylated proteins and proteasome through its ubiquitin-associated and ubiquitin-like domains. *FEBS Lett.* 566, 110–114.

Kulkarni, M., Ozgur, S., and Stoecklin, G. (2010). On track with P-bodies. *Biochem. Soc. Trans.* 38, 242–251.

Kurlawala, Z., Shah, P.P., Shah, C., and Beverly, L.J. (2017). The STI and UBA Domains of UBQLN1 Are Critical Determinants of Substrate Interaction and Proteostasis. *J. Cell. Biochem.* 118, 2261–2270.

Lancaster, A.K., Nutter-Upham, A., Lindquist, S., and King, O.D. (2014). PLAAC: A web and command-line application to identify proteins with prion-like amino acid composition. *Bioinformatics* 30, 2501–2502.

Le, N.T.T., Chang, L., Kovlyagina, I., Georgiou, P., Safren, N., Braunstein, K.E., Kvarita, M.D., Dyke, A.M.V., Legates, T.A., Philips, T., et al. (2016). Motor neuron disease, TDP-43 pathology, and memory deficits in mice expressing ALS-FTD-linked UBQLN2 mutations. *Proc. Natl. Acad. Sci. U. S. A.* 113, 7580–7589.

Li, Romero, Rani, Dunker, and Obradovic (1999). Predicting Protein Disorder for N-, C-, and Internal Regions. *Genome Inform. Ser. Workshop Genome Inform.* 10, 30–40.

Li, H.R., Chiang, W.C., Chou, P.C., Wang, W.J., and Huang, J. rong (2018). TAR DNA-binding protein 43 (TDP-43) liquid-liquid phase separation is mediated by just a few aromatic residues. *J. Biol. Chem.* 293, 6090–6098.

Li, P., Banjade, S., Cheng, H.-C., Kim, S., Chen, B., Guo, L., Llaguno, M., Hollingsworth, J. V, King, D.S., Banani, S.F., et al. (2012). Phase transitions in the assembly of multivalent signalling proteins. *Nature* 483, 336–340.

Lin, Y., Protter, D.S.W., Rosen, M.K., and Parker, R. (2015). Formation and Maturation of Phase-Separated Liquid Droplets by RNA-Binding Proteins. *Mol. Cell* 60, 208–219.

Sieburg, MA., Cleverdon, ER., and Hougland, JL. (2019). Biochemical Assays for Ghrelin Acylation and Inhibition of Ghrelin O-Acyltransferase. *Methods Mol. Biol.* 2009, 227–241.

Mackenzie, I.R., Nicholson, A.M., Sarkar, M., Messing, J., Purice, M.D., Pottier, C., Annu, K., Baker, M., Perkerson, R.B., Kurti, A., et al. (2017). TIA1 Mutations in Amyotrophic Lateral Sclerosis and Frontotemporal Dementia Promote Phase Separation and Alter Stress Granule Dynamics. *Neuron* 156, 1207–1222.

Malinowska, L., Kroschwald, S., and Alberti, S. (2013). Protein disorder, prion propensities, and self-organizing macromolecular collectives. *Biochim. Biophys. Acta - Proteins Proteomics* 1834, 918–931.

Martin, E.W., Holehouse, A.S., Peran, I., Farag, M., Incicco, J.J., Bremer, A., Grace, C.R., Soranno, A., Pappu, R. V., and Mittag, T. (2020). Valence and patterning of aromatic residues determine the phase behavior of prion-like domains. *Science*. 367, 694–699.

Marzahn, M.R., Marada, S., Lee, J., Nourse, A., Kenrick, S., Zhao, H., Ben-Nissan, G., Kolaitis, R., Peters, J.L., Pounds, S., et al. (2016). Higher-order oligomerization promotes localization of SPOP to liquid nuclear speckles. *EMBO J.* 35, 1254–1275.

McGurk, L., Gomes, E., Guo, L., Mojsilovic-Petrovic, J., Tran, V., Kalb, R.G., Shorter, J., and Bonini, N.M. (2018). Poly(ADP-Ribose) Prevents Pathological Phase Separation of TDP-43 by Promoting Liquid Demixing and Stress Granule Localization. *Mol. Cell* 71, 703-717.

Milkovic, N.M., Thomasen, F.E., Cuneo, M.J., Grace, C.R., Martin, E.W., Nourse, A., Lindorff-Larsen, K., and Mittag, T. (2020). Interplay of folded domains and the disordered low-complexity domain in mediating hnRNPA1 phase separation. *BioRxiv*.

- Mitreá, D.M., Cika, J.A., Guy, C.S., Ban, D., Banerjee, P.R., Stanley, C.B., Nourse, A., Deniz, A.A., and Kriwacki, R.W. (2016). Nucleophosmin integrates within the nucleolus via multi-modal interactions with proteins displaying R-rich linear motifs and rRNA. *Elife* 5, e13571.
- Mitreá, D.M., Cika, J.A., Stanley, C.B., Nourse, A., Onuchic, P.L., Banerjee, P.R., Phillips, A.H., Park, C.G., Deniz, A.A., and Kriwacki, R.W. (2018). Self-interaction of NPM1 modulates multiple mechanisms of liquid-liquid phase separation. *Nat. Commun.* 9, 842.
- Molliex, A., Temirov, J., Lee, J., Coughlin, M., Kanagaraj, A.P., Kim, H.J., Mittag, T., and Taylor, J.P. (2015). Phase Separation by Low Complexity Domains Promotes Stress Granule Assembly and Drives Pathological Fibrillization. *Cell* 163, 123–133.
- Murthy, A.C., Dignon, G.L., Kan, Y., Zerze, G.H., Parekh, S.H., Mittal, J., and Fawzi, N.L. (2019). Molecular interactions underlying liquid–liquid phase separation of the FUS low-complexity domain. *Nat. Struct. Mol. Biol.* 26, 637–648.
- Nott, T.J., Petsalaki, E., Farber, P., Jervis, D., Fussner, E., Plochowietz, A., Craggs, T.D., Bazett-Jones, D.P., Pawson, T., Forman-Kay, J.D., et al. (2015). Phase Transition of a Disordered Nuage Protein Generates Environmentally Responsive Membraneless Organelles. *Mol. Cell* 57, 936–947.
- Novotná, I., Blažíková, M., Staněka, D., Herman, P., and Malinsky, J. (2011). In vivo kinetics of U4/U6•U5 tri-snRNP formation in Cajal bodies. *Mol. Biol. Cell* 22, 513–523.
- Obradovic, Z., Peng, K., Vucetic, S., Radivojac, P., Brown, C.J., and Dunker, A.K. (2003). Predicting Intrinsic Disorder From Amino Acid Sequence. *Proteins Struct. Funct. Genet.* 53, 566–572.
- Pak, C.W., Kosno, M., Holehouse, A.S., Padrick, S.B., Mittal, A., Ali, R., Yunus, A.A., Liu, D.R., Pappu, R. V., and Rosen, M.K. (2016). Sequence Determinants of Intracellular Phase Separation by Complex Coacervation of a Disordered Protein. *Mol. Cell* 63, 72–85.
- Patel, A., Lee, H.O., Jawerth, L., Maharana, S., Jahnel, M., Hein, M.Y., Stoynov, S., Mahamid, J., Saha, S., Franzmann, T.M., et al. (2015). A Liquid-to-Solid Phase Transition of the ALS Protein FUS Accelerated by Disease Mutation. *Cell* 162, 1066–1077.
- Protter, D.S.W., and Parker, R. (2016). Principles and Properties of Stress Granules. *Trends Cell Biol.* 26, 668–679.

Qamar, S., Wang, G.Z., Randle, S.J., Ruggeri, F.S., Varela, J.A., Lin, J.Q., Phillips, E.C., Miyashita, A., Williams, D., Ströhl, F., et al. (2018). FUS Phase Separation Is Modulated by a Molecular Chaperone and Methylation of Arginine Cation- π Interactions. *Cell* 173, 720–734.

Riback, J.A., Katanski, C.D., Kear-Scott, J.L., Pilipenko, E. V., Rojek, A.E., Sosnick, T.R., and Drummond, D.A. (2017). Stress-Triggered Phase Separation Is an Adaptive, Evolutionarily Tuned Response. *Cell* 168, 1028–1040.

Romero, Obradovic, and Dunker (1997). Sequence Data Analysis for Long Disordered Regions Prediction in the Calcineurin Family. *Genome Inform. Ser. Workshop Genome Inform.* 8, 110–124.

Rubinstein, M., and Dobrynin, A. (1997). Solutions of associative polymers. *Trends Polym. Sci. (Regular Ed.)*. 2, 424-436.

Ruff, K.M., Roberts, S., Chilkoti, A., and Pappu, R. V. (2018). Advances in Understanding Stimulus-Responsive Phase Behavior of Intrinsically Disordered Protein Polymers. *J. Mol. Biol.* 430, 4619–4635.

Sabate, R., Rousseau, F., Schymkowitz, J., and Ventura, S. (2015). What Makes a Protein Sequence a Prion? *PLoS Comput. Biol.* 11, e1004013.

Saito, M., Hess, D., Eglinger, J., Fritsch, A.W., Kreysing, M., Weinert, B.T., Choudhary, C., and Matthias, P. (2019). Acetylation of intrinsically disordered regions regulates phase separation. *Nat. Chem. Biol.* 15, 51–61.

Schindelin, J., Arganda-Carreras, I., Frise, E., Kaynig, V., Longair, M., Pietzsch, T., Preibisch, S., Rueden, C., Saalfeld, S., Schmid, B., et al. (2012). Fiji: An open-source platform for biological-image analysis. *Nat. Methods* 9, 676–682.

Semenov, A.N., and Rubinstein, M. (1998). Thermoreversible Gelation in Solutions of Associative Polymers. 1. Statics. 31, 1373–1385.

Shapouri, F., Saeidi, S., de longh, R.U., Casagrande, F., Western, P.S., McLaughlin, E.A., Sutherland, J.M., Hime, G.R., and Familari, M. (2016). Tob1 is expressed in developing and adult gonads and is associated with the P-body marker, Dcp2. *Cell Tissue Res.* 364, 443–451.

Shin, Y., Berry, J., Pannucci, N., Haataja, M.P., Toettcher, J.E., and Brangwynne, C.P. (2017). Spatiotemporal Control of Intracellular Phase Transitions Using Light-Activated optoDroplets. *Cell* 168, 158–171.

Suntornnond, R., An, J., and Chua, C.K. (2017). Bioprinting of Thermoresponsive Hydrogels for Next Generation Tissue Engineering: A Review. *Macromol. Mater. Eng.* 302, 1600266.

Urry, D.W., Gowda, D.C., Parker, T.M., Luan, C. -H, Reid, M.C., Harris, C.M., Pattanaik, A., and Harris, R.D. (1992). Hydrophobicity scale for proteins based on inverse temperature transitions. *Biopolymers* 32, 1243–1250.

Uversky, V.N. (2017). Intrinsically disordered proteins in overcrowded milieu: Membrane-less organelles, phase separation, and intrinsic disorder. *Curr. Opin. Struct. Biol.* 44, 18–30.

Vernon, R.M., Chong, P.A., Tsang, B., Kim, T.H., Bah, A., Farber, P., Lin, H., and Forman-Kay, J.D. (2018). Pi-Pi contacts are an overlooked protein feature relevant to phase separation. *Elife* 7, e31486.

Walters, K.J., Goh, A.M., Wang, Q., Wagner, G., and Howley, P.M. (2004). Ubiquitin family proteins and their relationship to the proteasome: A structural perspective. *Biochim. Biophys. Acta - Mol. Cell Res.* 1695, 73–87.

Wang, A., Conicella, A.E., Schmidt, H.B., Martin, E.W., Rhoads, S.N., Reeb, A.N., Nourse, A., Ramirez Montero, D., Ryan, V.H., Rohatgi, R., et al. (2018a). A single N-terminal phosphomimic disrupts TDP-43 polymerization, phase separation, and RNA splicing. *EMBO J.* 37, e97452.

Wang, J., Choi, J.M., Holehouse, A.S., Lee, H.O., Zhang, X., Jahnel, M., Maharana, S., Lemaitre, R., Pozniakovsky, A., Drechsel, D., et al. (2018b). A Molecular Grammar Governing the Driving Forces for Phase Separation of Prion-like RNA Binding Proteins. *Cell* 174, 688–699.

Wang, J.T., Smith, J., Chen, B.C., Schmidt, H., Rasoloson, D., Paix, A., Lambrus, B.G., Calidas, D., Betzig, E., and Seydoux, G. (2014). Regulation of RNA granule dynamics by phosphorylation of serine-rich, intrinsically disordered proteins in *C. elegans*. *Elife* 3, e04591.

Ward, M.A., and Georgiou, T.K. (2011). Thermoresponsive polymers for biomedical applications. *Polymers (Basel)*. 3, 1215–1242.

Wilson, E.B. (1899). The structure of protoplasm. *Science*. 10, 33–45.

Xiang, S., Kato, M., Wu, L.C., Lin, Y., Ding, M., Zhang, Y., Yu, Y., and McKnight, S.L. (2015). The LC Domain of hnRNPA2 Adopts Similar Conformations in Hydrogel Polymers, Liquid-like Droplets, and Nuclei. *Cell* 163, 829–839.

Xue, B., Dunbrack, R.L., Williams, R.W., Dunker, A.K., and Uversky, V.N. (2010). PONDR-FIT: A meta-predictor of intrinsically disordered amino acids. *Biochim. Biophys. Acta - Proteins Proteomics* 1804, 996–1010.

Yang, Y., Jones, H.B., Dao, T.P., and Castañeda, C.A. (2019). Single Amino Acid Substitutions in Stickers, but Not Spacers, Substantially Alter UBQLN2 Phase Transitions and Dense Phase Material Properties. *J. Phys. Chem. B* 123, 3618–3629.

Yun Lee, D., Arnott, D., and Brown, E.J. (2013). Ubiquilin4 is an adaptor protein that recruits Ubiquilin1 to the autophagy machinery. *EMBO Rep.* 4, 373–381.

Zhang, D., Raasi, S., and Fushman, D. (2008). Affinity Makes the Difference: Nonselective Interaction of the UBA Domain of Ubiquilin-1 with Monomeric Ubiquitin and Polyubiquitin Chains. *J. Mol. Biol.* 377, 162–180.



Single Amino Acid Substitutions in Stickers, but Not Spacers, Substantially Alter UBQLN2 Phase Transitions and Dense Phase Material Properties

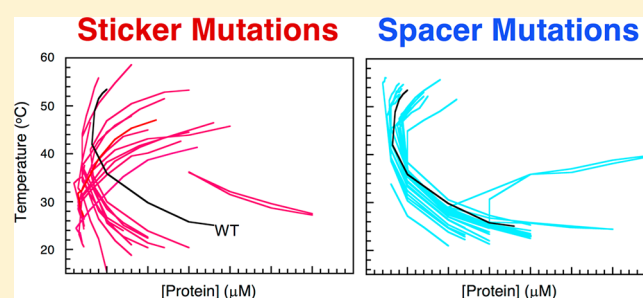
Published as part of *The Journal of Physical Chemistry virtual special issue "Young Scientists"*.

Yiran Yang,[†] Holly B. Jones,^{‡,§} Thuy P. Dao,^{||} and Carlos A. Castañeda^{*,§,||}

[†]Department of Chemistry, [‡]Department of Biology, [§]Interdisciplinary Neuroscience Program, and ^{||}Departments of Biology and Chemistry, Syracuse University, Syracuse, New York, United States

Supporting Information

ABSTRACT: UBQLN2 450–624 oligomerizes and undergoes temperature-responsive liquid–liquid phase transitions following a closed-loop temperature–concentration phase diagram. We recently showed that disease-linked mutations to UBQLN2 450–624 impart highly varying effects to its phase behavior, ranging from little change to significant decrease of saturation concentration and formation of gels and aggregates. However, how single mutations lead to these properties is unknown. Here, we use UBQLN2 450–624 as a model system to study the sequence determinants of phase separation. We hypothesized that UBQLN2 450–624 regions previously identified to promote its oligomerization are the “stickers” that drive interchain interactions and phase separation. We systematically investigated how phase behavior is affected by all 19 possible single amino acid substitutions at three sticker and two “spacer” (sequences separating stickers) positions. Overall, substitutions to stickers, but not spacers, substantially altered the shape of the phase diagram. Within the sticker regions, increasing hydrophobicity decreased saturation concentrations at low temperatures and enhanced oligomerization propensity and viscoelasticity of the dense phase. Conversely, substitutions to acidic residues at all positions greatly increased saturation concentrations. Our data demonstrate that single amino acid substitutions follow a molecular code to tune phase transition behavior of biopolymers.



■ INTRODUCTION

Liquid–Liquid phase separation (LLPS) is a process by which a solution of macromolecules demixes into a species-rich liquid dense phase in equilibrium with a species-poor dilute phase. LLPS is hypothesized to underlie the assembly of biomolecular condensates essential for various cellular processes.^{1,2} In phase-separating proteins, a major characteristic is multivalency, the existence of multiple associative motifs of intrinsically disordered segments or structured domains that form intra- and interchain interactions.^{3–5} Accumulating evidence shows that phase transition behavior is encoded in the amino acid sequence.^{6–8} Mutations can tune the conditions necessary for LLPS, as well as the material properties of these condensates in vitro and in vivo.^{9,10} Indeed, dysregulation of condensate dynamics, assembly, and/or disassembly is linked to diseases, including amyotrophic lateral sclerosis (ALS) among others. Therefore, deciphering the molecular code that drives phase transitions of biopolymers is key to understanding diseases, as well as designing stimuli-responsive polymers with emergent properties.

The “stickers” and “spacers” framework is emerging as useful language to describe the physical origins of LLPS behavior in proteins. Stickers are the associative motifs that drive LLPS,

whereas the spacers connect the sticker regions and tune LLPS behavior as well as impart flexibility.^{11–15} The chemical basis of sticker interactions that govern phase transition behavior varies across phase-separating systems. For instance, Arg and Tyr residues in the FUS family of proteins use cation– π and π – π stacking interactions to drive LLPS.⁸ The hydrophobic effect modulates LLPS of elastin and elastin-like proteins and other proteins such as Pab1.^{14–16} Aromatic residues are essential for mediating TDP-43 LLPS.¹⁷ Electrostatic interactions formed via clusters of either positively or negatively charged residues stabilize Ddx4 protein droplets.¹⁸ These experimental data must be combined to deduce the molecular grammar underpinning LLPS at physiological conditions for biological systems. Indeed, π – π contact propensity can be used to predict LLPS based solely on amino acid sequence.¹⁹

Evaluating the effects of amino acid substitutions on phase transition behavior requires elucidation of full phase diagrams that map the conditions where the solution phase separates into protein-dilute and protein-dense phases. For some

Received: January 31, 2019

Revised: March 25, 2019

Published: March 29, 2019

systems, the protein-dense phase also intersects a liquid–gel phase boundary, where the dense phase undergoes gelation, a transition from liquid droplets to a noncovalent physically cross-linked network of molecules.¹¹ The equilibrium protein concentrations in the protein-dilute and protein-dense phases are described by the binodal or coexistence curve comprising both low and high concentration arms. The low concentration arm defines the protein saturation concentration (c_s), below which the system will be mixed and homogeneous, and above which, the system will form a distinct second phase such as protein-dense liquid droplets.^{20–22} Coexistence curves are determined by the free energy of the system thereby including entropy of mixing, as well as the enthalpies of protein–protein, protein–solvent, and solvent–solvent interactions. The complex interplay of these terms provides the thermodynamic basis for LLPS in biological systems. Obtaining experimental phase diagrams and predicting these via computational modeling and/or simulation are ideal metrics to determine the molecular driving forces of phase separation and phase separation-driven gelation.^{11,23} Therefore, experimental systems are needed to address this goal, as emphasized in recent literature.^{22,24}

We established a model biopolymer system, the C-terminal construct of UBQLN2 (450–624), to which we could experimentally map the effects of single amino acid substitutions on phase transition behavior. We recently demonstrated that UBQLN2, a proteasomal shuttle factor involved in cellular protein quality control mechanisms, phase separates under physiological conditions, and that UBQLN2 450–624 generally mimics the LLPS behavior of full-length UBQLN2.²⁵ Furthermore, UBQLN2 450–624 can be easily expressed and purified from bacteria, enabling the establishment of a large mutagenesis library to study the sequence effects on phase transitions. We previously identified regions of UBQLN2 450–624 important for oligomerization and hypothesized that these same segments are the stickers that drive LLPS. To test this hypothesis, we systematically substituted each of the natural amino acids into three sticker and two spacer positions and obtained low-concentration arms of temperature–concentration phase diagrams. In agreement with the stickers and spacers framework, only sticker substitutions substantially altered the shape of temperature–concentration phase diagrams, whereas spacer substitutions only marginally affected coexistence curves. Increasing hydrophobicity of the amino acid substitution shifted coexistence curves such that UBQLN2 phase separated at lower temperatures and concentrations. Our data illustrate that single amino acid substitutions at designated positions in the amino acid sequence of a protein substantially modify phase transition behavior of biopolymers. These data can be used to benchmark analytical and computational models of phase transitions.

METHODS

Subcloning, Protein Expression, and Purification.

UBQLN2 mutants were generated from UBQLN2 450–624 using Phusion Site-Directed Mutagenesis Kit (Thermo Scientific). A tryptophan codon was added to the C-terminal end of all constructs to facilitate determination of protein concentration (Figure S1A). UBQLN2 450–624 and all the mutants were expressed and purified as described by Dao et al, 2018.²⁵ Briefly, the constructs were expressed in *Escherichia coli* Rosetta 2 (DE3) pLysS cells in Luria–Bertani (LB) broth at 37 °C overnight. Bacteria were pelleted, frozen, lysed, then purified via a “salting out” process. NaCl was added to the

cleared lysate to the final concentration of 0.5–1 M. UBQLN2 droplets were pelleted and then resuspended in 6 M urea, 20 mM sodium phosphate, 0.5 mM ethylenediaminetetraacetic acid (EDTA), 0.1 mM tris(2-carboxyethyl)phosphine (TCEP), 0.02% NaN₃ (pH 6.8). Leftover NaCl and urea were removed through HiTrap desalting column (GE Healthcare). All the cysteine mutants were subjected to size exclusion chromatography (SEC) over a Superdex 75 HiLoad 16/600 column (GE Healthcare) or an ENrich SEC 650 10 × 300 column (Biorad) to remove dimer contaminations. Sodium dodecyl sulfate-polyacrylamide gel electrophoresis (SDS-PAGE) gels were performed to confirm the purity of the proteins (Figure S2A). The identity and molecular weight of each mutant was verified using electrospray mass spectrometry in positive mode on a Shimadzu 8040 MS (Figure S2B). Purified proteins were frozen at –80 °C.

Spectrophotometric Absorbance/Turbidity Measurements. Protein samples were prepared by adding protein (from stock to a final concentration of 50 μM unless otherwise noted) to cold sodium phosphate buffer (pH 6.8, 20 mM NaPhosphate, 0.5 mM EDTA, 0.1 mM TCEP, 0.02% NaN₃) containing 200 mM NaCl and were kept on ice for at least 5 min before the assay. Absorbance at 600 nm was recorded as a function of temperature by a Beckman DU-640 UV/vis spectrophotometer using a temperature ramp rate of 2 °C/min increasing from 16 to 60 °C and then ramped down to 16 °C. Net absorbance values were recorded after subtracting the absorbance value of a buffer control. Results were averaged from data collected using proteins from at least two separate preps and four trials for each (total $n \geq 8$) (Figure S2C). Data were plotted using Mathematica (Wolfram Research).

Phase Diagram Measurements. For the lower critical solution temperature (LCST) phase transition, that is, mapping the phase boundary as temperature is increased, protein samples were prepared as described for the turbidity measurements. For the upper critical solution temperature (UCST) arm, protein samples were prepared by mixing protein and buffer/salt solutions that were incubated at 63 °C for at least 10 min. Absorbance at 600 nm was recorded as a function of temperature by a Beckman DU-640 UV/vis spectrophotometer using a temperature ramp rate of 2 °C/min decreasing from 60 to 16 °C. Two trials ($n = 2$) were conducted using four to five different concentrations of wild-type (WT) and mutant UBQLN2 450–624 proteins for each arm. The protein concentrations were chosen to cover as wide a range as possible to allow observation of phase separation during the temperature ramps but not at the starting temperatures (16 and 60 °C for LCST and UCST arms, respectively). Cloud-point temperatures were determined by fitting a Four Parameter Logistic Regression model to the data (Figure S3).

$$y = d + \frac{a - d}{1 + \left(\frac{x}{c}\right)^b} \quad (1)$$

Cloud-point temperatures used were the points of inflection (c). Cloud-point temperatures were then used to define the coexistence curve as a function of protein concentration. The temperature ramp rate was either 1 or 2 °C/min, whichever yielded the most reproducible, consistent turbidity profiles and phase diagrams. Specifically, a 1 °C/min ramp rate was used for the LCST arms of hydrophobic and aromatic substitutions.

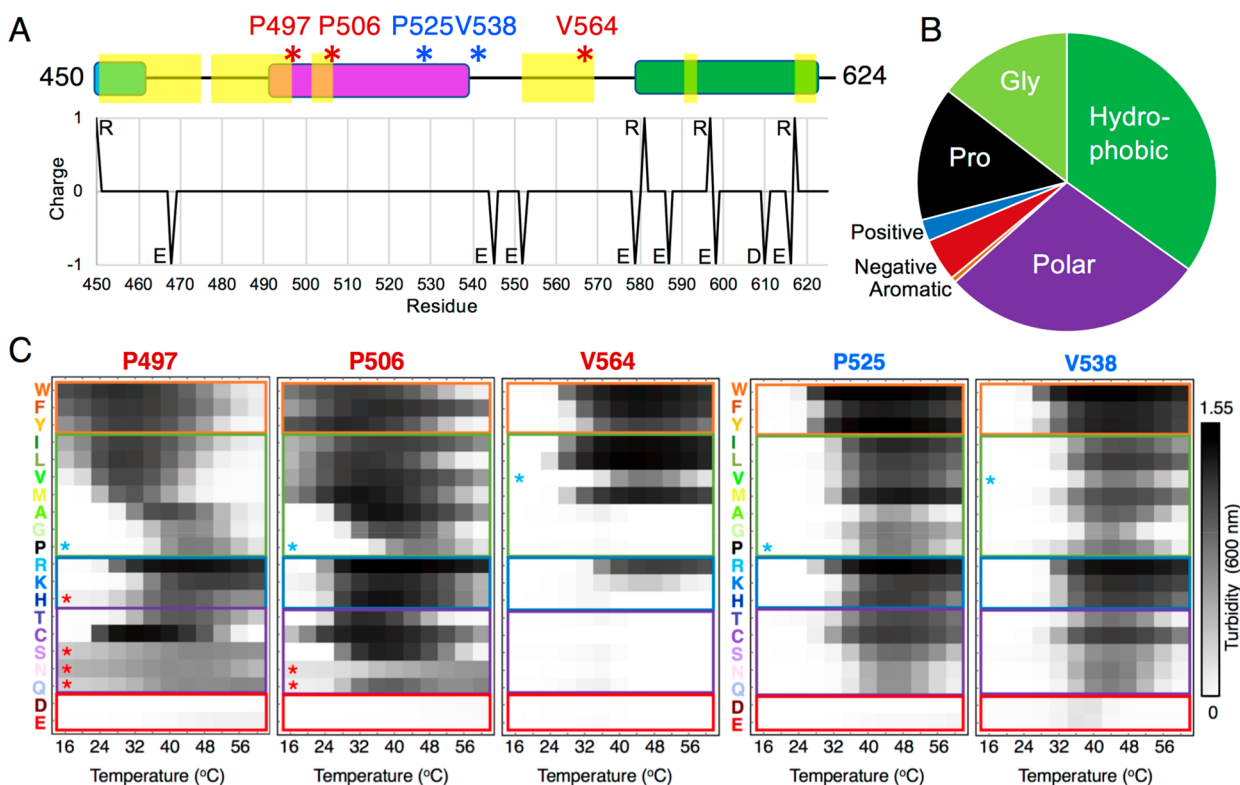


Figure 1. Turbidity assay screens for mutants in sticker and spacer regions of UBQLN2 450–624 with ST11-II, PXX, and UBA domains colored as cyan, magenta, and green, respectively. Highlighted in yellow are regions identified by NMR to promote UBQLN2 oligomerization and hypothesized to be stickers.²⁵ Red and blue labels represent sticker and spacer positions studied here, respectively. Immediately below marks the location of ionizable residues and their expected charge state at pH 7. All of the arginines and most of the negatively charged residues reside in the folded UBA domain. (B) Fraction of the different types of amino acids in UBQLN2 450–624, which is high in hydrophobic, polar, glycine, and proline and depleted of aromatic and charged residues. Pie chart follows the general organization in Ruff et al. 2018.²² (C) Results from spectrophotometric turbidity assay as a function of temperature comparing LLPS of different UBQLN2 mutants using 50 μM protein in 20 mM NaPhosphate and 200 mM NaCl (pH 6.8). The blue asterisks represent WT UBQLN2 turbidity profile for each position. The red asterisks represent mutants that form unevenly distributed aggregates at one point during the assay. P497H, S, N, and Q formed aggregates early in the experiment, whereas P506N and Q aggregated at temperatures above 44 $^{\circ}\text{C}$. Turbidity profiles of amino acid substitutions at each position are separated by amino acid type: aromatic, hydrophobic, basic, polar, and acidic. Hypothesized stickers and spacers are color-coded red and blue, respectively, at the top.

Fitting and plotting of data were done with Kaleidagraph (Synergy Software).

Bright-Field Imaging of Phase Separation. UBQLN2 450–624 constructs were prepared to contain 100 μM protein in 20 mM NaPhosphate, 200 mM NaCl, 0.1 mM TCEP, and 0.5 mM EDTA (pH 6.8). Samples were added to MatTek glass-bottom dishes that had been coated with 5% bovine serum albumin (BSA), to minimize changes as a result of surface interactions, and incubated at 37 $^{\circ}\text{C}$. Phase separation was imaged on an ONI Nanoimager (Oxford Nanoimaging Ltd.) equipped with a Hamamatsu sCMOS ORCA flash 4.0 V3 camera using an Olympus 100 \times /1.4 N.A. objective. Images were prepared using Fiji²⁶ and FigureJ plugin.²⁷

Droplet Fusion Assays. UBQLN2 450–624 constructs were prepared to contain 100 μM protein in 20 mM NaPhosphate and 0.5 mM EDTA (pH 6.8), except for P506W at 25 μM protein and P506E and V538E at 300 μM protein. Samples were added to MatTek glass-bottom dishes that had been incubated with 5% BSA (to minimize changes as a result of surface interactions) and incubated at 37 $^{\circ}\text{C}$. Phase separation was initiated with the addition of NaCl to a final concentration of 200 mM. After 10 min of incubation, droplet formation was imaged as time-lapsed sequences for 3 min on an ONI Nanoimager equipped with a Hamamatsu sCMOS

ORCA flash 4.0 V3 camera using an Olympus 100 \times /1.4 N.A. objective. Five trials were performed for each mutant. Droplets chosen for analysis were of similar size and ranged between 2 and 4 μm , except for V538E (8 μm) and P506E (5 μm). For each mutant, eight fusion events were chosen for analysis and saved as separate TIFF images including frames from the initial fusion event.

Relaxation times (time it takes for two fusing droplets to return to a round shape) were determined by manually measuring the major axis (a) and the minor axis (b) in pixels using Fiji software²⁶ and calculating the aspect ratio as $\alpha = a/b$. We monitored the fusion events in this way, until the droplets reached their most relaxed state, or until the aspect ratio was approximately equal to 1. The aspect ratio for each fusion event was fit to an exponential decay curve in Matlab (Mathworks).

$$y = (\alpha_0)e^{-x/\tau} + c \quad (2)$$

where α_0 is the initial aspect ratio, x is time, and τ gives the characteristic relaxation time.

Size Exclusion Chromatography. Purified UBQLN2 constructs at different concentrations (10, 100, and 500 μM) were subjected to chromatography over an ENrich SEC 650 10

× 300 column (Biorad) on a Biorad NGC FPLC system. Experiments were conducted using 250 μ L of protein at ambient temperature using 1 mL/min flow rate in pH 6.8 buffer containing 20 mM NaPhosphate, 0.5 mM EDTA, and 0.1 mM TCEP with no added NaCl.

RESULTS

Library Generation of UBQLN2 Mutants. We previously characterized the LLPS properties of full-length UBQLN2 and several deletion constructs, including UBQLN2 450–624.²⁵ We showed that UBQLN2 oligomerization is a prerequisite for UBQLN2's ability to phase separate *in vivo* and *in vitro*, as expected and observed for many other LLPS systems. For detailed biophysical analyses, we focused on UBQLN2 450–624 (Figure S1A), whose small size (~175 amino acids) enabled the use of nuclear magnetic resonance (NMR) spectroscopy to monitor backbone amide chemical shifts as a function of protein concentration on a residue-by-residue basis. We observed concentration-dependent chemical shifts for residues 450–509, 555–570, 592–596, and 615–620, indicating that these residues are involved in UBQLN2 oligomerization (Figures 1A and S1A,B). Here, we hypothesized that the residues in these segments comprise the sticker regions that drive UBQLN2 phase separation. The amino acid compositions of these sticker regions and of UBQLN2 450–624 are hydrophobic and polar (Figures 1B and S1A,C), consistent with other polymers that phase separate as temperatures increase such as elastin-like polypeptides (ELPs).¹⁵

We recently showed that ALS-linked mutations P497H, P497L, P497S, P506A, P506S, and P506T, but not P525S, significantly altered UBQLN2 450–624 LLPS properties.⁴³ Interestingly, on the basis of our NMR data, residues P497 and P506 are in a sticker region, and P525 is in a spacer region. We hypothesized that mutations in the sticker regions would greatly affect both the dense and dilute phases (e.g., saturation concentrations, droplet morphology, droplet fusion kinetics), whereas mutations in the spacer regions would not. To test this hypothesis, we sought to determine the effects of amino acid substitutions at these three positions as well as at an additional sticker position, V564, and spacer position, V538, in the UBQLN2 450–624 background, hereafter referred to as UBQLN2 (Figure 1A). All five positions reside in the intrinsically disordered segment between residues 450 and 580.²⁵ We generated all 19 possible amino acid substitutions at each of these positions for a total of 95 mutant constructs. We expressed and purified wild-type and mutant UBQLN2 proteins from *E. coli*. As done previously, we used salt-induced phase separation and centrifugation to separate UBQLN2 from the rest of the *E. coli* lysates and then desalted into non-phase separating pH 6.8 buffer containing 20 mM NaPhosphate. Proteins were more than 95% pure (Figure S2A).

Turbidity Assays Screened for Effects of Amino Acid Substitutions on LLPS. To systematically screen for the effects of UBQLN2 mutations on LLPS, we monitored the change of A_{600} values between 16 and 60 °C of samples containing a fixed protein concentration and buffer composition (see Methods). Previous work from our lab showed that high and low A_{600} values correlate with UBQLN2 droplet formation and droplet clearance, respectively.²⁵ To ensure reproducibility, we repeated these assays a minimum of eight times using at least two purified protein stocks (Figure S2C).

Wild-type UBQLN2 undergoes two temperature-responsive phase transitions (Figure 1C). First, UBQLN2 phase separates as temperature is increased between 16 and 45 °C. This phase transition has an LCST, below which the protein solution is always mixed, regardless of protein concentration. Second, a solution of phase-separated UBQLN2 becomes less turbid as temperature is increased between 45 and 60 °C. This second phase transition has a UCST, above which the protein solution is always mixed. Together, these data are indicative of phase behavior following a UCST + LCST closed-loop phase diagram (Figure 2A).²² Turbidity was generally reversible when temperature was decreased from 60 to 16 °C (Figure S2D). These results are consistent with our prior work.⁴³

Focusing first on the overall turbidity assay trends across all positions, we immediately noticed that mutations in sticker positions 497, 506, and 564 substantially impacted the temperature ranges where phase separation was observed, as compared to mutations in spacer positions 525 and 538. There is considerable variation in the extent of phase separation among the different amino acid substitutions in the sticker positions. It is important to note that, for positions 497, 506, and 525, the wild-type amino acid is proline, whereas for positions 538 and 564, it is valine. Regardless of the wild-type amino acid, the trends for spacer positions 525 and 538 were nearly identical. In contrast, the overall extent of phase separation for the sticker substitution at position 564 was greatly reduced compared to positions 497 and 506. The turbidity data across the five positions were consistent with our initial hypothesis that residues 497, 506, and 564 are stickers, whereas residues 525 and 538 are spacers (Figure 1C).

Second, we organized our turbidity assay results by amino acid type: hydrophobic (A, G, I, L, M, P, V), aromatic (F, W, Y), basic (H, K, R), acidic (D, E), and polar (C, N, Q, S, T). We note the difficulties in assigning amino acids to these classes, particularly G and P, due to their roles in modulating protein flexibility and solubility.²⁸ We presented our amino acid substitutions in terms of decreasing hydrophobicity, largely following the experimental hydrophobicity scale determined by Urry et al., 1992.²⁹ Among the sticker positions 497, 506, and 564, increased hydrophobicity promoted UBQLN2 LLPS and lowered the temperature threshold for phase separation. Aromatic substitutions at the sticker positions decreased the temperatures when phase separation was first observed, in many cases below 16 °C, the starting temperature of the experiment. Notably, the effects on the mutations on the turbidity profiles varied by position even among stickers. For example, UBQLN2 mutants with Ile or Phe substitutions at position 506 remained turbid for the entire temperature range (16–60 °C), whereas phase-separating solutions of P497F and P497I began clarifying at 40 °C. These observations illustrated that Ile and Phe substitutions to both P497 and P506 impact LCST and UCST phase transitions but via different mechanisms. Of the 95 mutants, only six visibly aggregated during the turbidity assay experiments: P497H, P497S, P497N, P497Q, P506N, and P506Q (Figure S2E). Of these, two are disease-linked mutations (P497H and P497S). Although the effects of the spacer mutations on LLPS were much less drastic compared to those in the sticker positions, we still observed large increases in the absolute intensity of the absorbance signal, especially among substitutions to aromatic and more hydrophobic residues. It is possible that these substitutions made the spacer positions more sticker-like, hence increasing the degree of phase separation of the solution.

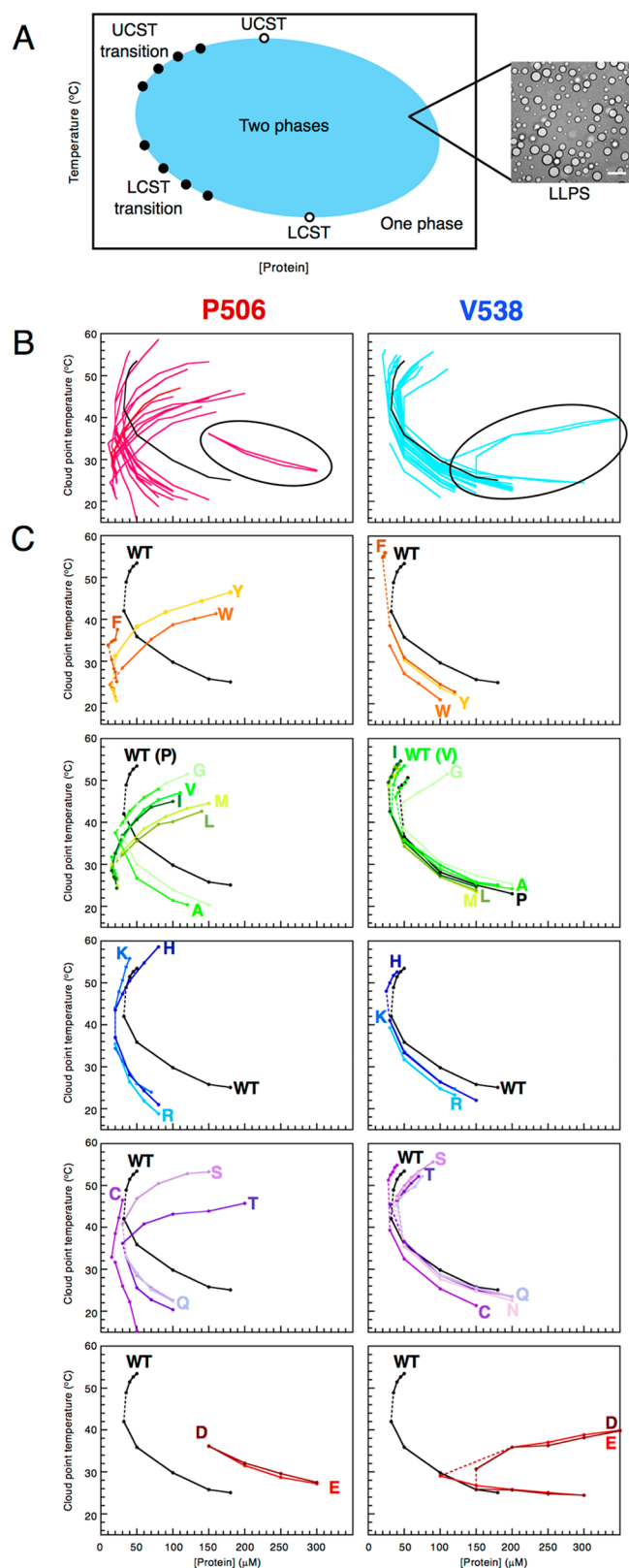


Figure 2. Temperature–Concentration phase diagrams for representative sticker and spacer residues in UBQLN2. (A) Schematic of a closed-loop phase diagram showing both UCST and LCST behaviors. The black dots represent the experimental data points for the low concentration arm obtained in this study to partially map the phase diagram. (B) Effects of amino acid substitutions in the sticker (pink, P506) region and in the spacer (cyan, V538) region compared to WT UBQLN2 (black). Circled in black are D and E mutants for each

Figure 2. continued

position. (C) Effects of amino acid substitutions separated by amino acid type: aromatic (F, W, Y), hydrophobic (A, G, I, L, M, P, V), basic (H, K, R), polar (C, N, Q, S, T), and acidic (D, E). The dashed lines are guides that connect the UCST phase transition cloud-point temperatures to the LCST ones. Both arms of P506N and the UCST arm of P506Q are missing due to formation of aggregates during the assays. The UCST arms for V538W, V538Y, V538R, V538K, P506D, and P506E are missing, since we observed either no turbidity or nonzero turbidity values at 60 °C at all concentrations tested.

Moreover, the turbidity assay does not directly measure the number of droplets but the scattering of the samples. Scattering is highly dependent on differences in the size of the droplets, which might change as the result of the substitutions. One notable similarity between stickers and spacers was the effect of Asp and Glu substitutions, both of which significantly disrupted phase separation at all positions tested. Together, these data emphasize that perturbations to LLPS properties of proteins are very sensitive to both the type of amino acid substitution and the position in the amino acid sequence.

Effects of Amino Acid Substitutions on Phase Diagrams. To quantitatively compare the effects of single amino acid substitutions on phase transitions of UBQLN2 and determine the driving forces for UBQLN2 phase separation, we experimentally obtained temperature–concentration phase diagrams for the 19 substitutions at two representative positions: a sticker residue (P506) and a spacer residue (V538) (Figure 2). At a protein concentration for which no LLPS was observed at the start of the experiment, we performed temperature-ramping turbidity assays and determined $T_{cp}(\text{infl})$, the cloud-point temperature at the inflection point of the transition (Figure S3).³⁰ There are other methods to characterize the conditions when phase transitions occur, including using microscopy to monitor onset or applying a threshold to changes in absorbance–temperature curves. For practical reasons, we chose the inflection point, $T_{cp}(\text{infl})$, for comparison across different protein samples. The experimental T_{cp} values at different protein concentrations were used to map the coexistence curves (Figure 2). Since UBQLN2 exhibits both LCST and UCST phase transition behavior, T_{cp} associated with the LCST transition was determined by increasing temperature from 16 to 60 °C, whereas T_{cp} values associated with the UCST transition were determined by starting turbidity assay experiments at 60 °C and ramping down to 16 °C (see Methods). We tried these experiments at low (μM) as well as high (up to 3 mM) protein concentrations. However, the protein solutions were always cloudy or contained aggregates at the higher concentration ranges at the start of the experiments (both 16 and 60 °C). Therefore, we focused on obtaining the low-concentration arm (c_s) of the coexistence curves (Figure 2A). As expected from the turbidity assays (Figure 1C), the experimental phase diagram for WT UBQLN2 resembles that of a UCST–LCST closed-loop phase diagram, indicating two temperature-responsive phase transitions between 16 and 60 °C (Figure 2B).

Strikingly, amino acid substitutions at sticker position 506 not only shifted the position of the coexistence curves but also changed the overall shape of the phase diagram (Figure 2B). Meanwhile, amino acid substitutions at spacer position 538

only mildly shifted coexistence curves but generally displayed a phase diagram with similar shape to that of WT. In other words, mutations at position 538 minimally perturbed the c_s needed for LLPS. These observations are entirely consistent with the expected behaviors of stickers and spacers.^{8,20} The major exceptions to these observations were acidic amino acid substitutions, for which the c_s values of the dilute phase were greatly increased for all positions (see below).

Among the classes of amino acid substitutions, aromatic and hydrophobic amino acid mutations at sticker position 506 substantially affected the phase diagram of UBQLN2. Furthermore, increasing hydrophobicity of the amino acid substitution correlated with decreasing c_s values of the LCST phase transition. The coexistence curves all shifted to the left as hydrophobicity of the amino acid substitution increased. These data are completely consistent with our prior work that showed lowered c_s of UBQLN2 for hydrophobic disease-linked mutations T487I and P497L.⁴³ Together, the data suggest the importance of the hydrophobic amino acids in driving UBQLN2 phase separation. Indeed, many of the amino acids in sticker regions are hydrophobic, as we previously characterized (Figure S1A).²⁵

At position 506, aromatic substitutions substantially changed the shape of UBQLN2's phase diagram, but differently depending on the amino acid. Tyr and Trp mutations shifted the UCST arm of the phase diagram downward compared to WT, with UCST cloud-point temperatures below 50 °C at least up to 200 μ M protein concentrations. On the one hand, the Phe substitution was always phase separated over the entire temperature range tested, except at low protein concentrations (<20 μ M). In contrast, the Phe substitution at position 538 minimally impacted the overall shape of the phase diagram, while all aromatic substitutions at this position imposed a leftward shift of the coexistence curves to lower protein concentrations. Notably, we could not obtain V538 Tyr and Trp UCST phase transition cloud points, since we could not establish clear baselines at 60 °C for any protein concentrations that exhibited turbidity during the temperature ramping assays. Therefore, these cloud-point values are likely to be greater than 60 °C. We speculate that the aromatic substitutions impart stickerlike properties to position 538, thus decreasing the c_s values for LLPS. It is apparent that π -stacking interactions involving aromatic amino acids promote LLPS in other systems, such as FUS and TDP-43.^{8,17}

Polar substitutions at the sticker but not spacer position affected the phase diagram of UBQLN2. This makes sense given the polar amino acid composition (Figure 1B). At position 506, both LCST and UCST transitions were perturbed. Interestingly, the LCST transitions of Ser, Thr, and Gln substitutions nearly superimposed, while the UCST arm of the coexistence curves decreased in the order C > S > T. We also noted that five of the six substitutions that produced aggregates (Figure S2E) were polar substitutions: P497S, P497Q, P497N, P506Q, P506N.

Basic amino acid substitutions shifted coexistence curves to the left, with little difference among the three basic amino acids (His, Lys, Arg). The effects were more substantial for the sticker position than for the spacer. Interestingly, acidic amino acid substitutions had the opposite effects and greatly increased the saturation concentrations needed for UBQLN2 LLPS, as well as narrowing the temperature region where the protein phase-separated. We speculate that these effects can be partially explained by the bulkiness of the side-chain

substitution (for Arg and Lys, whose side chains have some hydrophobic character) as well as the charge state of the UBQLN2 construct. At 25 °C, the predicted pI or isoelectric point of the UBQLN2 450–624 construct is \sim 4.4, with less than 7% of the protein containing ionizable residues (Figure 1B). This means that the protein is negatively charged at pH 6.8, the pH chosen for our experiments. Introduction of positive charges provides attractive Coulombic interactions between the substitution and the overall charge of the protein, thereby promoting intermolecular interactions between UBQLN2 molecules to drive phase separation. In contrast, acidic substitutions may do the opposite, potentially providing repulsive interactions between UBQLN2 molecules and decreasing phase separation.

Hydrophobic Sticker but Not Spacer Substitutions Altered Droplet Morphology and Increased Viscoelastic Properties. Mapping the lower concentration arms of the phase diagram allowed us to evaluate the effects of the substitutions on the dilute phase. However, what are the consequences of the substitutions on the dense phase? To answer this, we first used brightfield microscopy to investigate the morphology of UBQLN2 droplets of representative amino acid substitutions from the different classes of residues, including W (aromatic), G and L (hydrophobic), R (basic), Q (polar), and E (acidic) across the five positions studied here (Figure 3A). In general, the droplet morphologies at these different positions correlated well with the turbidity assay results. Mutants exhibiting similar turbidity profiles as WT UBQLN2 (e.g., P525 and V538 mutants) produced spherical droplets of similar size as WT. Mutants that exhibited significantly enhanced turbidity (P497W, P497L, P506W, P506L) also formed amorphous droplets (Figures 1C and 3A). Microscopy also confirmed the existence of aggregates as observed in the turbidity assays for P497Q (P506Q aggregates were observed at temperatures higher than 37 °C during the turbidity assays and therefore were not seen under the microscope). Surprisingly, acidic substitution E, which showed little or no turbidity at the condition tested, appeared to form small aggregate-like species at all five positions at our experimental conditions. Over time, these aggregate-like species sometimes morphed into droplets as observed for V538E (Figure 3A). Consistent with our hypothesis, mutations at spacer positions 525 and 538 (except V525R, P525E, and V538E) had minimal effects on the morphology of the droplets, while mutations at sticker positions 497, 506, and 564 elicited different morphologies ranging from round like WT-like to amorphous droplets and/or aggregates.

To describe the effects of amino acid substitutions on the properties of the dense phase quantitatively, we analyzed droplet fusion kinetics. We noticed that, for many substitutions, two fusing droplets relaxed into spherical shapes within seconds, while for other substitutions, spherical shapes were not achieved within a 3 min experimental window (Figure 3B). Since the sphericity of droplets stems from surface tension, the rates of droplet fusion report on droplet viscosity and surface tension.³¹ To assess the liquidity of mutant UBQLN2 droplets, we measured the time it took for two fusing droplets to return to a spherical shape (or round in two dimensions). We extracted relaxation times from droplet fusion measurements for seven amino acid substitutions at the sticker and spacer positions, 506 and 538, respectively, of protein samples that had been incubated in phase-separating conditions for 10 min (Figure 3B,C). Remarkably, droplets for

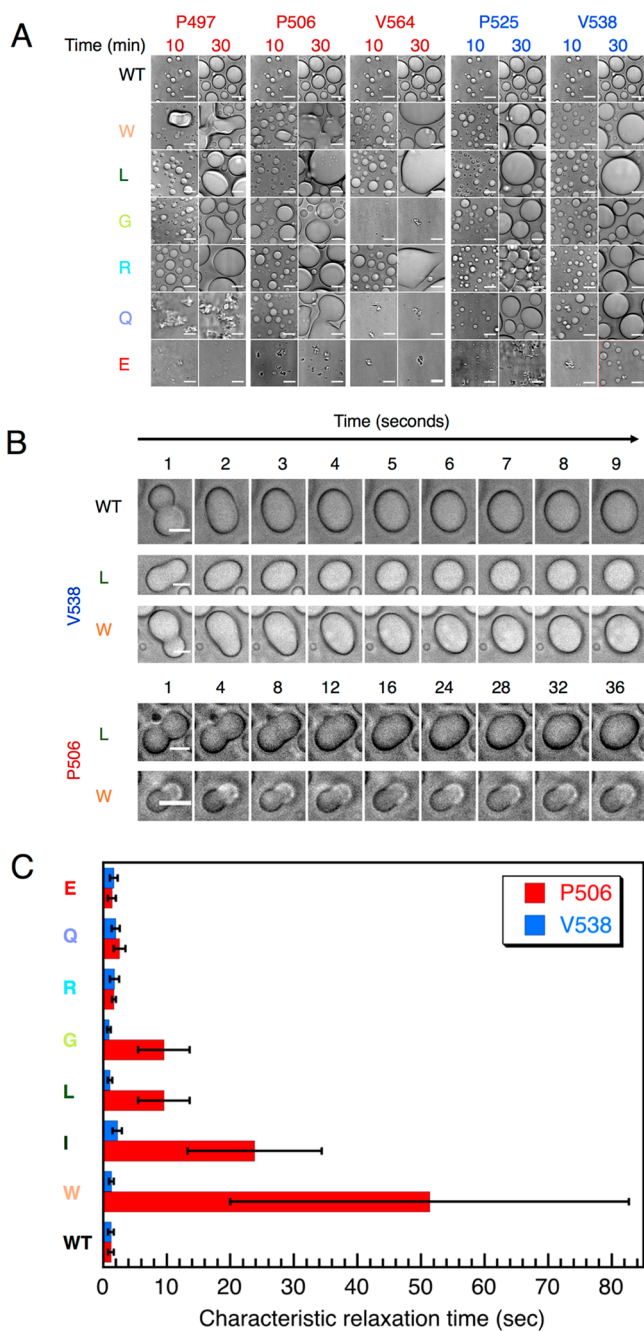


Figure 3. Amino acid substitutions in the sticker, but not spacer, regions affect droplet properties. (A) Light microscopy of different UBQLN2 mutants over 10 and 30 min at 37 °C using 100 μM protein at sticker (P497, P506, V564) and spacer (P525, V538) positions. Scale bar = 5 μm . (B) Snapshots of droplet fusion over a nine second window (for WT and V538L and V538W) and a 36 s window (for P506L and P506W), indicating differences in droplet fusion kinetics between substitutions at a sticker position (P506) and a spacer position (V538). Droplets were imaged 10 min after incubating 100 μM protein (except for P506W (25 μM), P506E and V538E (300 μM)) at 37 °C in buffer containing 20 mM NaPhosphate and 200 mM NaCl (pH 6.8). Scale bar = 2 μm . (C) Average characteristic relaxation times for WT and mutant droplet fusion. Error bars represent the standard deviation over eight droplets.

V538 mutants fused quickly and with similar relaxation times as that for WT UBQLN2, despite the markedly different types of amino acid substitutions tested. These observations are fully

consistent with the spacer characteristics expected for position 538, in that spacer amino acid substitutions minimally perturbed phase separation properties. In contrast, the type of amino acid substitution at sticker position 506 had a substantial impact on the rate of droplet relaxation. Bulky aromatic and hydrophobic substitutions resulted in significantly slowed droplet relaxation events, but not for polar and ionizable substitutions. These data suggest that hydrophobic and aromatic amino acids promote UBQLN2 intermolecular interactions that increase viscoelasticity of UBQLN2 droplets as well as drive UBQLN2 phase separation (see below).

Hydrophobic and Aromatic Sticker Substitutions Increase UBQLN2 Oligomerization. As UBQLN2 oligomerization is a prerequisite for phase separation,²⁵ we probed UBQLN2 self-association propensity using SEC under non-phase separating conditions (i.e., 20 mM NaPhosphate without added NaCl). We previously demonstrated that WT UBQLN2 is monomeric at low protein concentrations (up to $\sim 100 \mu\text{M}$) but forms higher-order oligomers at higher concentrations ($\sim 500 \mu\text{M}$).²⁵ Indeed, SEC peak elution volumes for WT decreased as protein concentration increased between 10 and 500 μM , as expected for UBQLN2 oligomerization. Therefore, we subjected representative mutants at each position to size exclusion chromatography using three protein concentrations (10, 100, 500 μM).

All of the mutants studied exhibited concentration-dependent oligomerization; increasing protein concentrations led to a decrease in elution volume (Figure 4). Strikingly, almost all of the spacer mutants (P525 and V538) exhibited a concentration dependence that followed the pattern of WT UBQLN2. The only exception was P525E, where a small population of large particles eluted near the void volume ($\sim 9 \text{ mL}$). Of all the E mutants, P525E showed the most aggregates by microscopy (Figure 3A). Among the sticker mutants, four oligomerized substantially more than WT: P497W, P497L, P506W, and P506L. Sedimentation velocity analytical ultracentrifugation experiments showed that hydrophobic mutations T487I and P497L also produced high-order oligomers.⁴³ V564W and V564L oligomerized slightly more than WT but not to a significant extent, since the wild-type amino acid is valine, which is already hydrophobic. These data suggest that aromatic and hydrophobic substitutions promote UBQLN2 self-association and thus drive LLPS at lower protein concentrations than WT (Figure 2) and enhance the viscoelasticity of droplets (Figure 3).

DISCUSSION

How amino acid substitutions alter thermoresponsive phase transition behavior of proteins is critical to elucidating the driving forces of phase separation. Here, we demonstrated that both LCST and UCST phase transition behaviors of UBQLN2 can be differentially tuned by single amino acid substitutions. The observations herein provide evidence that the stickers and spacers framework is useful for predicting the positions in a given amino acid sequence that drive phase separation behavior.^{8,12,20} Regardless of amino acid type, substitutions at sticker but not spacer positions elicited major changes to the overall shape and characteristics of the phase diagram (Figures 2 and 5).

Our original hypothesis considered the stickers of UBQLN2 to be residues that exhibited large concentration-dependent changes in amide chemical shifts obtained by NMR spectroscopy.²⁵ In the stickers and spacers framework, the number of

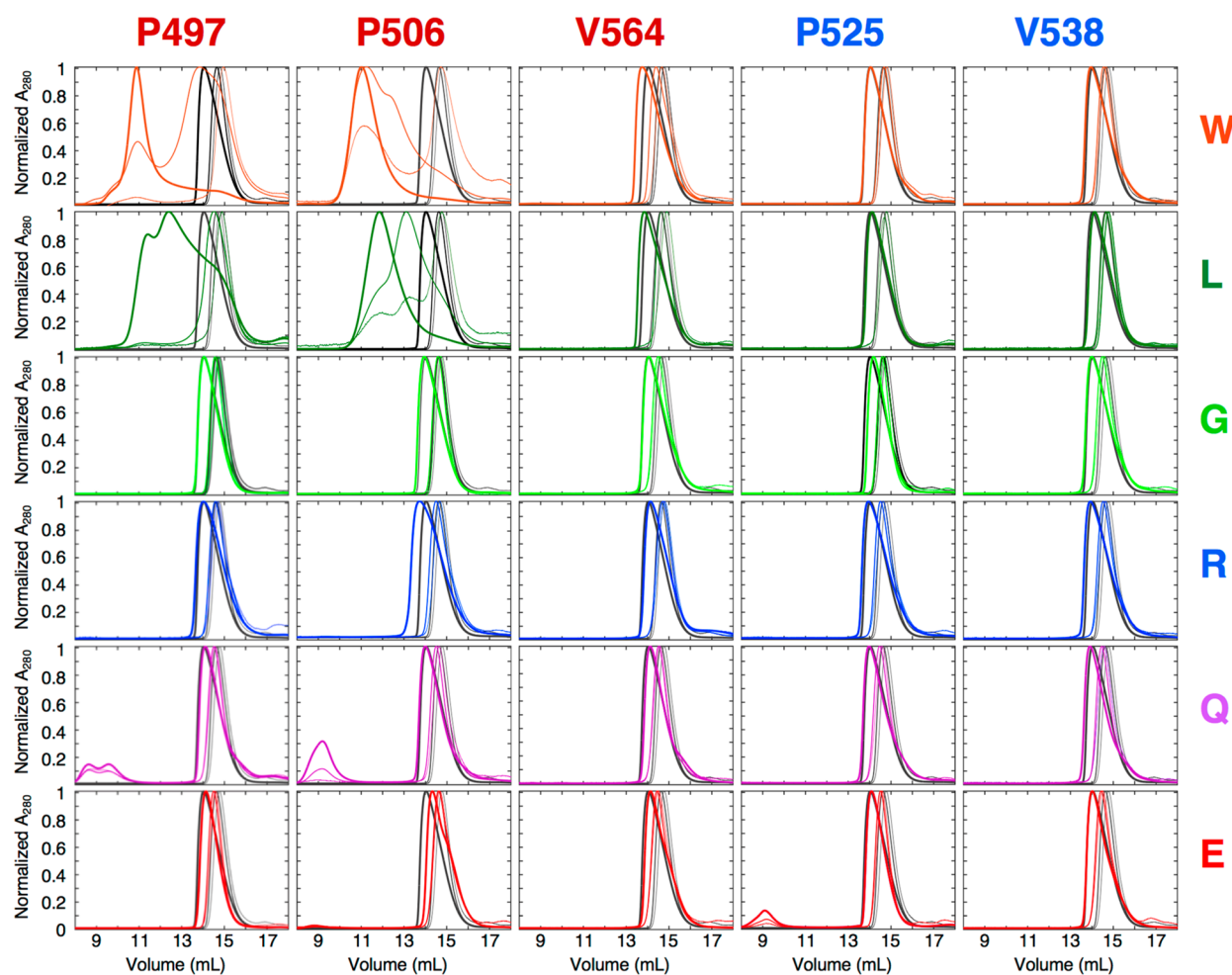


Figure 4. Oligomerization propensities of different UBQLN2 mutants. Representative SEC profiles of UBQLN2 mutants at 10 μM (thinnest line), 100 μM (medium-thick), and 500 μM (thickest) protein concentrations. For each mutant, WT SEC curves were plotted in gray for visual comparison.

stickers and their “stickiness” control the saturation concentrations (c_s) and the coexistence curve for LLPS, whereas spacer residues weakly modulate these parameters. These expectations are completely in line with our observations on amino acid substitutions at the three stickers (P497, P506, and V564) and two spacers (P525, V538) (Figure 1C,B). Strikingly, not only did single amino acid substitutions alone substantially shift c_s values but the effects of these substitutions followed particular trends to create a rich molecular code that governs UBQLN2 LLPS.

Self-association and LLPS of UBQLN2 are mediated by hydrophobicity involving either aliphatic or aromatic residues (Figure 2, Figure 4), in line with the hydrophobic composition of the amino acid sequence (Figure 1B). At position 506, decreased c_s values for the LCST phase transition correlated with increased hydrophobicity of amino acid substitution (Figure S5). Indeed, while we did not obtain phase diagrams for P497 mutants, the LCST transition temperatures for aromatic and hydrophobic substitutions at P497 followed the same trend as that at P506 (Figure 1C). LCST phase transitions require hydrophobicity.^{22,25,32} UBQLN2 also has high proline and glycine content (Figure 1B), which is a frequent component of proteins that undergo LCST phase transitions, such as Pab1, tropoelastins, and the spindle-associated BuGZ protein.^{14,15,33}

UBQLN2 exhibits a closed-loop phase diagram with both LCST and UCST phase transitions, such that the protein solution is well-mixed either above the UCST or below the LCST (Figure 2A). The thermodynamics of the underlying phase transitions can be explained by the entropic and enthalpic forces experienced by nonpolar particles in water as a function of temperature.³⁴ At low temperature, solubility of hydrophobic particles is high, partially due to water structuring around the hydrophobic groups. As temperature increases, the entropic cost to organize water also increases to a point at which solvent molecules are released from surrounding hydrophobic side chains, promoting demixing (phase separation) to minimize the free energy of the system. In polymer solutions, dehydration of hydrophobic groups is accompanied by attractive polymer–polymer interactions that also contribute to demixing.³⁵ As temperature increases further, entropy also increases promoting a UCST transition where homogeneous mixing of the polymer solution occurs. A decrease in polymer–polymer and solvent–solvent interactions also promotes mixing.³⁶ This UCST transition is not always observed, as biopolymers generally denature at high temperatures, but UBQLN2 450–624 remains well-behaved up to 60 °C.⁴³

As illustrated in Figure 1B, more than 25% of UBQLN2 450–624 contains polar residues (Q, N, S, T). Therefore, the

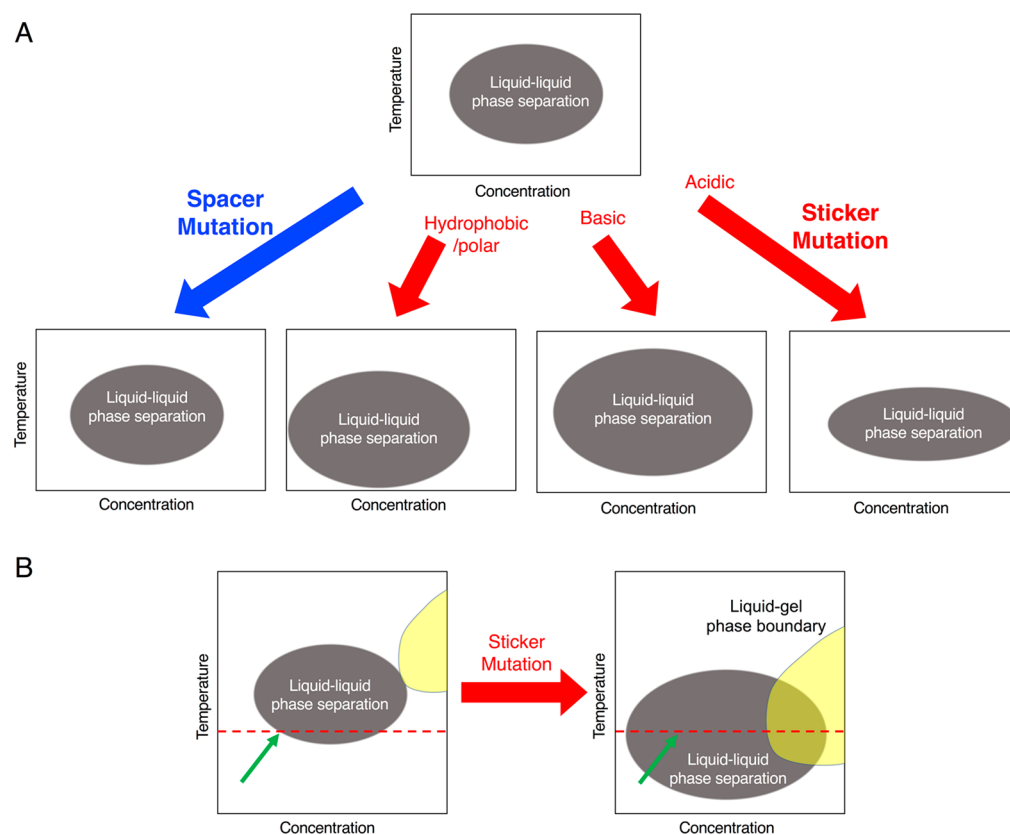


Figure 5. Illustration of effects of UBQLN2 sticker and spacer substitutions on temperature–concentration phase diagrams. (A) Effects of spacer and different types of sticker substitutions on the shape of the phase diagram. Amino acid substitutions in sticker regions move the location and shape of the phase boundaries. However, high concentration arms are hypothetical and for illustration purposes only. We hypothesize that the high concentration arms of some of the sticker mutants also move as we observed changes to the material properties of the dense phase. (B) Effects of mutations on phase diagrams and viscoelasticity. Gray and yellow shapes represent regions where the dense phase is liquid-like and gel/aggregate-like, respectively. (left) Green arrow represents a condition where dense phase is liquid. (right) Green arrow represents a condition where dense phase is solid-like (i.e., gel-like consistency).

driving forces underlying UBQLN2 phase separation are likely due to a combination of the hydrophobic effect and polar interactions. Of note, polymers rich in polar residues (N, Q) undergo a collapse transition reminiscent of the intrachain collapse in hydrophobic biopolymers, even though the underlying forces for polar collapse likely include other interactions such as intrachain hydrogen bonding and amide–solvent interactions.^{28,37} Interestingly, the c_c values for the LCST transition correlated well with the hydrophobicity of the amino acid substitution at P506 when all nonionizable residues were considered (Figure S5B). Polar substitutions also promoted aggregation (Figure S2E).

The polar groups in UBQLN2 likely modulate the UCST transition, as favorable polymer–polymer interactions among polar and/or ionizable tracts in intrinsically disordered proteins (IDPs) such as FUS and hnRNPA1 are considered drivers of UCST transitions in biopolymers.^{6,9} An increase and decrease in the UCST part of coexistence curves correspond to stronger and weaker polymer–polymer interactions, respectively. Complicating matters, hydrophobic groups also modulate UCST, and the effects of hydrophobic amino acid substitutions on the UCST transitions in UBQLN2 are certainly complex. At P506, increased hydrophobicity moderately tracks with decreased cloud-point temperatures for the UCST transition (Figure S5A). Our observations are opposite of what was seen in designed IDP polymers, for which UCST cloud points increased with increasing hydrophobicity.³⁸ Interestingly, our

turbidity data profile for hydrophobic substitutions at P497 are in better agreement with Quiroz et al.³⁸ We must acknowledge that prolines are structure-disrupting amino acids. In addition, peptide bonds preceding prolines can isomerize between *cis* and *trans* conformations. Therefore, the differences in observed turbidity profiles for proline substitutions at different positions could be partially explained by changes to backbone conformation and flexibility. These observations emphasize the heterogeneity of the phase transition behavior for the same type of amino acid substitution even among the sticker positions.

Remarkably, Asp and Glu mutations at any of the five tested positions in UBQLN2 reduced phase separation and significantly compressed the phase-separating regime in the UBQLN2 phase diagram (Figure 2). Importantly, these acidic mutations are also phosphomimetic substitutions. These data highlight the potential impact of post-translational modifications such as phosphorylation on modulating phase separation behavior. However, the effect is likely very dependent on the electrostatics of the protein system involved.^{8,39}

Material properties of the dense phase are also modified by amino acid substitutions.^{9,40} The liquid–liquid phase diagram therefore includes liquid–gel phase boundaries as schematized in Figure 5.⁶ Indeed, the stickers and spacers framework is one formalism that quantitatively addresses gelation.¹³ We observed that hydrophobic and aromatic amino acid substitutions only in sticker position P506 showed significantly

slowed droplet fusion kinetics (Figure 3), and those same mutants exhibited increased oligomerization propensity (Figure 4). At least in the UBQLN2 system, material properties of the dense phase appear linked to the propensity for UBQLN2 to oligomerize. We also noted that mutations that increased the propensity of oligomerization promoted UBQLN2 LLPS and led to slowed droplet fusion kinetics.⁴³ However, this is not always the case, as spacer mutations significantly slowed droplet fusion kinetics in the FUS family of proteins,⁸ and physicochemical properties of spacers in multidomain proteins modulate the liquid–liquid and liquid–gel phase boundaries.¹¹

In summary, our work here provides a rich data set to be used as a benchmark for analytical and computational models of phase separation. While mean-field theories such as Flory–Huggins approximate phase separation behavior for several systems,^{18,41} sequence-dependent frameworks will be essential to capture the nuances of phase-separating systems such as UBQLN2.⁴² The stickers and spacers framework has already been used to successfully examine the underlying forces of phase separation in the FET family of RNA-binding proteins.⁸ Unraveling the complexities of solvent–solvent, polymer–polymer, and polymer–solvent interactions will establish the molecular code of phase-separating systems.

CONCLUSIONS

In this work, we put forth UBQLN2 450–624 as a model system to study the physicochemical molecular determinants of phase separation. We employed a battery of spectrophotometric, microscopy, and size exclusion chromatography experiments to systematically elucidate how amino acid substitutions at different positions in the protein sequence modulate phase separation. Experimental phase diagrams revealed that we can describe UBQLN2 as an associative polymer with stickers and spacers that drive and modulate phase separation behavior. Single amino-acid substitution can substantially shift coexistence curves in a residue type-dependent manner. It is our expectation that our experimental data can be used to rigorously design and benchmark analytical models and molecular simulations of phase separation. This work can be used to elucidate effects of disease-linked mutations in phase-separating systems as well as to design thermoresponsive biopolymers.

ASSOCIATED CONTENT

Supporting Information

The Supporting Information is available free of charge on the ACS Publications website at DOI: 10.1021/acs.jpcb.9b01024.

Figures of UBQLN2 sequence information, representative gels, and mass spectrometry of UBQLN2 mutants, reproducibility of turbidity assays and size exclusion chromatography experiments, and correlations between saturation concentrations and hydrophobicity (PDF)

AUTHOR INFORMATION

Corresponding Author

*E-mail: cacastan@syr.edu.

ORCID

Carlos A. Castañeda: 0000-0001-9634-0867

Author Contributions

The manuscript was written through contributions of all authors. All authors have given approval to the final version of the manuscript.

Notes

The authors declare no competing financial interest.

Biography



Carlos A. Castañeda received his Ph.D. from the Program in Molecular Biophysics at Johns Hopkins University working with Dr. Bertrand Garcia-Moreno on using NMR spectroscopy and electrostatics calculations to measure and calculate the pK_a values of ionizable groups in proteins. As an NSF postdoctoral fellow, he worked with David Fushman at the University of Maryland-College Park on studying the structure and function of all polyubiquitin chain types using NMR spectroscopy, small angle scattering, and computational modeling. In his independent lab at Syracuse University, where he is an assistant professor of Biology and Chemistry, Carlos focuses on elucidating the role of protein quality control mechanisms in neurological disorders, such as amyotrophic lateral sclerosis (ALS). Since discovering that UBQLN2 undergoes liquid–liquid phase separation in vitro and in vivo, his lab has focused on determining the molecular basis for phase separation in ubiquilins and other proteins using a combination of experimental and computational tools. For this work, Carlos has received two grants from the ALS Association and an NSF CAREER award in 2018.

ACKNOWLEDGMENTS

This work was supported by ALS Association Grant No. 18-IIP-400 and the National Science Foundation (CAREER Award No. 1750462) to C.A.C. We thank A. Sorzano and participants at the Gibbs Conference on Biothermodynamics for useful discussions. The Shimadzu 8040 mass spectrometer was partially supported by a Shimadzu equipment grant to C.A.C.

REFERENCES

- (1) Brangwynne, C. P.; Eckmann, C. R.; Courson, D. S.; Rybarska, A.; Hoege, C.; Gharakhani, J.; Jülicher, F.; Hyman, A. A. Germline P Granules Are Liquid Droplets That Localize by Controlled Dissolution/Condensation. *Science* **2009**, *324*, 1729–1732.
- (2) Hyman, A. A.; Weber, C. A.; Jülicher, F. Liquid-Liquid Phase Separation in Biology. *Annu. Rev. Cell Dev. Biol.* **2014**, *30*, 39–58.
- (3) Banani, S. F.; Rice, A. M.; Peeples, W. B.; Lin, Y.; Jain, S.; Parker, R.; Rosen, M. K. Compositional Control of Phase-Separated Cellular Bodies. *Cell* **2016**, *166*, 651–663.
- (4) Li, P.; Banjade, S.; Cheng, H.-C.; Kim, S.; Chen, B.; Guo, L.; Llaguno, M.; Hollingsworth, J. V.; King, D. S.; Banani, S. F.; et al.

Phase Transitions in the Assembly of Multi-Valent Signaling Proteins. *Nature* **2012**, *483*, 336–340.

(5) Lin, Y.; Protter, D. S. W.; Rosen, M. K.; Parker, R. Formation and Maturation of Phase-Separated Liquid Droplets by RNA-Binding Proteins. *Mol. Cell* **2015**, *60*, 208–219.

(6) Lin, Y.; Currie, S. L.; Rosen, M. K. Intrinsically Disordered Sequences Enable Modulation of Protein Phase Separation through Distributed Tyrosine Motifs. *J. Biol. Chem.* **2017**, *292*, 19110–19120.

(7) Pak, C. W.; Kosno, M.; Holehouse, A. S.; Padrick, S. B.; Mittal, A.; Ali, R.; Yunus, A. A.; Liu, D. R.; Pappu, R. V.; Rosen, M. K. Sequence Determinants of Intracellular Phase Separation by Complex Coacervation of a Disordered Protein. *Mol. Cell* **2016**, *63*, 72–85.

(8) Wang, J.; Choi, J.-M.; Holehouse, A. S.; Lee, H. O.; Zhang, X.; Jahnel, M.; Maharana, S.; Lemaitre, R.; Pozniakovskiy, A.; Drechsel, D.; et al. A Molecular Grammar Governing the Driving Forces for Phase Separation of Prion-like RNA Binding Proteins. *Cell* **2018**, *174*, 688–699.

(9) Molliex, A.; Temirov, J.; Lee, J.; Coughlin, M.; Kanagaraj, A. P.; Kim, H. J.; Mittag, T.; Taylor, J. P. Phase Separation by Low Complexity Domains Promotes Stress Granule Assembly and Drives Pathological Fibrillization. *Cell* **2015**, *163*, 123–133.

(10) Patel, A.; Lee, H. O.; Jawerth, L.; Maharana, S.; Jahnel, M.; Hein, M. Y.; Stoykov, S.; Mahamid, J.; Saha, S.; Franzmann, T. M.; et al. A Liquid-to-Solid Phase Transition of the ALS Protein FUS Accelerated by Disease Mutation. *Cell* **2015**, *162*, 1066–1077.

(11) Harmon, T. S.; Holehouse, A. S.; Rosen, M. K.; Pappu, R. V. Intrinsically Disordered Linkers Determine the Interplay between Phase Separation and Gelation in Multivalent Proteins. *eLife* **2017**, *6*, No. e30294.

(12) Rubinstein, M.; Dobrynin, A. V. Solutions of Associative Polymers. *Trends Polym. Sci.* **1997**, *5*, 181–186.

(13) Semenov, A. N.; Rubinstein, M. Thermoreversible Gelation in Solutions of Associative Polymers. *Macromolecules* **1998**, *31*, 1373–1385.

(14) Riback, J. A.; Katanski, C. D.; Kear-Scott, J. L.; Pilipenko, E. V.; Rojek, A. E.; Sosnick, T. R.; Drummond, D. A. Stress-Triggered Phase Separation Is an Adaptive, Evolutionarily Tuned Response. *Cell* **2017**, *168*, 1028–1040.

(15) Yeo, G. C.; Keeley, F. W.; Weiss, A. S. Coacervation of Tropoelastin. *Adv. Colloid Interface Sci.* **2011**, *167*, 94–103.

(16) Zai-Rose, V.; West, S. J.; Kramer, W. H.; Bishop, G. R.; Lewis, E. A.; Correia, J. J. Effects of Doxorubicin on the Liquid-Liquid Phase Change Properties of Elastin-Like Polypeptides. *Biophys. J.* **2018**, *115*, 1431–1444.

(17) Li, H.-R.; Chiang, W.-C.; Chou, P.-C.; Wang, W.-J.; Huang, J. TAR DNA-Binding Protein 43 (TDP-43) Liquid-Liquid Phase Separation Is Mediated by Just a Few Aromatic Residues. *J. Biol. Chem.* **2018**, *293*, 6090–6098.

(18) Nott, T. J.; Petsalaki, E.; Farber, P.; Jarvis, D.; Fussner, E.; Plochowitz, A.; Craggs, T. D.; Bazett-Jones, D. P.; Pawson, T.; Forman-Kay, J. D.; et al. Phase Transition of a Disordered Nuage Protein Generates Environmentally Responsive Membraneless Organelles. *Mol. Cell* **2015**, *57*, 936–947.

(19) Vernon, R. M.; Chong, P. A.; Tsang, B.; Kim, T. H.; Bah, A.; Farber, P.; Lin, H.; Forman-Kay, J. D. Pi-Pi Contacts Are an Overlooked Protein Feature Relevant to Phase Separation. *eLife* **2018**, *7*, No. e31486.

(20) Posey, A. E.; Holehouse, A. S.; Pappu, R. V. Chapter One - Phase Separation of Intrinsically Disordered Proteins. *Methods Enzymol.* **2018**, *611*, 1–30.

(21) Rubinstein, M.; Colby, R. H. *Polymer Physics*; Oxford University Press: Oxford, UK, 2003.

(22) Ruff, K. M.; Roberts, S.; Chilkoti, A.; Pappu, R. V. Advances in Understanding Stimulus-Responsive Phase Behavior of Intrinsically Disordered Protein Polymers. *J. Mol. Biol.* **2018**, *430*, 4619–4635.

(23) Alberti, S.; Gladfelter, A.; Mittag, T. Considerations and Challenges in Studying Liquid-Liquid Phase Separation and Biomolecular Condensates. *Cell* **2019**, *176*, 419–434.

(24) Dzuricky, M.; Roberts, S.; Chilkoti, A. Convergence of Artificial Protein Polymers and Intrinsically Disordered Proteins. *Biochemistry* **2018**, *57*, 2405–2414.

(25) Dao, T. P.; Kolaitis, R.-M.; Kim, H. J.; O'Donovan, K.; Martyniak, B.; Colicino, E.; Hehnl, H.; Taylor, J. P.; Castañeda, C. A. Ubiquitin Modulates Liquid-Liquid Phase Separation of UBQLN2 via Disruption of Multivalent Interactions. *Mol. Cell* **2018**, *69*, 965–978.

(26) Schindelin, J.; Arganda-Carreras, I.; Frise, E.; Kaynig, V.; Longair, M.; Pietzsch, T.; Preibisch, S.; Rueden, C.; Saalfeld, S.; Schmid, B.; et al. Fiji: An Open-Source Platform for Biological-Image Analysis. *Nat. Methods* **2012**, *9*, 676–682.

(27) Mutterer, J.; Zinck, E. Quick-and-Clean Article Figures with FigureJ. *J. Microsc.* **2013**, *252* (1), 89–91.

(28) Holehouse, A. S.; Pappu, R. V. Collapse Transitions of Proteins and the Interplay Among Backbone, Sidechain, and Solvent Interactions. *Annu. Rev. Biophys.* **2018**, *47*, 19–39.

(29) Urry, D. W.; Gowda, D. C.; Parker, T. M.; Luan, C.-H.; Reid, M. C.; Harris, C. M.; Pattanaik, A.; Harris, R. D. Hydrophobicity Scale for Proteins Based on Inverse Temperature Transitions. *Biopolymers* **1992**, *32*, 1243–1250.

(30) Osváth, Z.; Iván, B. The Dependence of the Cloud Point, Clearing Point, and Hysteresis of Poly(N-Isopropylacrylamide) on Experimental Conditions: The Need for Standardization of Thermoresponsive Transition Determinations. *Macromol. Chem. Phys.* **2017**, *218*, 1600470.

(31) Feric, M.; Vaidya, N.; Harmon, T. S.; Mitrea, D. M.; Zhu, L.; Richardson, T. M.; Kriwacki, R. W.; Pappu, R. V.; Brangwynne, C. P. Coexisting Liquid Phases Underlie Nucleolar Sub-Compartments. *Cell* **2016**, *165*, 1686–1697.

(32) Martin, E. W.; Mittag, T. Relationship of Sequence and Phase Separation in Protein Low-Complexity Regions. *Biochemistry* **2018**, *57*, 2478–2487.

(33) Jiang, H.; Wang, S.; Huang, Y.; He, X.; Cui, H.; Zhu, X.; Zheng, Y. Phase Transition of Spindle-Associated Protein Regulate Spindle Apparatus Assembly. *Cell* **2015**, *163*, 108–122.

(34) Moelbert, S.; Normand, B.; De Los Rios, P. Solvent-Induced Micelle Formation in a Hydrophobic Interaction Model. *Phys. Rev. E. Stat. Nonlin. Soft Matter Phys.* **2004**, *69*, 061924.

(35) Matsarskaia, O.; Braun, M. K.; Roosen-Runge, F.; Wolf, M.; Zhang, F.; Roth, R.; Schreiber, F. Cation-Induced Hydration Effects Cause Lower Critical Solution Temperature Behavior in Protein Solutions. *J. Phys. Chem. B* **2016**, *120*, 7731–7736.

(36) Falahati, H.; Haji-Akbari, A. Thermodynamically Driven Assemblies and Liquid-Liquid Phase Separations in Biology. *Soft Matter* **2019**, *15*, 1135–1154.

(37) Wuttke, R.; Hofmann, H.; Nettels, D.; Borgia, M. B.; Mittal, J.; Best, R. B.; Schuler, B. Temperature-Dependent Solvation Modulates the Dimensions of Disordered Proteins. *Proc. Natl. Acad. Sci. U. S. A.* **2014**, *111*, 5213–5218.

(38) Quiroz, F. G.; Chilkoti, A. Sequence Heuristics to Encode Phase Behaviour in Intrinsically Disordered Protein Polymers. *Nat. Mater.* **2015**, *14*, 1164–1171.

(39) Monahan, Z.; Ryan, V. H.; Janke, A. M.; Burke, K. A.; Rhoads, S. N.; Zerze, G. H.; O'Meally, R.; Dignon, G. L.; Conicella, A. E.; Zheng, W.; et al. Phosphorylation of the FUS Low-complexity Domain Disrupts Phase Separation, Aggregation, and Toxicity. *EMBO J.* **2017**, *36*, 2951–2967.

(40) Kato, M.; Han, T. W.; Xie, S.; Shi, K.; Du, X.; Wu, L. C.; Mirzaei, H.; Goldsmith, E. J.; Longgood, J.; Pei, J.; et al. Cell-Free Formation of RNA Granules: Low Complexity Sequence Domains Form Dynamic Fibers within Hydrogels. *Cell* **2012**, *149*, 753–767.

(41) Brady, J. P.; Farber, P. J.; Sekhar, A.; Lin, Y.-H.; Huang, R.; Bah, A.; Nott, T. J.; Chan, H. S.; Baldwin, A. J.; Forman-Kay, J. D.; et al. Structural and Hydrodynamic Properties of an Intrinsically Disordered Region of a Germ Cell-Specific Protein on Phase Separation. *Proc. Natl. Acad. Sci. U. S. A.* **2017**, *114*, E8194–E8203.

(42) Lin, Y.-H.; Forman-Kay, J. D.; Chan, H. S. Theories for Sequence-Dependent Phase Behaviors of Biomolecular Condensates. *Biochemistry* **2018**, *57*, 2499–2508.

(43) Dao, T. P.; Martyniak, B.; Canning, A. J.; Lei, Y.; Colicino, E. G.; Cosgrove, M. S.; Hehly, H.; Castañeda, C. A. ALS-linked mutations affect UBQLN2 oligomerization and phase separation in a position- and amino acid-dependent manner. *Structure* **2019**, DOI: [10.1016/j.str.2019.03.012](https://doi.org/10.1016/j.str.2019.03.012).

Curriculum Vitae

Holly Brianne Jones

Hjones08@syr.edu

Education

M.S. Biology

2020 Syracuse University, Syracuse, New York
Thesis title: Elucidation of UBQLN2 liquid-liquid phase separation mechanisms via point mutations and domain deletions

B.S. Biological Sciences

2018 Eastern Illinois University, Charleston, Illinois
Major GPA: 4.0/4.0

B.S. Kinesiology and Sports Science: Exercise Science

2018 Eastern Illinois University, Charleston, Illinois
Major GPA: 4.0/4.0

Publications

Radu F. Semeniuc, Thomas J. Reamer, Kaitlyn A. Hammock, **Holly B. Jones**, Mark D. Smith, and Kraig A. Wheeler. (2018). Second generation O-alkyldithiocarbonates: Easy access to a new class of metalloligands. *Inorganica Chimica Acta*, 475. 161-171

Yiran Yang, **Holly B. Jones**, Thuy P. Dao, and Carlos A. Castañeda. (2019). Single Amino Acid Substitutions in Stickers, but Not Spacers, Substantially Alter UBQLN2 Phase Transitions and Dense Phase Material Properties. *J. Phys. Chem. B* 123. 3618–3629.

Teaching and Professional Experience

General Biology I and II Teaching Assistant, 2018-2019

Syracuse University, Syracuse, NY

- Assist with lab preparation, teach two lab sections, lead class discussion
- Hold open tutoring hours, provide/write quizzes and tests

Chemistry/Biology/Kinesiology Tutor, Fall 2015-2018

Eastern Illinois Athletics, Charleston, IL

- Help plan, modify, and implement study habits for student athletes
- Hold open labs and study sessions, provide/write practice quizzes and tests

Research Assistant, Summer 2016

University of Illinois Medical School of Entomology, Champaign, IL

- Assisted with molecular procedures, field work, and upkeep of laboratory
- Data analysis and record keeping

Anatomy and Physiology Teaching Assistant, Spring 2016-Spring 2017

Eastern Illinois University Biology Department, Charleston, IL

- Assisted with lab preparation, procedures, and individual student help
- Held open labs, wrote and graded quizzes

Research Experience

Syracuse University, Biology and Chemistry, *06/2018-current*

Advisor: Dr. Carlos Castañeda

- Express and purify UBQLN2 constructs
- Perform gel filtration experiments to monitor UBQLN2 self-association
- Monitored mutant UBQLN2 droplet dynamics using light and fluorescence microscopy

Eastern Illinois University, Inorganic Chemistry, *01/2017-2018*

Advisor: Dr. Radu Semeniuc

- Synthesized and purified starting materials
- Designed biomimetic ligands to coordinate transmetallic centers
- Analysis using ^1H NMR, ^{13}C NMR, IR spectroscopy, TLC, UV spectroscopy, x-ray diffraction crystallography

Eastern Illinois University, Fish Biomechanics, *08/2016-12/2016*

Advisor: Dr. Anabela Maia

- Designed and implemented research analyzing the oxygen consumption and kinetics of Longear Sunfish
- Recorded data with use of flow tank and probes, used software to analyze fish kinematics
- Incorporated group meetings and discussions, practiced presenting and analyzing publications

Eastern Illinois University, Mosquito Lab, *05/2016-08/2016*

Advisor: Dr. Antony Oluoch

- Sample collection: used traps at multiple cross county sites for diverse insect sample
- Analyzed mosquito morphology using microscopy
- Species identification using DNA extraction/isolation, PCR, gel electrophoresis and western blot